**LUCAS BORGES FERNANDES**
**VITOR BORGES FERNANDES**

# EXPERIMENTAL ANALYSIS OF A 1997 HONDA CIVIC VTi REAR AIR DIFFUSER

UNIVERSIDADE FEDERAL DE UBERLÂNDIA
FACULDADE DE ENGENHARIA MECÂNICA
2022

**LUCAS BORGES FERNANDES**
**VITOR BORGES FERNANDES**

# EXPERIMENTAL ANALYSIS OF A 1997 HONDA CIVIC VTi REAR AIR DIFFUSER

Undergraduate thesis submitted to the Course of Aeronautical Engineering from the Federal University of Uberlândia as a part of requirement for obtaining the BACHELOR'S DEGREE ON AERONAUTICAL ENGINEERING.

Tutor: Prof. Dr. Odenir de Almeida

UBERLÂNDIA – MG
2022

**LUCAS BORGES FERNANDES**
**VITOR BORGES FERNANDES**

# EXPERIMENTAL ANALYSIS OF A 1997 HONDA CIVIC VTi REAR AIR DIFFUSER

Undergraduate thesis **APROVED** by the Course of Aeronautical Engineering from the Faculty of Mechanical Engineering of the Federal University of Uberlândia.

Thesis Committee Composition:

_____

Prof. Dr. Odenir de Almeida

_____

Prof. Dr. Giuliano Gardolinski Venson

_____

Eng. Samara Cunha Rosa

_____

Me. João Paulo Eguea

**Uberlândia, 15th September 2022**

Este trabalho é dedicado ao nosso querido amigo Nelson Batista Neto, proprietário do Honda Civic VTi, usado como modelo para este projeto. Sua amizade fará falta, e sua memória ficará gravada para sempre em nossos corações.

# ACKNOLEGEMENTS

First, we would like to thank God for His unconditional love and grace, in the fact that He sent His only Son to die in our place, making us righteous before Him, and resurrect to give us eternal life. We are also grateful for our wives and family for all the love, care, and support during our graduation period. Thanks to the Federal University of Uberlândia (UFU) and more specifically the Faculty of Mechanical Engineering (FEMEC) for providing a high-level academic formation that is concluded on the production of this manuscript.

We personally thank Prof. Dr. Odenir de Almeida for all the support in all aspects regarding the wind tunnel experiments and for all the knowledge that was taught to us about the theory of vehicular aerodynamics. We also thanks Reinaldo, the laboratory technician, for all the excellent work in the preparation of the model, used in wind tunnel tests, including the model assembly, the model surface treatment, and the installation of the pressure taps. We are very grateful to Nelson Batista for allowed us to use his own car for this paper and all support he gave us to make this project real.

FERNANDES, L. B., and FERNANDES, V. B. **Experimental Analysis of a 1997 Honda Civic VTi Rear Air Diffuser**. 2022. 124 f. Trabalho de Conclusão de Curso (Graduação em Engenharia Aeronáutica) - Universidade Federal de Uberlândia, Uberlândia, 2022.

# RESUMO

Os carros de competição têm um único propósito, entregar o melhor desempenho dentro das pistas. Sempre se busca a melhor relação entre o arrasto aerodinâmico e o *downforce* para que maiores velocidades em retas e curvas sejam atingidas e assim reduzir os tempos de volta. A instalação de dispositivos aerodinâmicos, como, aerofólios, *spoilers*, geradores de vórtices, difusores de ar, entre outros, é um meio de conseguir esse objetivo. A exposição dos componentes mecânicos e estruturais na parte inferior do veículo contribui de maneira significativa para o aumento do coeficiente de arrasto total, e por isso veículos modificados para competição devem dotar de dispositivos que amenizem esse fenômeno e ao mesmo tempo intensificam o coeficiente de sustentação negativo. Este trabalho apresenta um estudo experimental do escoamento ao redor do Honda Civic VTi 1997 modificado para participar em competições de *time attack*. O modelo foi construído seguindo a forma base do carro buscando manter fidelidade ao veículo existente. No túnel de vento, foram realizados testes com o modelo em escala de 1:10, com e sem difusor, o qual variou-se o ângulo da rampa de subida a partir de 0° até o ângulo máximo de 10.51°, com o intervalo de 2°, totalizando 6 configurações (0°, 2°, 4°, 6°, 8° e 10.51°). Posteriormente foram instaladas *endplates* nos difusores de 2°, 4°, 6° e 8°. Todos os ensaios foram realizados com o modelo utilizando o assoalho liso a uma velocidade de 20 m/s. Foi utilizado o método de visualização parietal por tufos para identificar a mudança no padrão do escoamento para cada difusor utilizado na parte de trás do modelo. Também se utilizou o método de visualização por pintura, com o qual foi possível observar os pontos de descolamento do escoamento. Foram instaladas 22 tomadas de pressão na parte superior do modelo para a obtenção da curva de distribuição de pressão, e assim foram realizadas medidas para os casos em que a instalação dos difusores apresentou os melhores resultados. O difusor de 2 graus apresentou o melhor resultado possibilitando uma redução de 6% da força de arrasto total do modelo. Ao adicionar as *endplates*, os resultados mostraram que não houve mudanças significativas no coeficiente de arrasto, exceto para a configuração de 6 graus, que resultou em uma diminuição de aproximadamente 5% na força de arrasto quando comparado ao modelo base.

Esse trabalho visa servir como referência para análises futuras e deste modo realizar um estudo numérico (CFD) e a aplicação de outras rotinas experimentais é recomendado. A investigação de mecanismos de redução de arrasto e dos efeitos de outras modificações na geometria é sugerida para as próximas etapas.

[1]Keywords: Aerodinâmica; Difusor; Carro de Corrida; Túnel de Vento; Downforce; Arrasto; Honda Civic.

FERNANDES, L. B., and FERNANDES, V. B. **Experimental Analysis of a 1997 Honda Civic VTi Rear Air Diffuser**. 2022. 124 f. Trabalho de Conclusão de Curso (Graduação em Engenharia Aeronáutica) - Universidade Federal de Uberlândia, Uberlândia, 2022.

# ABSTRACT

Racing cars have a single purpose, to deliver the best performance on the tracks. Always looking for the best relationship between aerodynamic drag and downforce so that higher speeds on straights and curves are achieved and thus reduce lap times. The installation of aerodynamic devices, such as airfoils, spoilers, vortex generators, air diffusers, among others, are some ways to achieve this objective. The exposure of mechanical and structural components on the underside of the vehicle contributes significantly to the increase in the total drag coefficient, and therefore vehicles modified for competition must have devices that mitigate this phenomenon and at the same time intensify the negative lift coefficient. This work presents an experimental study of the flow around the Honda Civic VTi 1997 modified to participate in time attack competitions. The model was built following the base form of the car, seeking to maintain fidelity to the existing vehicle. In the wind tunnel, tests were carried out with the model on a scale of 1:10, with and without a diffuser, in which the angle of the ascent ramp was varied from 0° to the maximum angle of 10.51°, with the interval of 2°, totaling 6 settings (0°, 2°, 4°, 6°, 8° and 10.51°). Later, endplates were installed in the 2°, 4°, 6° and 8° diffusers. All tests were performed with the model using the smooth floor at a speed of 20 m/s. The parietal tuft visualization method was used to identify the change in flow pattern for each diffuser used at the back of the model. The painting visualization method was also used, with which it was possible to observe the flow detachment points. 22 pressure taps were installed in the upper part of the model to obtain the pressure distribution curve, and thus measurements were carried out for the cases in which the installation of diffusers presented the best results. The 2-degree diffuser presented the best result, allowing a reduction of 6% of the total drag force of the model. When adding the endplates, the results showed that there were no significant changes in the drag coefficient, except for the 6-degree setting, which results in an approximately 5% decrease in drag force when compared to the base model. This work aims to serve as a reference for future analysis and thus performing a numerical study (CFD) and the application of other experimental routines is recommended. The investigation of drag

reduction mechanisms and the effects of other geometry modifications is suggested for the next steps.

[1]Keywords: Aerodynamics; Diffuser; Race Car; Wind-tunnel; Downforce; Drag; Honda Civic.

# LIST OF FIGURES

# LIST OF TABLES

# LIST OF SYMBOLS

| | |
|---|---|
| $C_L$ | Lift Coefficient |
| $C_D$ | Drag Coefficient |
| $L$ | Lift force |
| $D$ | Drag force |
| $C_P$ | Pressure coefficient |
| $\bar{\bar{C}}_{Pi}$ | Streamwise-distance-averaged pressure coefficient |
| $\bar{\bar{C}}_{Pl}$ | Whole underbody mean effect pressure coefficient |
| $\bar{\bar{C}}_{Pf}$ | Floor mean effect pressure coefficient |
| $\bar{\bar{C}}_{Pd}$ | Diffuser mean effect pressure coefficient |
| $\bar{C}_P$ | Overall pressure-recovery coefficient of the diffuser |
| $C_{P1}$ | Diffuser inlet pressure coefficient |
| $C_{P2}$ | Diffuser outlet pressure coefficient |
| $V_b$ | Freestream velocity |
| $Re$ | Reynolds Number |
| $\dot{V}$ | Flow Rate |
| $V_1$ | Venturi tube inlet velocity |
| $V_2$ | Venturi tube throat velocity |
| $A_1$ | Venturi tube inlet transversal section area |
| $A_2$ | Venturi tube throat transversal section area |
| $p_1$ | Venturi tube inlet static pressure |
| $p_2$ | Venturi tube throat static pressure |

| | |
|---|---|
| $\rho$ | Air density |
| $U_0$ | Air flow velocity |
| $P$ | Static pressure |
| $P_0$ | Freestream pressure |
| $A_{ref}$ | Referential area |
| $F$ | Local lift force |
| $\alpha_i$ | Induced angle of attack |
| $\alpha_d$ | Slant angle |
| $D_i$ | Induced Drag |
| $L_{ref}$ | Reference dimension |
| $\mu$ | Fluid dynamic viscosity |
| $\Delta C_D$ | Delta drag coefficient |
| $h$ | Ground clearance |
| $h_0$ | Height difference of diffuser inlet and outlet |
| $L_B$ | Bluff body length |
| $L_D$ | Diffuser length |
| $H$ | Bluff body height |
| $W$ | Bluff body width |
| $p_f$ | Flat underbody floor static pressure |
| $p_d$ | Diffuser floor static pressure |
| $p_u$ | Upper body static pressure |
| $p_n$ | Nose static pressure |
| $p_b$ | Base static pressure |

# SUMMARY

# CHAPTER I

## Introduction

Aerodynamics is an aspect of great importance in racing car design, in which it is aimed to obtain the highest performance on racetracks. From the very beginning, racing car engineers have realized the importance of aerodynamic forces to vehicle performance and began to develop methods to optimize the air flow over the car. The goal was to make the cars faster, which may be accomplished by changing the shape of the vehicle. One example is the 1916 Peugeot Indianapolis 500 (Figure 1.1) winner with a tapering boat tail, that decreased the total drag force by smoothing the air flow at the car's rear.

Figure 1.1 – 1916 Peugeot Indianapolis 500 winner


Source: https://www.finemodelcars.info/peugeot-l45-gp.html

As cars increased in speed, engineers realized that aerodynamics can be used to improve vehicle performance in curves by increasing its grip as the car's lift force is reduced. The grip could be even increased by generating aerodynamics forces downward (down force), resulting in the appearance of devices like inverted wing in several categories of motorsport, such as Formula 1, IndyCar, Le Mans, and the extinct Can-Am.

Figure 1.2 – 1970 McLaren M8F Chevrolet


Source: https://www.conceptcarz.com/vehicle/z15080/mclaren-m8f.aspx

Figure 1.3 – 1968 Lotus 49B Ford


Source: https://motorsportoldtimes.wordpress.com/2013/07/15/o-lendario-lotus-49/

The major idea is to increase the normal load on the tires for increased grip without the corresponding addition of mass, in other words, enhance the negative lift (downforce). The Figure 1.2 is an example of design to decrease the drag and lift forces. The smooth shape of the car,

covered wheels and adding devices, like inverted rear wing, were solutions that remain until today. Figure 1.3 shows one of the first F1 cars to use inverted wings to improve car performance in corners, by increasing downforce. Lotus was the first team to bring this to the category in 1968, and in the same year, they became world champions. Another race car example is the IndyCar 1967 Lotus 56 (Figure 1.4). This car was designed to race in the Indianapolis 500 reaching a top speed of 276 km/h in that year due to its design. It's noticeable difference in the design of F1 and Indy cars. The Lotus 56 was designed to minimize drag; they covered some mechanical parts, like suspension arms and exhaust pipes, to prevent air flow interactions with these structures and reduce turbulence.

Figure 1.4 – 1968 Lotus 56 at the Indianapolis 500


Source: https://robbreport.com/motors/cars/slideshow/top-10-racecars-indy-500-history/1968-lotus-56/

The movement and performance of a car is constrained mainly by two factors: rolling resistance and aerodynamic drag. The rolling resistance is caused by the contact between the ground and the tire, and it is proportional to the frictional coefficient between these two. On the other hand, the drag force is a result of the car and the air interaction, being proportional to the wind speeds squared.

Figure 1.5 – Resistance force versus vehicle speed

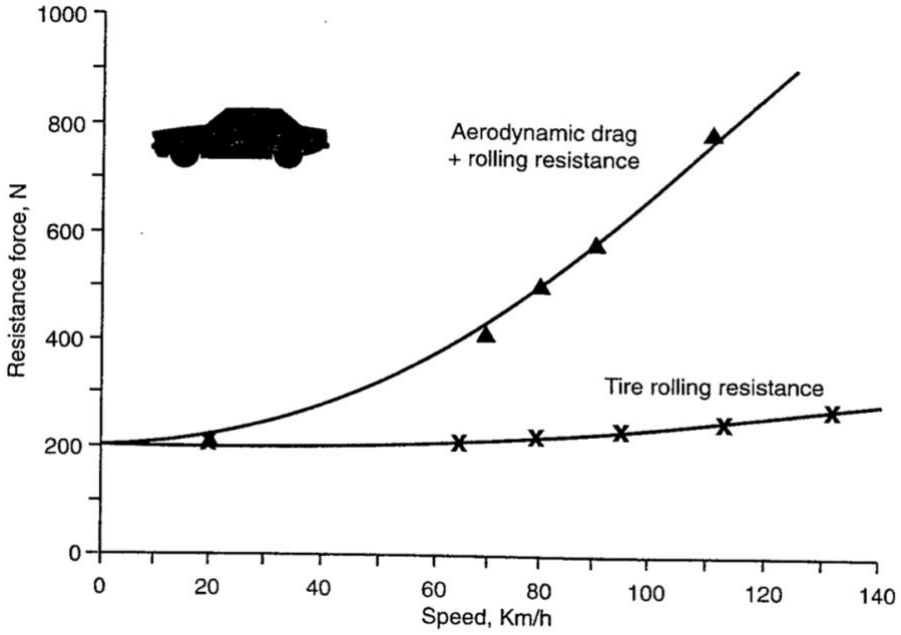


Source: (Katz, 1995)

Katz (1995) analyzed the influence of rolling resistance and drag in a car's resistance force to motion. The results (Figure 1.5) indicated that the drag force is the major responsible force the car's resistance forces, increasing proportionally to its speed squared. However, when aerodynamic forces are considered, the resistance force drastically increases, which indicates that drag is the main responsible for opposition to car motion, principally on high speeds. To illustrate how drag influences race car performance, Carrol Smith (1978) demonstrates (Figure 1.6), with a Formula 5000 base model, that higher the velocity, the higher the power required by the car to overcome the drag forces. The drag force was converted to horsepower for better illustration.

Figure 1.6 – Drag Horsepower vs Road Speed

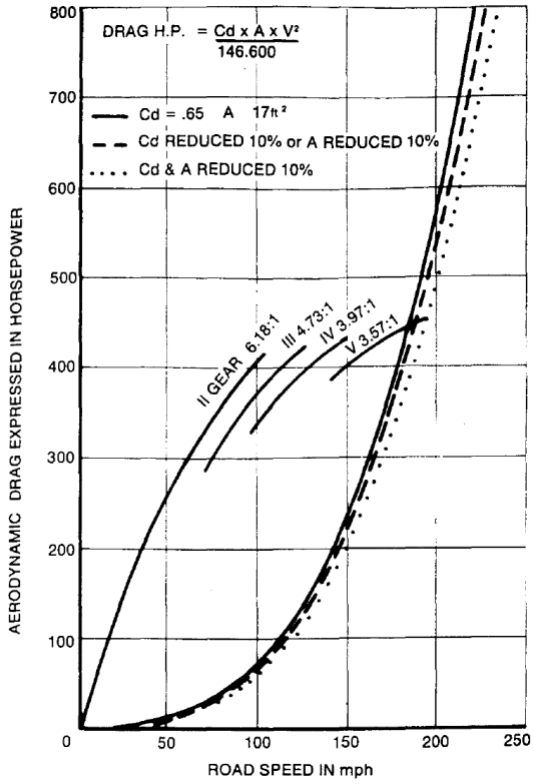


Source: (Smith, 1978)

The results indicate that for low speeds, below than 50 mph (80 km/h), drag forces have less influences on cars performance, and it becomes noticeable above this speed, when the curve slope increases drastically. According to (DUXBURY; HOLDING, 2022) the average speed during a lap for most race cars is over 70 mph. The article shows that at the Circuit of the Americas, the average speed for an F1 car was 128.18 mph, for an IndyCar it was 116.46 mph. As for a WTCR car, at the Hungaroring racetrack, the value was 78.44 mph. At those speeds, it may be inferred that the aerodynamic drag is one of the biggest concerns of race car designers for reducing lap times.

Racing engineers have always been involved in a dilemma, with the increase in downforce, the drag forces become higher either. One of the solutions to contour this situation without adding more aerodynamics appendices, was to make the car's underbody flat. In the figure below, it is possible to see the relation between these forces on a 2009 Formula 1 base car, and the importance of a flat underbody.

Figure 1.7 – Relation between downforce and drag on a 2009 F1 base car

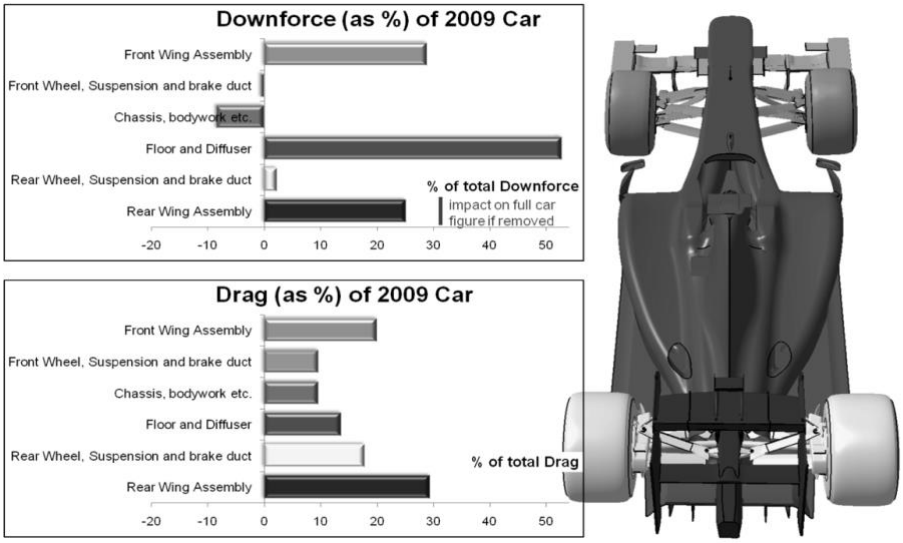


Source: (Toet, 2013)

The downforce and drag breakdown of a F1 car (Figure 1.7) shows that the floor and diffuser together are responsible for generating more than 50% of total car's downforce, while accounting for approximately 13% of the total vehicle's drag. Due to the big surface area and flat shape, the main amount of drag is generated by friction between air flow and the body.

An interesting development in the effort to use the vehicle's body to create aerodynamic benefits occurred when race car engineers in the late 1970s paid attention to the then well-known fact, that the lift, as well as the downforce, of a wing increases with ground proximity (KATZ, 1995). This effect becomes noticeable when the ground clearance is less than 1 chord length of an airfoil, bringing an opportunity to use the race car's body to create downforce. As a result, the undertray of race cars became a smooth surface, mimicking a wing shape (KATZ, 1995). It was the introduction of the ground effect principle in race cars.

Figure 1.8 illustrates the increase in cornering speed as a function of the evolution of aerodynamics over the years. It is possible to observe a significant improvement in the cornering capability from the 70's due to the inverted wings close to the ground. It is noticed that in the 80s there is an even more expressive increase due to the introduction of the underbody capable of generating increased downforce due to the ground effect.

Figure 1.8 – Maximum Relative Cornering Speed vs Decades

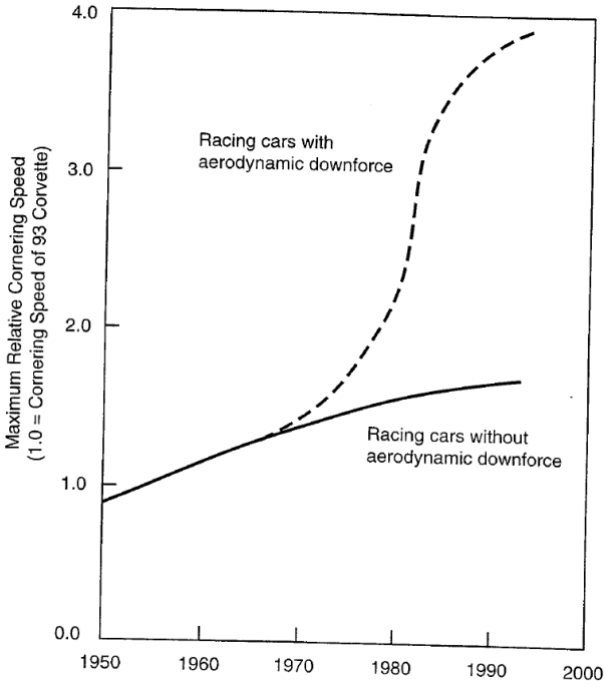


Source: (Katz, 1995)

Figure 1.9 shows the schema of the underbody shape used by Lotus 78 and 79. This illustrates an example of using inverted wings on body shape to increase ground effect. In addition to that, a side skirt (yellow bars at the bottom of the car) was used to prevent the external flow from interfering with flow under the car. Later, in 1983 Formula 1 technical regulation banned this underbody design, as it became dangerous to lose the suction effect and, as result, the downforce at high-speed corners. If the skirts broke, or if the car raised up significantly going over a bump or kerb, the seal would break, causing the air pressure under the car increase to rapidly as the airflow was disturbed and the underbody tunnels lost their effectiveness, causing the cars to effectively lose almost all their downforce instantaneously.

Figure 1.9 – Illustration of an inverted wing underbody

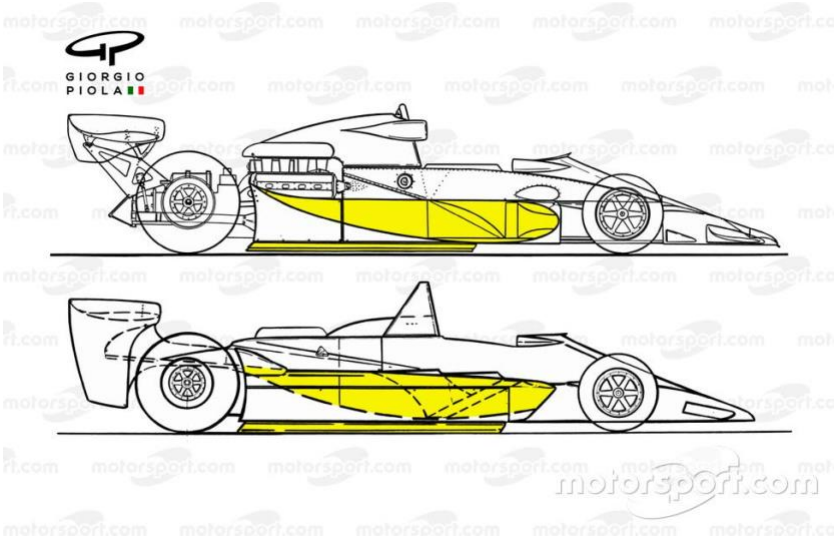


Source: https://motorsport.uol.com.br/f1/news/analise-tecnica-lotus-79-como-um-erro-ajudou-a-criar-um-icone-da-f1/4795093/

Figure 1.10 – Lotus Type 78 known as ‘wing car’


Source: Wikipedia

This configuration of the undertray was unique for that specific situation, but many other solutions involving generating downforce under the vehicle were developed along race car history. The most recent example is the 2022 Formula 1 car. Two of the fundamental changes in the aerodynamics of the 2022 car when compared with the 2021, are the underbody and diffuser. The idea is very similar to the 80’s decade in which the underfloor generates the major amount of

downforce. The floor has two main tunnels, the diffuser is a little further forward, and the exit area is bigger. The biggest difference is that the raised leading edge and its internal vertical turning vanes helps to control the turbulence from another car, making it more efficient and safer.

Figure 1.11 – 2022 Ferrari F1-75 Formula 1 underbody

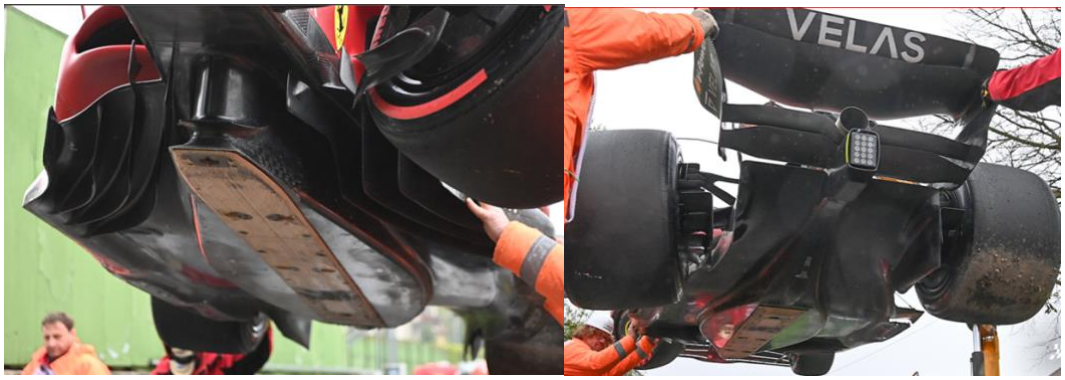


Source: https://twitter.com/autosport/status/1517571759431688192

Figure 1.12 – 2022 Formula 1 baseline model at wind tunnel test

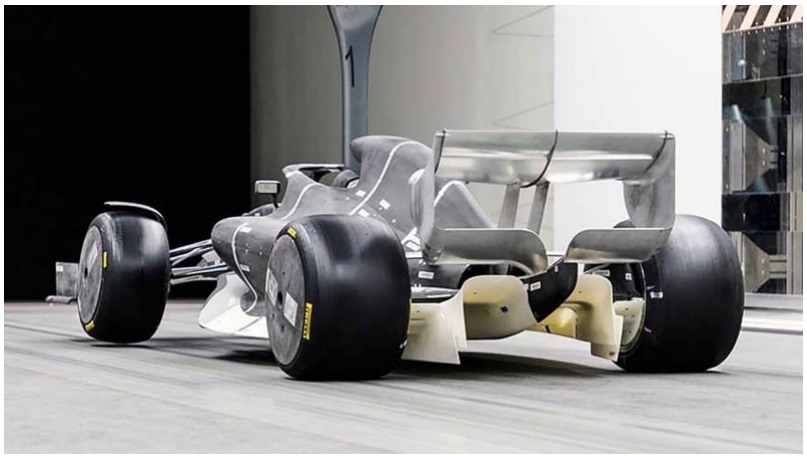

Source: https://www.formula1.com/en/latest/article.first-look-formula-1s-2021-car-in-the-wind-tunnel.6ye3S7Pb8NRX1K7PjTBxtS.html

There are numerous examples like the mentioned above, in which devices were created and adapted to improve the car's performance in lap times. Most of race cars are equipped with a flat underbody and rear air diffuser (Figures 1.13 to 1.15), since the underbody represents a large

surface area of the car very close to the ground, making it an important advantage point for increasing the car's performance.

Figure 1.13 – 2018 Toyota TS050 LMP1 underbody


Source: https://www.tamiyausa.com/shop/124-sports-car-series/toyota-gazoo-racing-ts050/

Figure 1.14 – 2015 Team Penske Chevrolet IndyCar underbody

Source: http://www.espn.com.br/noticia/512252_onda-de-graves-acidentes-e-risco-de-morte-assombram-as-500-milhas

Figure 1.15 – 2017 Porsche 911 RSR rear diffuser


Source: https://www.evo.co.uk/porsche/911/203110/porsche-911-rsr-v-gt3-r-v-gt3-cup-track-only-911s-driven

Production sports car development followed a similar pattern to that of racing vehicles, as their high performance make the automobile drag and downforces of great concern. Ferrari recognized that the entire underbody requires as much attention as the upper surface, and then brought solutions from racing experience to the 1995 Ferrari F355, which was the first model of the brand to equip a flat underbody (KATZ, 1995). The Figure 1.11 shows the smooth underside of the car with venturi tunnels, and despite no official aerodynamic data available, the Italian brand suggest in the 1995 sales brochure, that the vehicle produces about 170 kg of downforce at 290 km/h, this translates to a lift coefficient of about $C_L = -0.24$.

Figure 1.16 – 1994 Ferrari F355 Berlinetta underbody

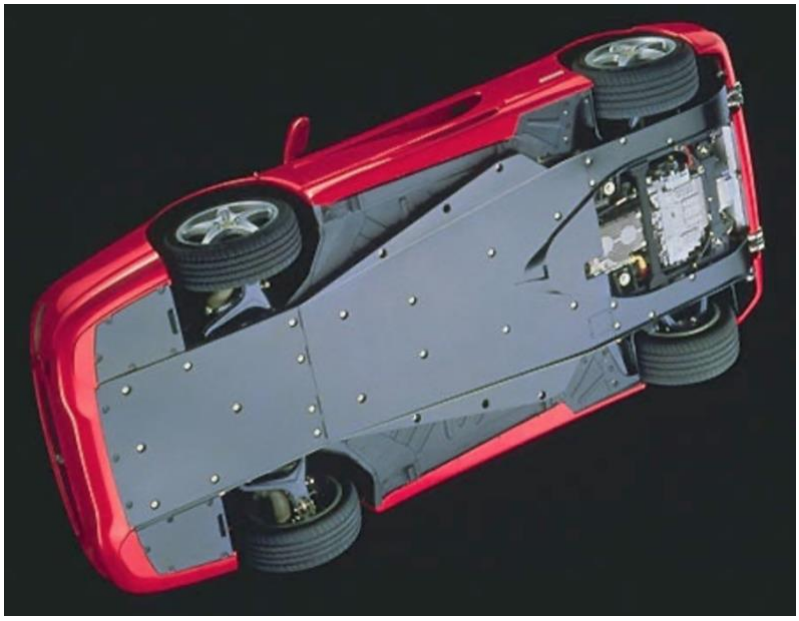

Source: https://www.ferrari.com/en-EN/auto/f355-berlinetta

An interesting point is that, to preserve the smooth styling of the car, Ferrari used no external aerodynamics aids such as large inverted wings (Figure 1.17). Therefore, apart from the small rear spoiler, most of the downforce is generated by the underbody and diffusers.

Figure 1.17 – 1994 Ferrari F355 Berlinetta

Source: https://www.ferrari.com/en-EN/auto/f355-berlinetta

A well-known fact is that motorsport racing is a laboratory for road cars, where automotive industries test their technologies. The aerodynamic field is no different, since a lot of solutions existing in passengers and sports cars came from racing experience. The main idea is to minimize drag forces to reduce fuel consumption, as there are major concerns are CO2 emissions and reduce lift forces to improve stability at highway speeds and thus improve safety. Examples of some aerodynamic devices on road vehicles are shown in Figures 1.18 to 1.21.

Figure 1.18 – 2015 Audi A4 underbody panels


Source: https://www.audiownersclub.com/forums/topic/19384-undercarriageunderbody-images-or-diagrams/

Figure 1.19 – 2017 KTM X-Bow RR

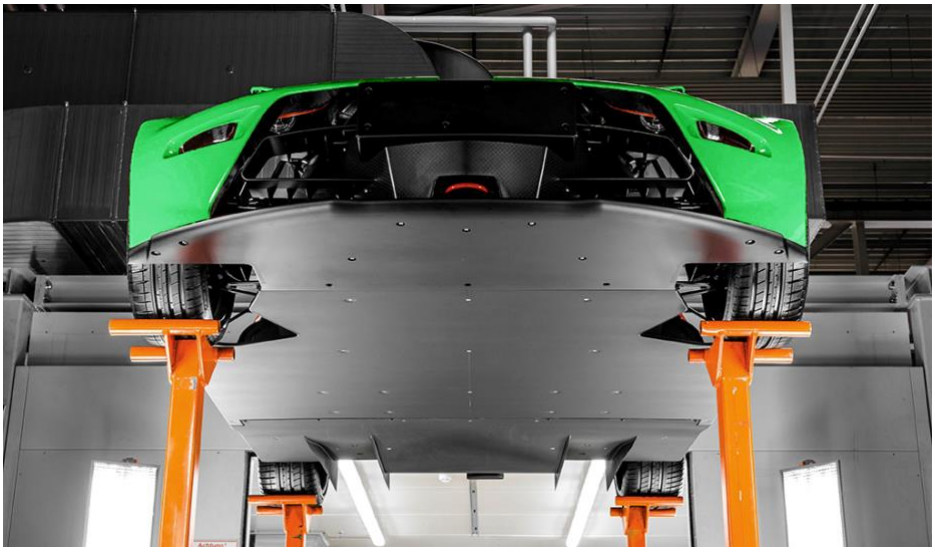

Source: https://www.ktm.com/en-ru/models/x-bow/ktm-x-bow-r.html

Figure 1.20 – 2021 Ford GT rear air diffuser

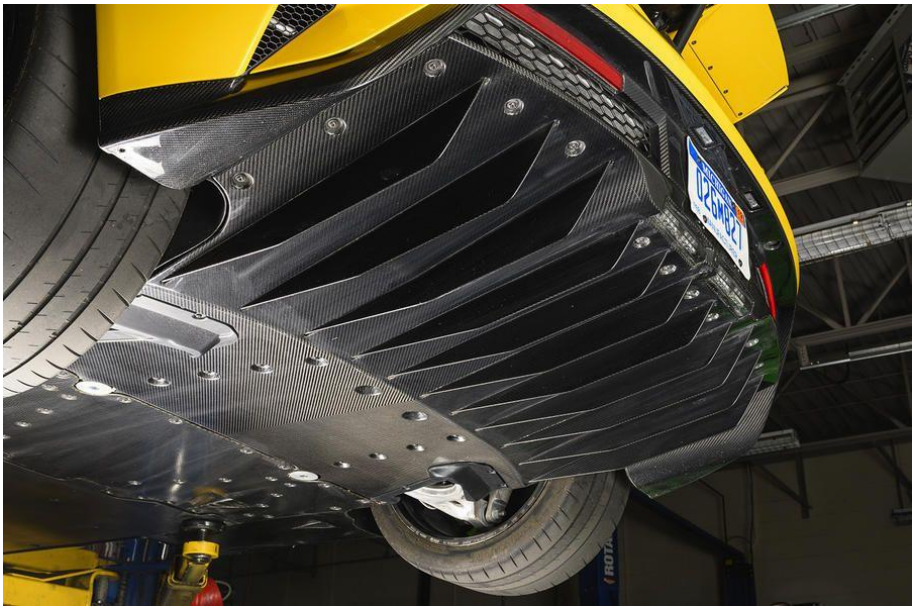

Source: https://www.autoexpress.co.uk/99434/new-ford-gt-2017-review-pictures

The concern with fuel consumption and safety, made the car industries adopt ways to make the cars more efficient, in terms of economy and better handling. A solution is the flat or half-flat underbody, used to reduce flow interaction with exposed mechanical and structural parts under the vehicle. At the back, they add an air diffuser to help to extract the air flow from vehicle's underneath that increases downforce. Most road cars don't have all those devices, since they don't reach high speeds frequently, suffering less influence from aerodynamic forces, and the increase on production and maintenance costs, reflecting their selling prices.

Professional motorsport racing requires big investments, an excellent team of engineers and mechanics, and a professional and experienced racing driver. Hours of CFD simulations, wind tunnel and road test are essential to develop a winning car, making motorsport expensive for most people. There are some motorsport categories that count with lower investment, some of them use road cars tuned to compete. The regulations allow teams to adapt those vehicles by changing suspension setup, powertrain components, weight reduction and add some aerodynamics appendices. Recent examples are the Brazilian Copa HB20 and extinct UK Renault Clio Cup (Figures 1.22 and 1.23).

Figure 1.21 – 2019 Copa HB20


Source: https://racingonline.com.br/copa-hb20/copa-hb20-define-campeoes-de-2019-em-interlagos/

Figure 1.22 – 2019 Renault Clio Cup

Source: https://www.autosport.com/btcc/news/btcc-support-series-renault-uk-clio-cup-to-end-after-2019-season-5282086/5282086/

For those who do not want to compete or can't afford professional racing, there is another alternative, which is the Track Day event. In its literal translation Track Day means day on the track. It is an organized non-competitive sporting event, in which qualified or amateur drivers can drive their own vehicle, cars or motorcycles, on a professional or private racetrack, and the categories are determinates by the event organization. The categories are usually defined by traction, tire compounds and engine specs like naturally aspirated or turbocharged engines. There are no restrictions for modifications and drivers are free to race with their own cars, modified or not.

Figure 1.23 – 2020 TRS Race Team Track Day event


Source: (yocarsbr.com.br)

In this context, this study is aimed to the general description of the external flow around a hatchback vehicle modified to race. A simplified scaled model based on a 1997 Honda Civic VTi road car (Figure 1.25) modified to race on track day events was used in this work. The main modifications were a new set of springs and dampers, air intake, exhaust system, programmable fuel injection, valvetrain, fuel injectors, and weight reduction.

Figure 1.24 – 1997 Honda Civic VTi


Source: (Own Autor)

This study is intended to analyze experimentally the flow over the vehicle and propose aerodynamics improvements by designing a smooth underbody with a rear air diffuser. The main goal is to analyze the car’s undertray effect in relation to drag forces, and the advantages and disadvantages on a vehicle's performance. The experiments are performed with a 1:10 scale version in a subsonic wind-tunnel.

The second chapter is dedicated to the description of the fundamentals of automotive aerodynamics and the rear air diffuser, summarizing the literature's conclusions. A discussion of all the academic work on the matter is presented in the third chapter. Fourth chapter is dedicated to present the definition of the car generic model and experimental methods. Chapter five summarizes the results and discussions concerning wind tunnel tests and the rear air diffuser geometric variation effects.

# CHAPTER II

## Phenomenology

This chapter is dedicated to the description of the fundamentals of automotive aerodynamic analysis and to summarize previous conclusions on the flow present around a hatchback vehicle.

## 2.1. Fundamentals of Fluid Mechanics

For didactic purposes, the analyzed surfaces can be assumed a generic body shape insert on flow with constant velocity and viscosity. For the vast region of the flow field away from the body, the velocity gradients are relatively small, and friction can be disregarded. However, for the thin region of the flow close to the surface the velocity gradients are large, and friction starts to have a great influence on the flow; this thin viscous region adjacent to the body is called the boundary layer. For most aerodynamic problems, the boundary layer is very thin compared with the rest of the flow (ANDERSON, 2011).

Figure 2.1 – Velocity profile through a boundary layer

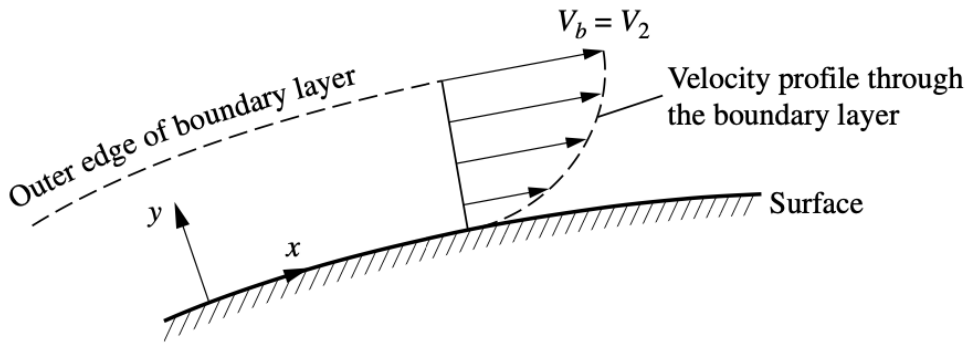


Source: (Anderson, 2011)

Due to friction, the air molecules immediately adjacent to the body surface have zero velocity relative to the surface. This is called the no-slip condition, and it is the cause of the velocity gradients within the boundary layer. Figure 2.1 illustrates the velocity profile through the boundary layer. The velocity starts at zero at the surface and increases continuously to its value of $V_b$ at the outer edge, where $V_b$ is the freestream velocity.

Figure 2.2 – Boundary layer close a vehicles surface

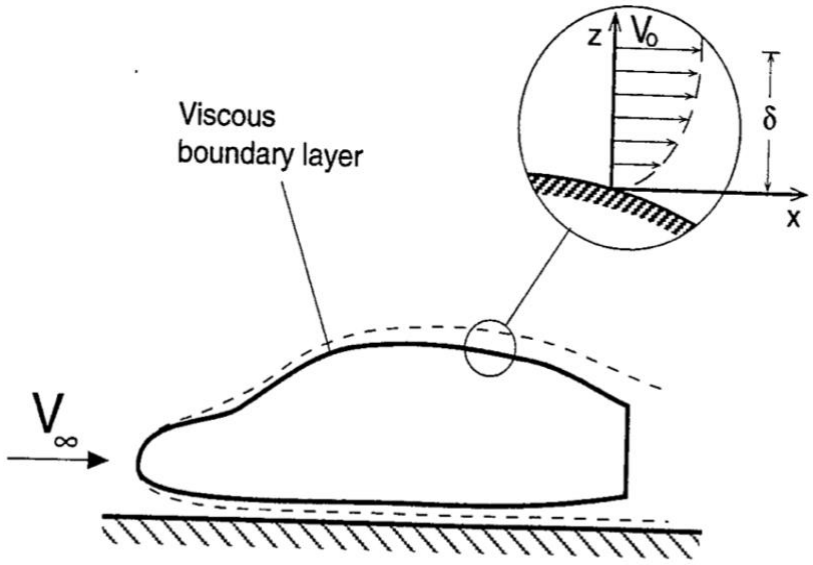


Source: (Katz, 1995)

The boundary layer can be laminar or turbulent. Usually begins as laminar and gradually becomes turbulent with the increase in local distance or flow velocity. The region where this change occurs is called the region of transition. The turbulent boundary layer is thicker, and the momentum loss is larger, which implies more friction, thus more drag.

Figure 2.3 – Variation of the boundary layer thickness along a flat plate

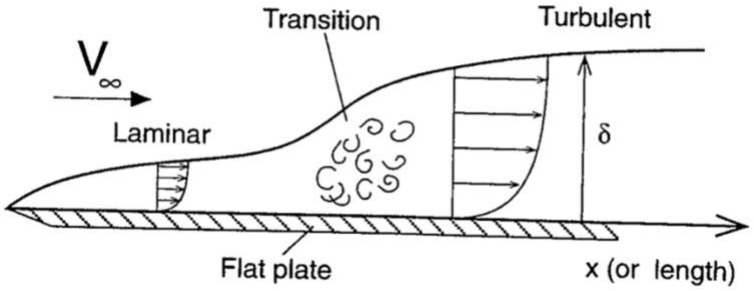


Source: (Katz, 1995)

At determinate local distance, pressure starts to increase in flow direction, and if the adverse pressure gradient is too high it will slow down the boundary layer flow too much, especially near the wall, pushing the boundary layer backwards causing reversed flow (recirculation region). This condition causes flow separation, dramatically changing the pressure distribution over the surface resulting in a large increase in drag called pressure drag.

Figure 2.4 – Separation of the boundary layer

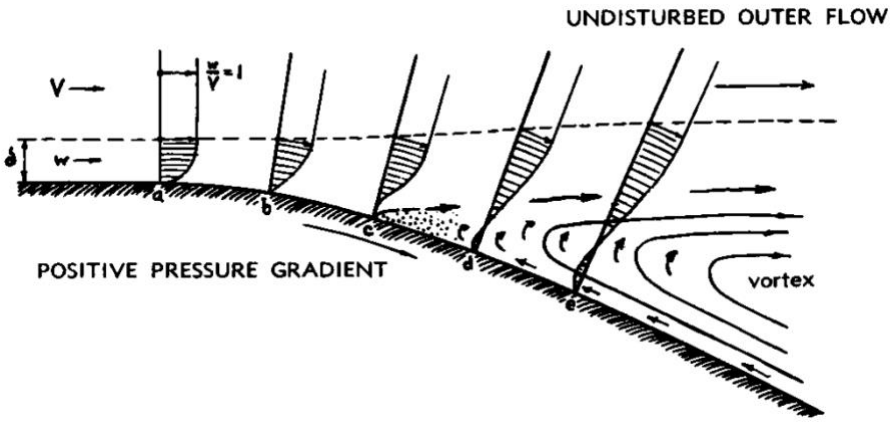


Source: (Hoerner, 1965)

For every aerodynamic problem, the viscous effects must be considered. Fluid viscosity influences directly in the dynamic of boundary layer, flow detachments and turbulence structures

formation. The quantification of those effects is accounted by the Reynolds number, a non-dimensional that represents the ratio between inertial and viscous forces created in the air and is defined by the equation (2.1):

$$Re = \frac{\rho U_0 L_{ref}}{\mu} \tag{2.1}$$

where $L_{ref}$ is the reference dimension and $\mu$ is the fluid dynamic viscosity (in automotive aerodynamics, the reference dimension is vehicle's length). The Reynolds number can be used for scaling effects in aerodynamics analyses, for example, the Reynolds number for a quarter-scale car model for certain flow velocity is still ¼ of the full-size car $Re$ number and quantifies the product of speed times size, which is very helpful in experimental tests.

Every problem in fluid mechanics involve speed and pressure variations, and this rules the flow behavior through or inside a body. The Venturi tube is the example of the relation between the flow velocity, transversal section area and static pressure. It consists of a converging inlet and diverging outlet with a narrowed center section as shown in the Figure 2.5.

Figure 2.5 – Flow through a Venturi tube

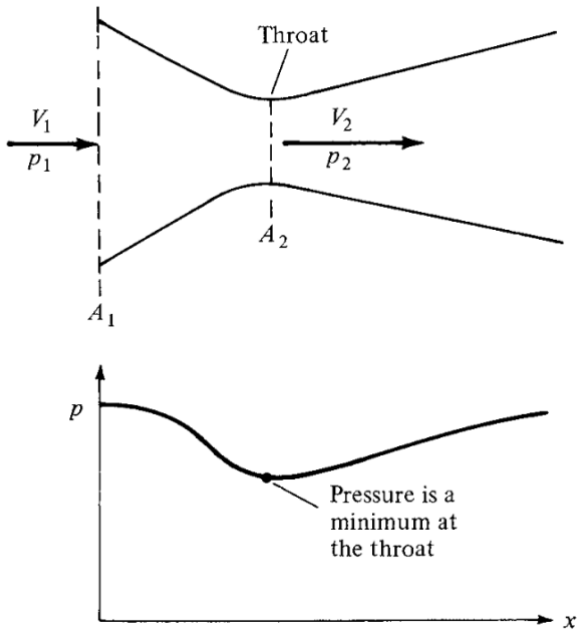


Source: (Anderson, 2011)

The flow rate trough the tube can be expressed by the equation (2.2):

$$\dot{V} = VA \tag{2.2}$$

where $V$ is the flow velocity and $A$ is the transversal section area.

For an incompressible and subsonic flow according to the principle of conservation of mass, the mass of a fluid is constant during its motion (TOTH; BOBOK, 2017), so the same amount of mass on the inlet ($A_1$) must be equals to the amount on the throat ($A_2$), that is, the flow rate in the throat is equal to the flow rate in the pipeline.

$$V_1 A_1 = V_2 A_2 \tag{2.3}$$

Since the flow rate must be constant and the inlet and outlet areas are different the flow velocity needs to change to guarantee the conservation of mass. By the equation (2.3) it can be assumed that for a small area the flow speed must be higher.

Applying the Bernoulli's equation to the venturi tube it is possible to compare the pressure and velocity between two points in the flow. The equation can be expressed as shown below:

$$\frac{p_1}{\rho} + \frac{V_1^2}{2} = \frac{p_2}{\rho} + \frac{V_2^2}{2} \tag{2.4}$$

where $\rho$ is the flow specific mass, $p_1$ and $p_2$ are the static pressure relative to the inlet and throat area respectively.

According to the Eq. (2.4), when the velocity increases in a convergent duct, the pressure decreases; conversely, when the velocity decreases in a divergent duct, the pressure increases (ANDERSON, 2011). The flow enters the duct with velocity $V_1$ and pressure $p_1$. The velocity increases in the convergent portion of the duct, reaching a maximum value $V_2$ at the minimum area of the duct. Also, in the convergent section, the pressure decreases and reaches a minimum value $p_2$, as sketched in Figure 2.5. In the divergent section downstream of the throat, the velocity decreases, and the pressure increases.

## 2.2. Fundamentals of Automotive Aerodynamics

The study of automotive aerodynamics involves both internal and external flow. The movement of air around a moving vehicle affects all its components in one way or another. The intake and engine cooling flow, internal ventilation, acoustic noise, brake cooling and general external flow, which influence the forces and moments acting on the vehicle, affects, directly or indirectly, on vehicle's stability and consumption.

To evaluate aerodynamic loads, it is necessary to know the surface pressure distribution. Laminar and turbulent boundary layer flows depend strongly on the pressure distribution which is imposed by the external flow. Surface pressure distribution can be determined on wind tunnel experiments by measuring static pressure with sensors at specific points of the car, and then integrating those pressures over the vehicle body. For these situations, a non-dimensional pressure coefficient, $C_P$, is used, representing the difference between the static pressure and the freestream pressure. To make it independent of speed, it is divided by dynamic pressure:

$$C_P = \frac{P - P_0}{\frac{1}{2}\rho U_0^2} \tag{2.5}$$

where $P$ is local pressure and $P_0$ is pressure on the freestream. For incompressible flow, $C_P > 0$ indicates that flow is slower than $U_0$ and $C_P < 0$ means that local flow is faster than freestream and $C_P = 1$ represents a stagnation point.

Figure 2.6 shows the pressure distribution over a general automobile shape. At the front, there is a stagnation point, where $C_P = 1$. The flow accelerates over the hood and $C_P$ becomes negative. As air flow reaches the windshield, it slows down and increases the pressure. At the start of the roof, flow reaccelerates and reaches the minimum pressure value. Across the back side of the vehicle the whole sequence is reversed, but thus not return to $C_P = 1$, because the flow separates behind the car. At the lower side of the car, the stagnation point remains the same, but pressure decreases due to the ground proximity that accelerates the flow creating a venturi effect. At the back, pressure returns to rise but does not equate to 1. As a result of flow detachment, the pressure in the back is lower than at the front, which creates the called pressure drag which will be explained later in this chapter.

Figure 2.6 – Pressure distribution over a baseline vehicle

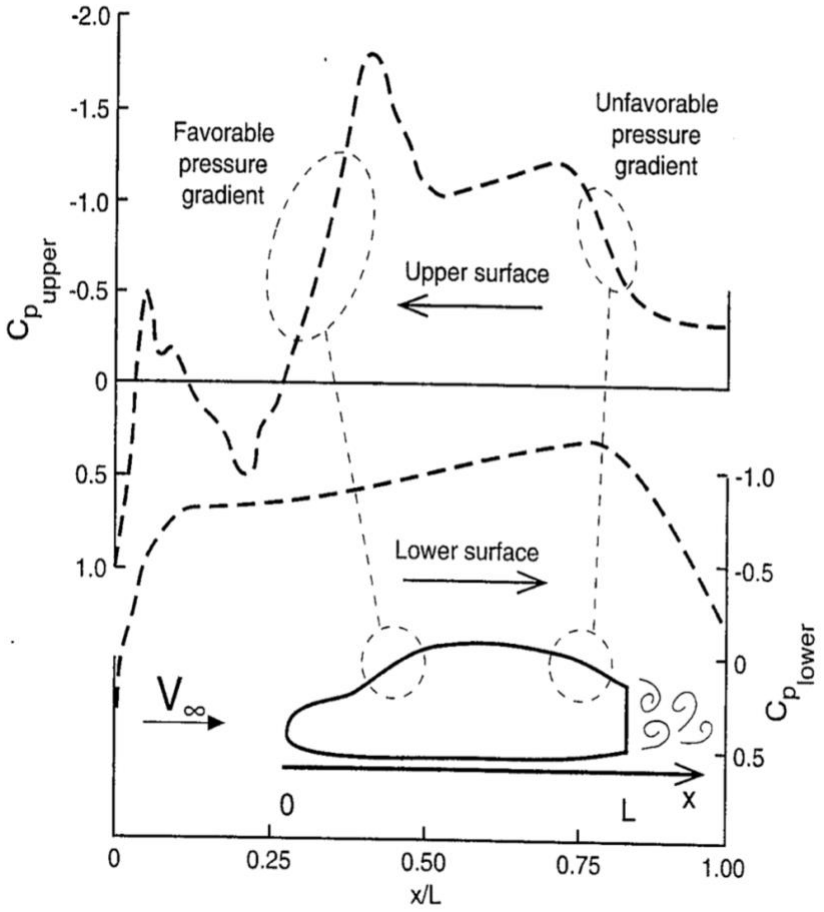


Source: (Katz, 1995)

There are two main categories of aerodynamics forces acting on a vehicle. The first is pressure, which acts basic in two directions, normal to the car's surface and is responsible for the vehicle's lift, and parallel to the body's surface which contributes to drag. The second is the shear force (e.g., friction), which acts parallel to the body's surface and contributes only to drag. The resultant force that is acting over the vehicle, can be divided basically in three components as shown in the Figure 2.7.

Figure 2.7 – Coordinate system used to represent the aerodynamic loads over a vehicle

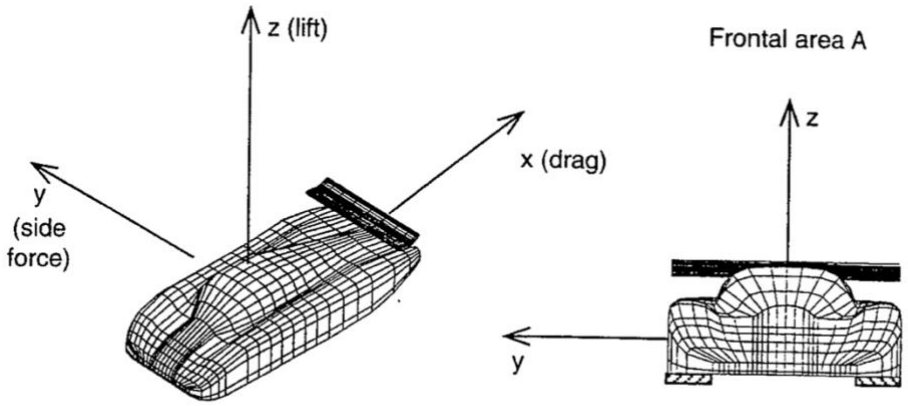


Source: (Katz, 1995)

Lift is the vertical component that acts on the vehicle's body, perpendicular to the velocity vector, responsible for reducing adherence of the tires. Generated by the difference in pressure distribution on the upper and lower surface of the car, and due to the air reaction force, according to the third law of Newton, since the vehicle body changes the flow direction through viscous forces (Coanda Effect), a reaction force is generated by the air in the opposite direction, in the vehicle body. Lift is measured using the lift coefficient $C_L$ defined by the following equation:

$$C_L = \frac{Lift}{\frac{1}{2}\rho U_0^2 A_{ref}} \tag{2.6}$$

A common way to increase lift without changing the geometry characteristics of the body, is to change its incidence angle (angle of attack, a). It is the angle between the central line of the body and the velocity vector. At low-to-moderate angles of attack, $C_L$ varies linearly with a. In this region, the flow moves smoothly over the airfoil and is attached over most of the surface, as shown in the streamline picture at the left of Figure 2.8. However, as a becomes large, the flow tends to separate from the top surface of the airfoil, creating a large wake behind the airfoil. The consequence of this separated flow is a decrease in lift and a large increase in drag; this condition is called airfoil stall (ANDERSON, 2011). The figure below shows the variation of lift by changing the angle of attack for a generical airfoil, but this behavior is similar on inverted wing in racecars and inclined surfaces like rear windshield and rear air diffusers.

Figure 2.8 – Lift coefficient variation with angle of attack for an airfoil

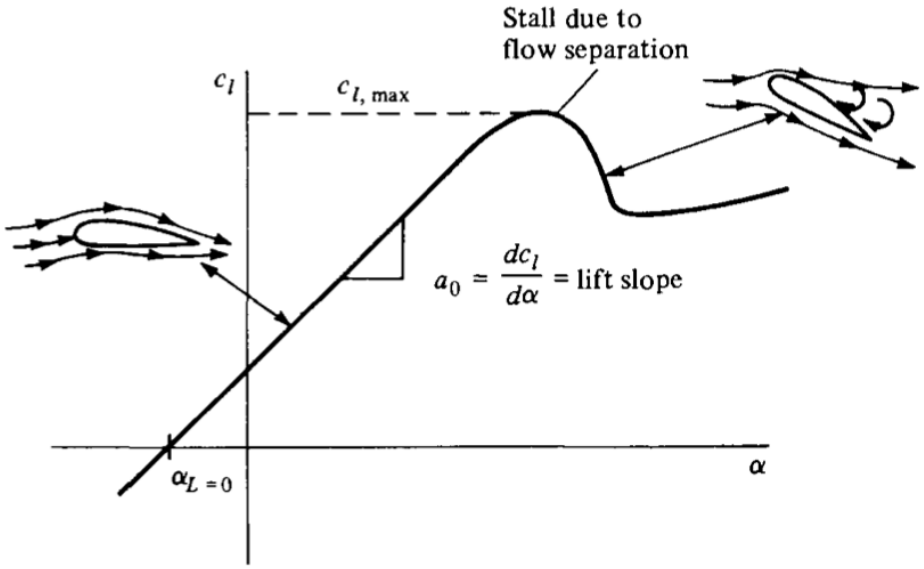


Source: (Anderson, 2011)

Drag is the aerodynamic force component along the flow direction, opposite the body's motion. It is generated by the pressure difference between the front and the back of the vehicle (pressure drag), by friction between the flow and the car's body (friction drag) and due to Lift (induced drag).

Pressure drag is caused by pressure differences between the body front and hear sides, being increased by the detachment of the boundary layer, when flow separation occurs causes recirculation and low-pressure zones in the back of the vehicle. Friction drag is caused by the fluid viscosity and surface rugosity as a flow resistance is created by this interaction, generating shear stresses on the surface of the body. The induced drag is the drag force produced by a lifting surface because of the lift (SMITH, 1978). Due to the difference in pressure between the lower side of the body and the upper side, a pair of tridimensional vortices are formed (Figure 2.9).

Figure 2.9 – Wing-tips vortices effect

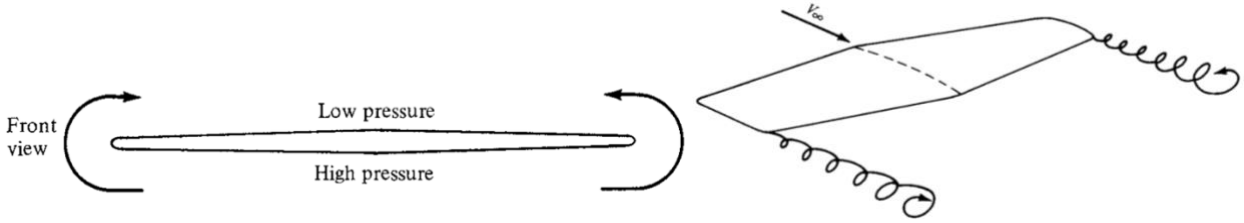


Source: (Anderson, 2011)

These wing-tip vortices downstream of the wing induce a small downward component of air velocity close to the wing, that is called downwash, denoted by $w$ (Figure 2.10). This downward component combines with the freestream velocity to produce a local relative wind, which is inclined in relation with flow direction. This difference is called induced angle of attack ($\alpha_i$). Since local lift force is perpendicular to local relative wind direction (in the Figure 2.10 is expressed by $F = L/cos\ \alpha_i$), a horizontal component is formed which is the induced drag ($D_i$).

Figure 2.10 – Lift-Induced drag

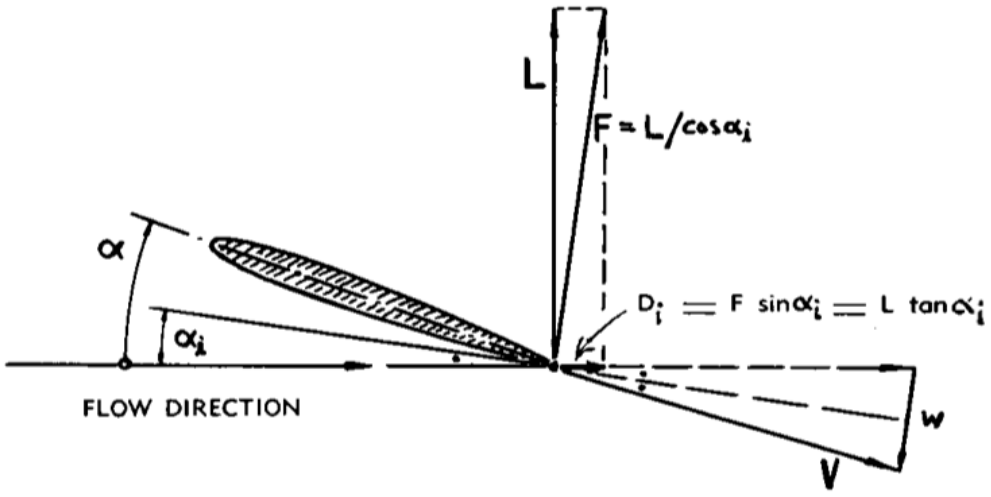


Source: (Hoerner, 1965)

Drag is measured by the drag coefficient $C_D$ shown in the Eq. (2.7).

$$\mathrm{C_D} = \frac{\mathrm{Drag}}{\frac{1}{2}\rho \mathrm{U_0^2 A_{ref}}} \tag{2.7}$$

where, for both cases, ρ is the air density, $U_0$ is the freestream velocity and $A$ is a reference area (for automotive applications the frontal area is common use as reference area). These are two non-dimensional coefficients used to quantify the two forces to compare forces virtually in any condition (flow velocity and density) and geometry.

The side force is very important when strong crosswinds are involved. In general cases the two main forces considered are lift and drag. However, for race cars, when cornering, there will appear a side component acting in the car's center of pressure, which influences directly on the vehicle's stability.

## 2.3. Hatchback Vehicle Aerodynamics

Flow around a car is very complex and asymmetric, with numerous regions of flow detachment and vortex generation. The presence of side mirrors, engine cooling systems, air intake, wheels and mechanical parts at the car's underbody generates undesirable disturbances, by the interaction of these structures with the air flow, which enhance drag. This flow is strongly governed by separation and the effect of viscosity is no longer confined to comparatively small zones close to the surface of the body (boundary layer). Furthermore, it is not possible to distinguish several independent flow fields, that is, flow fields around a car body must be treated as a whole (HUCHO, 1987).

Figure 2.11 – Flow around a vehicle

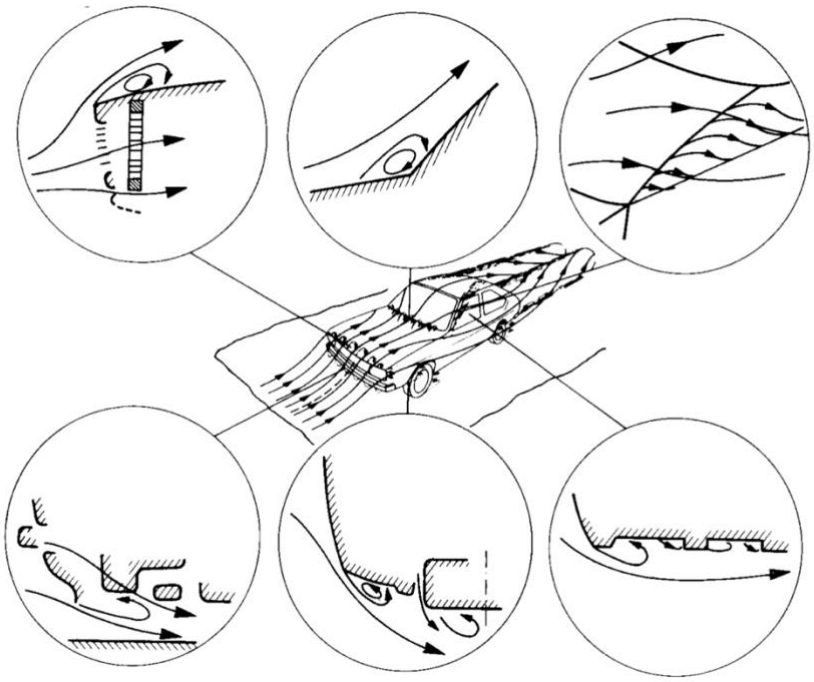

Source: (Hucho, 1987)

The shape of the car is directly associated with the magnitude of the forces generated. Some regions have more influence on the flow field and need to be better understood for the purpose of this work. The front, underbody and rear end are those regions that needed more attention.

First, the shape of the vehicle front will determine where the stagnation point is located. This point determines which portion of the flow passes over the vehicle and how much air flows between the bottom of the car and the road. Generally, a low stagnation point is favorable for low drag, like shown in the Figure 2.12. The front also determines the formation or not of recirculation bubbles over the hood.

Figure 2.12 – Stagnation point effect on vehicle's drag

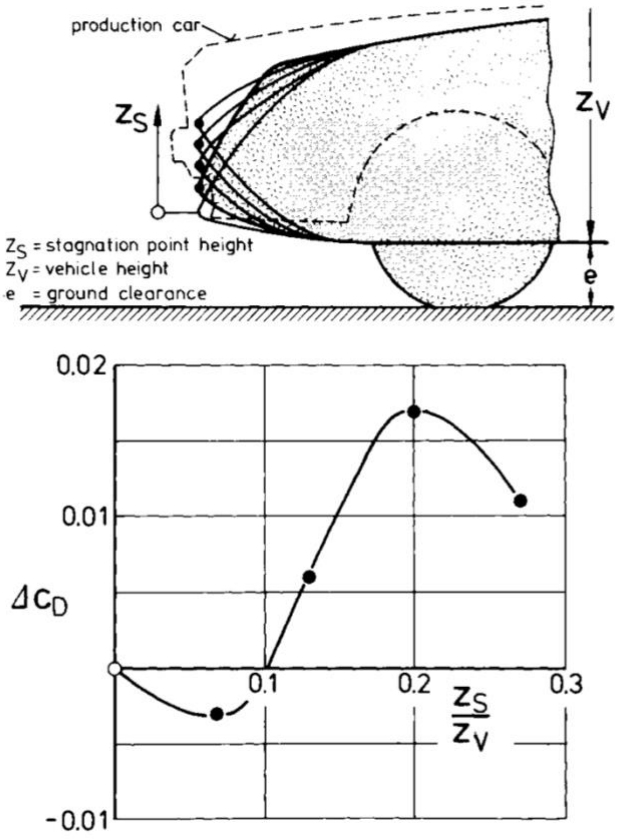


Source: (Hucho, 1987)

Rear end, on the other hand, define where the flow detachment will occur. There are two most common ways for flow detachment. First, when the boundary layer becomes thicker and lose momentum to continue attach to the body due to viscous effects. Second, in most cases of hatchback cars, when the rear ends abruptly so the flow is incapable to follow the curvature because of inertial effects. Due to these two phenomena, a low-pressure zone is generated in the back of the car. Rear end also determines the flow direction when it leaves the car, which can increase or decrease rear lift force.

For a hatchback vehicle there are two different forms of separation that occur at the rear end: the quasi-two-dimensional shape in the form of a wake and the three-dimensional as a longitudinal vortex pair. The geometry of the rear end will determine how and where those separation occurs. In principle there are three different vortex systems as shown on Figure 2.13:

Vortex C, emanating at the C-pillars; vortex A and vortex B are generated in the quasi-manner at the edges A and B respectively. They are of the viscous type and their vorticity is low. Generally, Vortex A is anti-clockwise and vortex B is clockwise.

Figure 2.13 – Vortex system for a hatchback configuration

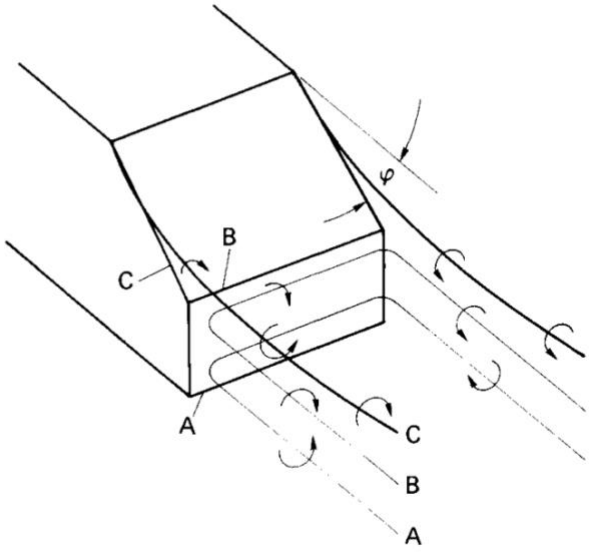


Source: (Hucho, 1987)

Figure 2.14 – Flow pattern for different types of rear end configurations

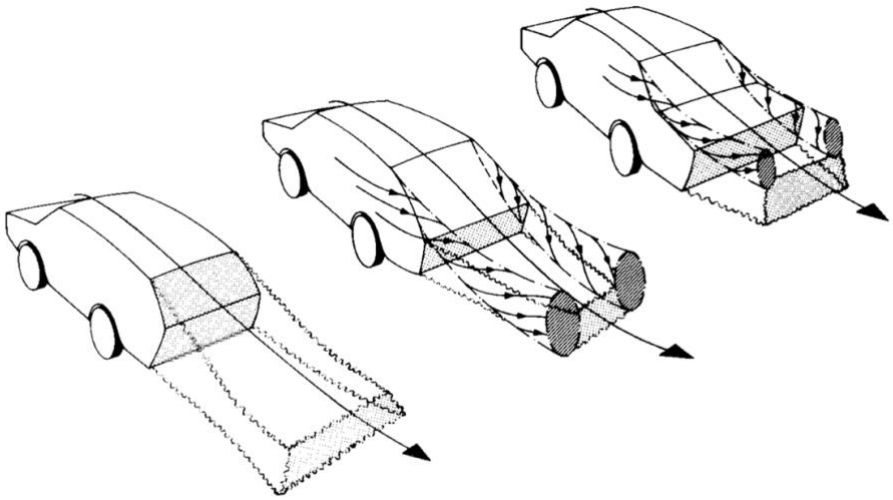

Source: (Hucho, 1987)

At the higher angle of inclination of the rear end, $\theta = 15°$ (Figure 2.15-c), the C-pillar vortex pair has developed. It induces a downwash, which forces the external flow downward in the area of the rear end and keeps it attached. At $\theta = 30°$ the C-pillar vortices are highly pronounced, the drag reaches its maximum value, and vortices are so strong that flow remains attached over almost all of the sloping back; however, the flow separates in front of the rear edge (HUCHO, 1987). At angles of $\theta > 30°$ the flow separates at the upper edge of the roof, the vortex structure breaks down and the drag and lift contribution of the slanted surface is much smaller (region II – Fully separated case) as shown in Figure 2.15. According to (KATZ, 1995), for hatchback vehicles the rear window inclination angle should be less than $\theta = 25°$ or more than $\theta = 35°$.

Figure 2.15 – The influence of the rear end slant angle on lift and drag forces

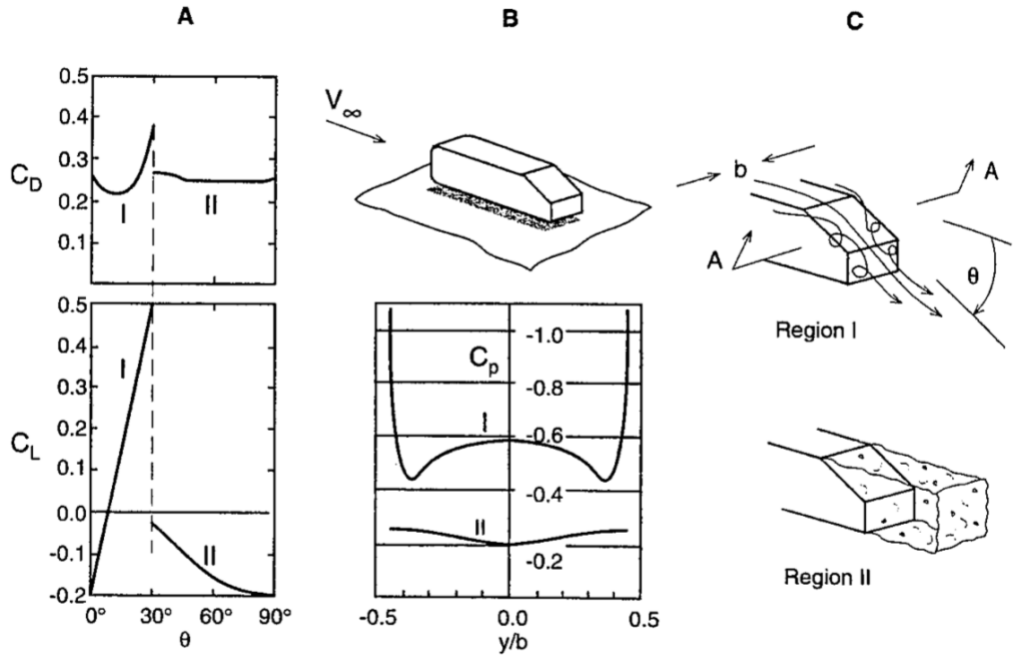


Source: (Katz, 1995)

Is shown in Figure 2.16 the detachment points between two different layouts, and the size of turbulent zones created. Although the flow in these separation bubbles is unsteady, its time average identifies a macrostructure in which the separation bubbles contain circulation, and the axes of the vortices run primarily perpendicular to the undisturbed flow and parallel to the line of separation (HUCHO, 1987).

Figure 2.16 – Analyses of detachment point between two different rear end

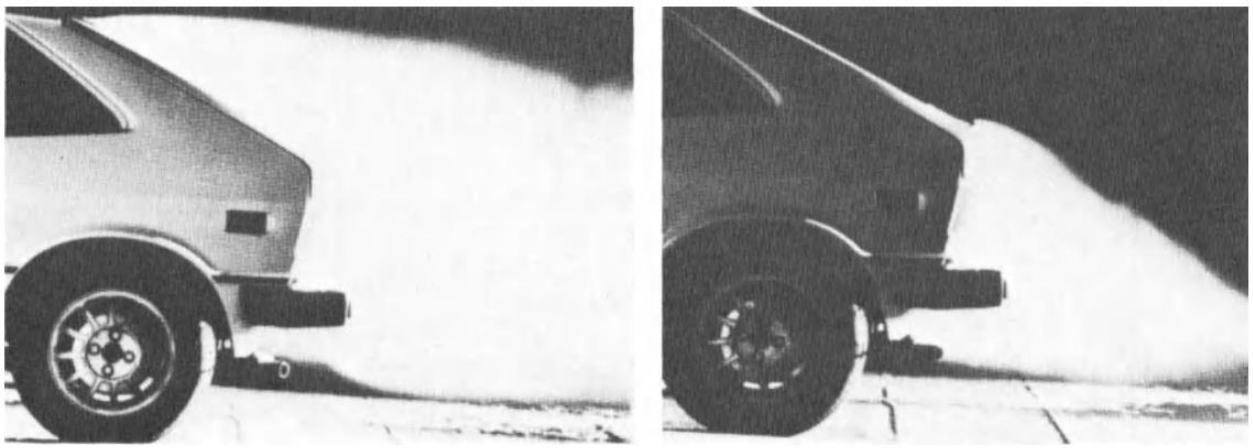

Source: (Hucho, 1987)

On hatchback configuration, the wake is bigger when compared with sedan models, because of the anticipation of flow detachment that occurs in general at the top of the rear window, due C pillar inclination. According to Yakkundi; Mantha; Sunnapwar (2017), and Bhagirathsinh; Rathod; Arvind; I Joshi (2012) the drag forces on hatchback vehicles are higher when compared with sedans due the influence of these vortex wake, as indicated on Figures 2.17 to Figure 2.19.

Figure 2.17 – Drag force for a hatchback car with increase of speed

**Table – II Force and drag values as computed from fluent force reports for HATCHBACK**

| Velocity m/s | Pressure force ( N) | Pressure drag($D_P$) | Viscous force (N) | Viscous drag ($D_F$) | Total force ( N) | Total drag ( D= $D_P$ + $D_F$) |
|---|---|---|---|---|---|---|
| 27.00 | 1428220.0 | 0.62 | 930298.0 | 0.41 | 2358518.0 | 1.03 |
| 36.00 | 1084201.0 | 0.47 | 1297746.6 | 0.56 | 2381947.4 | 1.03 |
| 45.00 | 578075.0 | 0.25 | 125407,5 | 0.55 | 677332.5 | 0.80 |
| 60.00 | 1444793.1 | 0.63 | 1770340.5 | 0.77 | 3215133.6 | 1.40 |

Source: (Yakkundi, Mantha and Sunnapwar, 2017).

Figure 2.18 – Drag force for a sedan car with increase of speed

| Table – IV Force and drag values as computed from fluent force reports for SEDAN. | | | | | | |
|---|---|---|---|---|---|---|
| Velocity m/s | Pressure force ( N) | Pressure drag($D_P$) | Viscous force (N) | Viscous drag ($D_F$) | Total force ( N) | Total drag ( D= $D_P + D_F$) |
| 27.00 | 561505.60 | 0.18 | 619451.45 | 0.20 | 1180957.10 | 0.38 |
| 36.00 | 613300.00 | 0.20 | 638065.80 | 0.21 | 1251365.90 | 0.41 |
| 45.00 | 629972.00 | 0.21 | 660149.00 | 0.22 | 1290121.40 | 0.42 |
| 60.00 | 614830.40 | 0.20 | 728290.61 | 0.24 | 1343121.00 | 0.44 |

Source: (Yakkundi, Mantha and Sunnapwar, 2017)

Figure 2.19 – Comparison of drag forces between a sedan and hatch vehicle

| MODEL | SPEED(KMPH) | DRAG FORCE(N) |
|---|---|---|
| Sedan car | 60 | 0.612 |
| | 75 | 0.718 |
| | 90 | 0.934 |
| | 105 | 1.122 |
| Hatch back car | 60 | 0.684 |
| | 75 | 0.964 |
| | 90 | 1.457 |
| | 105 | 1.783 |

Source: (Bhagirathsinh, Rathod, Arvind and I Joshi, 2012)

In the case of the underbody, the flow is more complex, chaotic, and difficult to predict due to its interaction with the mechanical parts under the vehicle. The many regions of vortex generation, hot air from the engine cooling system, dirty air flow from the wheels and external side flow interactions creates a significant amount of drag. The reduction in drag by smoothing the underbody is significant according to Buchheim et al. (Figure 2.20). in the development of the Audi 100. Complete paneling of the underside provides a reduction of drag amounting to $\Delta C_D = -0.045$. When at the rear of the vehicle is installed an air diffuser, it is possible to achieve a value of $\Delta C_D = -0.070$ (HUCHO, 1987).

Figure 2.20 – Drag reduction by smoothing the underbody for the Audi 100

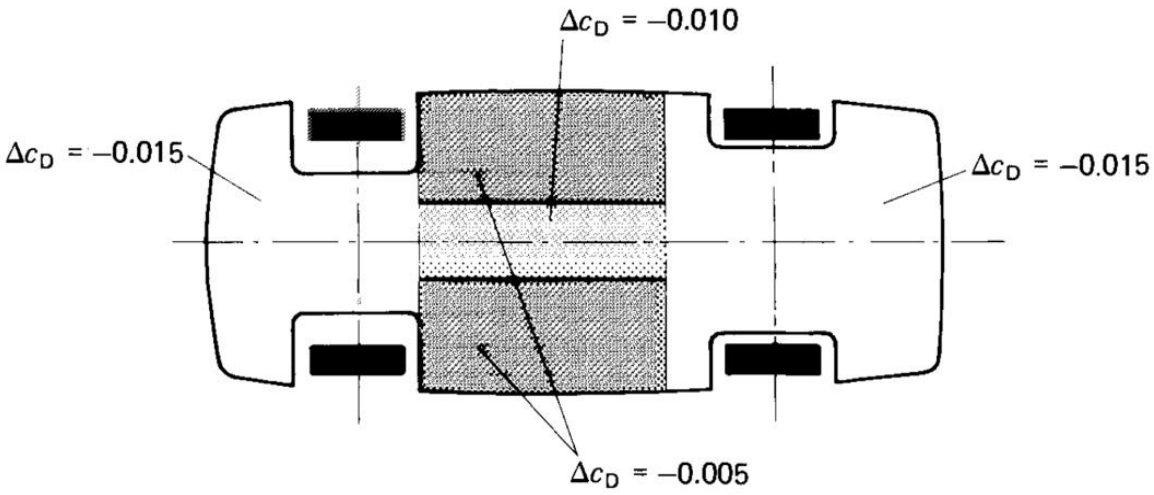


Source: (Hucho, 1987)

## 2.4. Rear Air Diffuser

The air diffuser is an upwardly ramped surface at the rear of vehicle's underbody with or without lengthwise end plates extending from the start to the end of the elevation, and its function is to bring the low pressure of the air underneath the cars back to the atmospheric pressure using an appropriate geometry in order to have minimum induced turbulences (KATZ, 2006).

As the vehicle travels along the road, the air flows at the same traveling speed of the vehicle. The airflow that travels underneath the vehicle, along its underbody surface exits into the atmosphere by flowing through the underbody diffuser. As the airflow travels through the diffuser channel(s) the resultant aerodynamic effect generated acts on the car's performance, due to the suction created by the diffuser (EHIRIM, 2018). The work principle of the diffusers can be explained by the venturi effects.

Figure 2.21 – Pressure distribution between Ahmed model with air diffuser and venturi tube

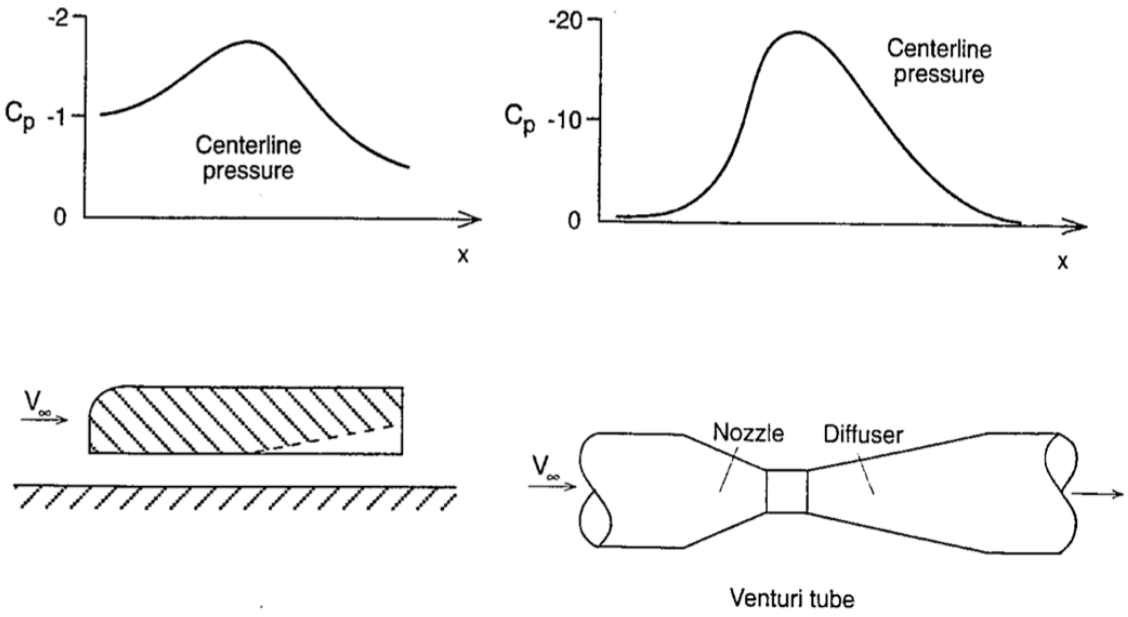


Source: (Katz, 1995)

As the underbody airflow travels underneath the car, the start of the elevating ramp surface of the diffuser further accelerates and lowers the pressure of the airflow traveling through the diverging area of the diffuser. The diverging expansion of the diffuser area then acts as a region where the airflow expands, thereby reducing its speed and increasing its pressure before it exits the diffuser into the atmosphere, which helps to decrease drag force by the pressure recovery at the rear end. Through this interaction between the vehicle's diffuser and its underbody airflow, the suction effect (low pressure) created by the diffuser translates into downforce acting on the vehicle (EHIRIM, 2018).

Figure 2.22 – Schematic of the centerline pressure behavior along the flat underbody and diffuser sections of a bluff body

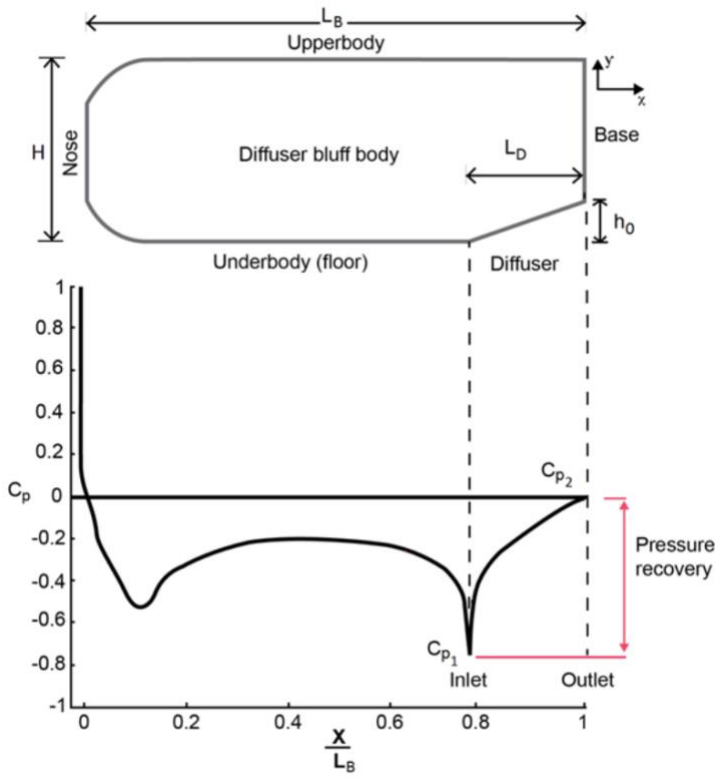


Source: (Knowles; Saddington, 2018)

Figure 2.22 illustrates a typical pressure distribution of the Ahmed body, along the underbody floor with the suction peak at the diffuser inlet and the pressure recovery along the diffuser length. The performance of a ground-effect diffuser is quantified by the static pressure on its ramp surface represented by the pressure coefficient:

$$C_P = \frac{P - P_0}{0.5\rho U_\infty^2} \tag{2.8}$$

The pressure distribution on the entire surface of the diffuser creates a net downforce and net drag force on the body (Eq. 2.9 and 2.10). The surface pressure distribution can be integrated over the body surface to provide an estimate of the pressure forces acting, if it is assumed that centerline pressures sufficiently represent average pressures across the bluff body's width $W$ at all cross sections.

$$L = -W\left[\left[\int_0^{L_B-L_D} p_f(x)dx + \int_{L_B-L_D}^{L_B} p_d(x)dx\right] - \int_0^{L_B} p_u(x)dx\right] \quad (2.9)$$

$$D = W\left[\int_0^{H} p_n(y)dy - \left[\int_0^{h_0} p_d(y)dy + \int_{h_0}^{H} p_b(y)dy\right]\right] \quad (2.10)$$

where $h_0$ is the height difference between the top of the diffuser exit and the bluff body floor plane, $L_B$ and $L_D$ are represent the lengths of the overall bluff body and diffuser respectively, $H$ is the bluffy body height, and the subscripts $f,\ d,\ u,\ n,\ b$ denote static pressures for the flat underbody floor, diffuser, upper body, nose, and base of the bluff body respectively.

Cooper et al. (1998, 2000) derived the performance of a ground-effect diffuser in an inviscid and incompressible flow. To investigate underbody flow, a simple bluff body design was tested with varying underbody geometry and ride heights. The expression below represents the streamwise-distance-averaged pressure coefficient $\bar{\bar{C}}_{Pi}$, over a streamwise length $x_i$:

$$\bar{\bar{C}}_{Pi} = \frac{1}{x_i}\int_0^{x_i} C_P\,(x)dx \quad (2.11)$$

With the underbody composed by the floor and diffuser sections, the specific value of the mean effective pressure coefficient along the streamwise length of the whole underbody $\bar{\bar{C}}_{Pl}$ was resolved into two pressure coefficient components: the mean effective pressure coefficients of the diffuser $\bar{\bar{C}}_{Pd}$, and underbody (floor) upstream of the diffuser $\bar{\bar{C}}_{Pf}$:

$$\bar{\bar{C}}_{Pl} = \left(1 - \frac{L_D}{L_B}\right)\bar{\bar{C}}_{Pf} + \left(\frac{L_D}{L_B}\right)\bar{\bar{C}}_{Pd} \quad (2.12)$$

Then the overall pressure-recovery coefficient of the diffuser $\bar{C}_P$ was formulated:

$$\bar{C}_P = \frac{(C_{P2} - C_{P1})}{(1 - C_{P1})} \quad (2.13)$$

where $C_{P1}$ and $C_{P2}$ representing the pressure coefficients at the diffuser inlet and outlet respectively. Cooper et al. (2000) developed in detail the mathematical derivation for $\bar{\bar{C}}_{Pd}$, resulting in the equation below:

$$\bar{\bar{C}}_{Pd} = 1 - \frac{(1 - C_{P2})}{\sqrt{1 - \bar{C}_P}} \quad (2.14)$$

From Eq. (2.14), it can be observed that the diffuser centerline pressure distribution is non-linear. However, the diffuser's pressure recovery performance determines how much of downforce is generated from the entire underbody. From Eq. (2.12) it is noticeable that if $\bar{\bar{C}}_{Pd}$ more negative, than $\bar{\bar{C}}_{Pl}$ is also more negative, which means that the downforce is greater.

The clearance between the car and the ground is important parameter that influences in downforce generation by the diffuser. Considering an incompressible flow, reducing the area under the vehicle accelerates the air flow through the underbody decreasing the pressure until its minimum value (peak of downforce). Further reduction in the ride height leads to an abrupt reduction in downforce due to the appearance of large separation/stall on the suction surface. At very low ride heights, viscous effects cause an increase of blockage area due to the increase of wall boundary layers with velocity profiles occupying the largest fraction of flow cross-section. This distorted velocity profile surely blocks part of the flow cross-section, which reduces the area ratio of the diffuser and the flow rate under the body (TOET et al., 2021).

Figure 2.23 – Lift and drag coefficient variation with ground clearance for a generic model with underbody diffuser

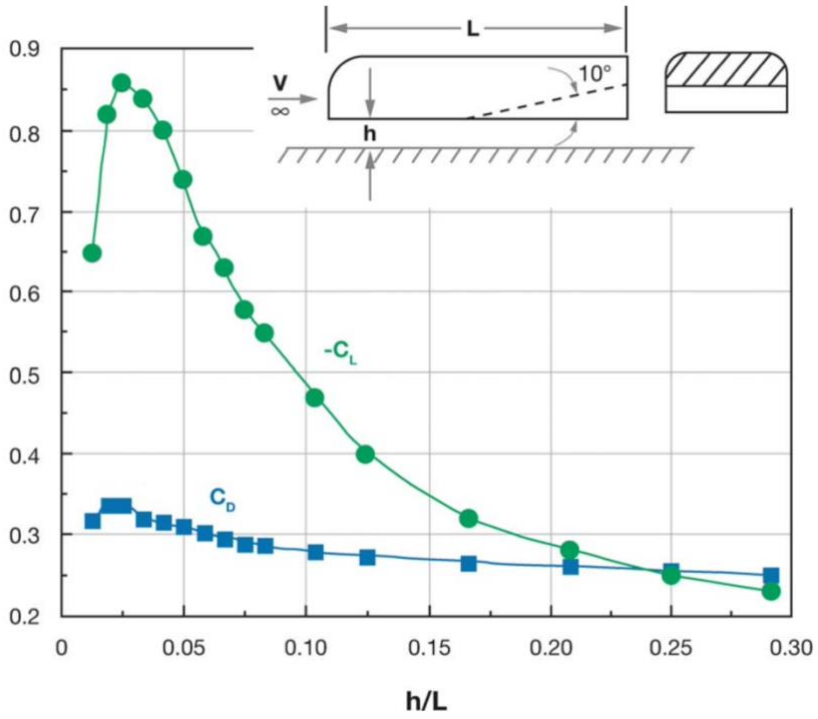


(Katz, 2006)

The Figure 2.23 shows an Ahmed body with diffuser angle of $10°$ where the stall happens at $^{h}/_{L} \cong 0.025$. In racing cars, the displacement (ride height) between its underbody diffuser and the racetrack surface is low enough to enable the effectiveness of the diffuser.

The geometry of the diffuser is another parameter that affects directly on its efficiency and thus on the performance of the vehicle. The slant angle of the diffuser will determine the amount of drag and downforce generated underneath the vehicle. If the angle of the diffuser is close to zero the boundary layer flow will not detach, but the air speed will not be reduced enough to make a laminar transition of the air at the end of the car when to two airstreams meet, which reduces the diffuser's ability to recover pressure at the rear end. The increase of the angle induces a reduction in drag until its minimum value (Figure 2.24), but this effect is only assured with a smooth underside, that allows the flow to be attached. For a large slant angle ($\alpha_d$), more suction and downforce can be created, however at a certain point the drag starts to increase due to flow detachment and side vortex effects (Figure 2.25), caused by an abrupt change in flow direction.

Figure 2.24 – Effects of diffuser geometry on vehicle's performance

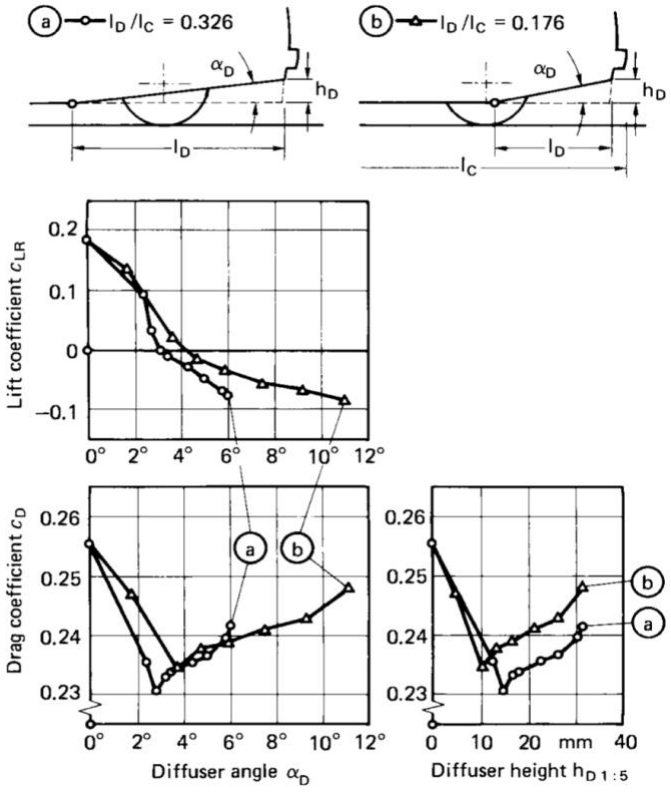


Source: (Hucho, 1987)

The formation of a pair of longitudinal vortices (three-dimensional separation), occurs at the underbody rear end as shown in Figure 2.25. Since there is a low-pressure zone on the inlet of the diffuser, the high-pressure air of freestream near it, tends to decrease this difference, so lateral inflows on the sides of the diffuser surface into the underbody region, causing a rotating streamwise vortical structure pair upward, created by the pressure gradient between the diffuser and the outer region (GUERRERO; CASTILLA; EID, 2022).

Figure 2.25 – Side vortex effects on diffusers without endplates

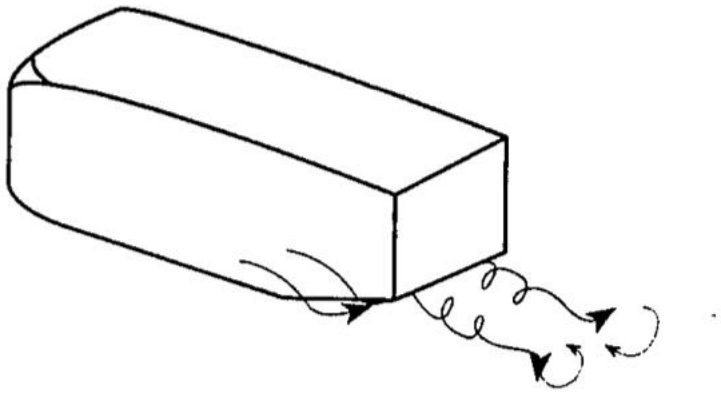

Source: (Katz, 1995)

These vortices roll up under the diffuser, taking high energy air from the outside of the body and introducing it into the diffuser. However, they also take high energy air from below the level of the body and mix it into the airflow under the diffuser. This phenomenon enables the diffuser to function at high angles without detaching and losing effectiveness. The presence of the pair of side vortices in the diffuser redirects the flow upward, inducing some level of upward washing; by Newton's 3rd Law of action-reaction, a reaction force acts on the diffuser in the opposite direction, resulting in downward force. At higher angles these vortex structure breaks down and the flow separates from the diffuser as shown in Figure 2.26.

A common problem with cars is that they all suffer from the turbulence generated by the movement of the wheels, and this interact with the rest of the car. In the case of the floor, if the wheels are close, since they are rotating elements, this turbulence can interfere with the flow in this region, causing detachment, which makes the diffuser inefficient. Wheelhouse also creates

disturbance on the air flow by generation of vortices, and according to (HUMANIC et al., 2015) the presence of wheelhouse has a significant effect on drag and lift forces. To guarantee the efficiency of the diffuser and ensure that the flow passing through it is not disturbed, strakes or fins, and endplates are introduced. Those appendices help to prevent the formation of the side vortex pairs and protect the air flow at the diffuser from wheel and wheelhouse wake. They create small vortices at their edges that help expel external flow and seal up the diffuser, making the airflow to follow its path without harmful interference.

Figure 2.26 – Fins and endplates of Ford GT GTE rear air diffuser

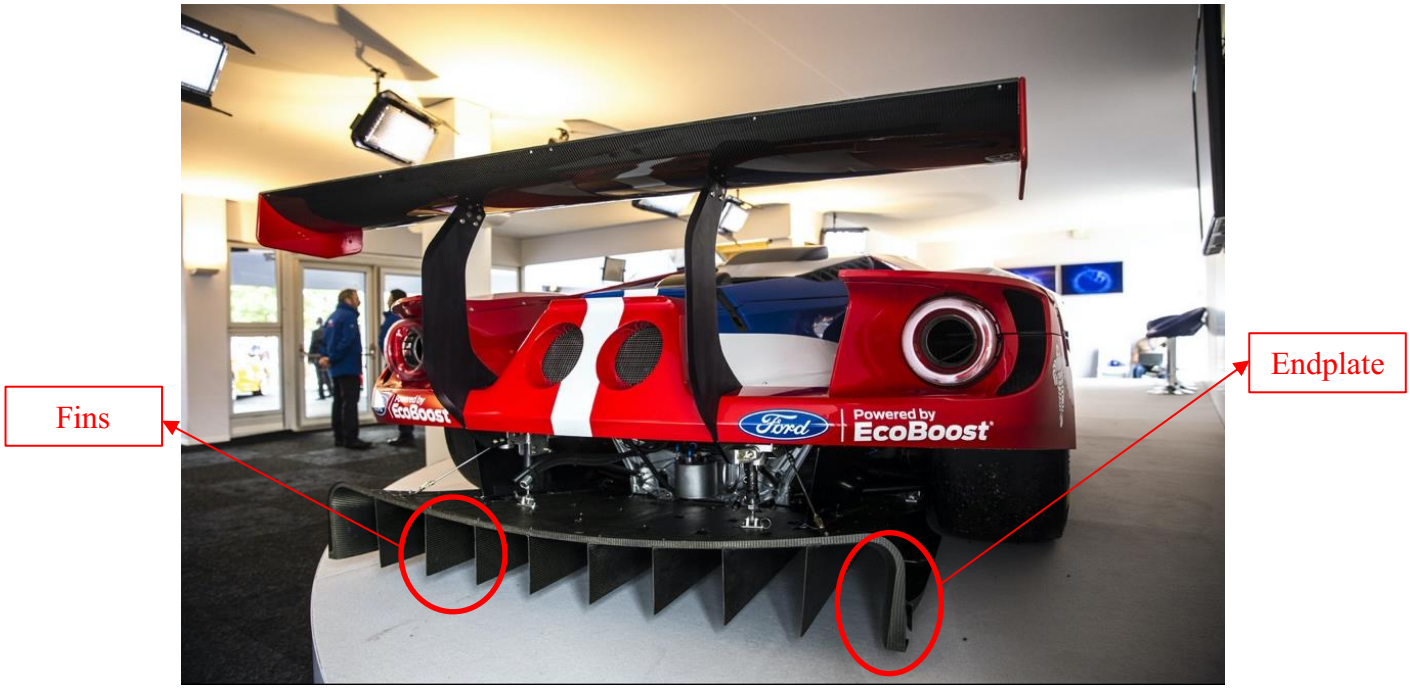


Source:
https://www.caricos.com/cars/f/ford/2016_ford_gt_le_mans_racecar/1920x1080/18.html

The following description is based on results of (HUMINIC et al., 2015) that numerically investigated the flow around a generic car model with and without wheels and underbody diffuser. The proposed geometry (Figure 2.27) and the found results are recurrent in the literature.

Figure 2.27 – Ahmed body with wheels and underbody diffuser

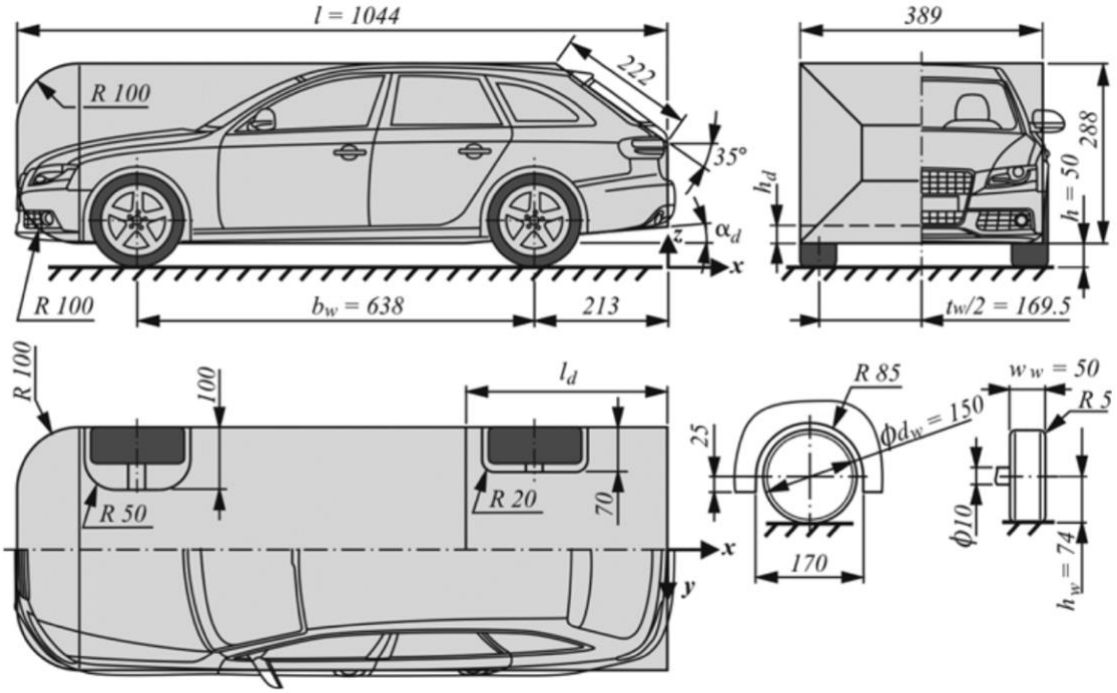


Source: (Huminic, 2015)

For the body without wheels, the lift is always negative, and it decreases linearly with the angle of the diffuser due to a continuous increment of vortices induced on the sides of the diffuser by lateral inflows into the underbody region.

The Figure 2.28 indicates that for high diffusers angles and length, the lift generated decreases. The upper plot on the figure represents an Ahmed body with diffusers and wheels, and it is noticeable that the lift decrement follows a curve due to the interferences of the vortices induced at the side of the diffuser by lateral inflow into the underbody region, with those generated by the wheels. The decreasing rate becomes smaller with the increasing of the diffuser angle. Also, without a diffuser, the body on wheels generates positive lift. This behavior was also observed for cases of relatively smaller diffuser angles and length. Lift becomes negative for body with wheels if $l_d/l \geq 0.2$ and $\alpha_d \geq 3^{\circ}$.

Figure 2.28 – Lift and drag coefficients for body with diffuser, with and without wheels

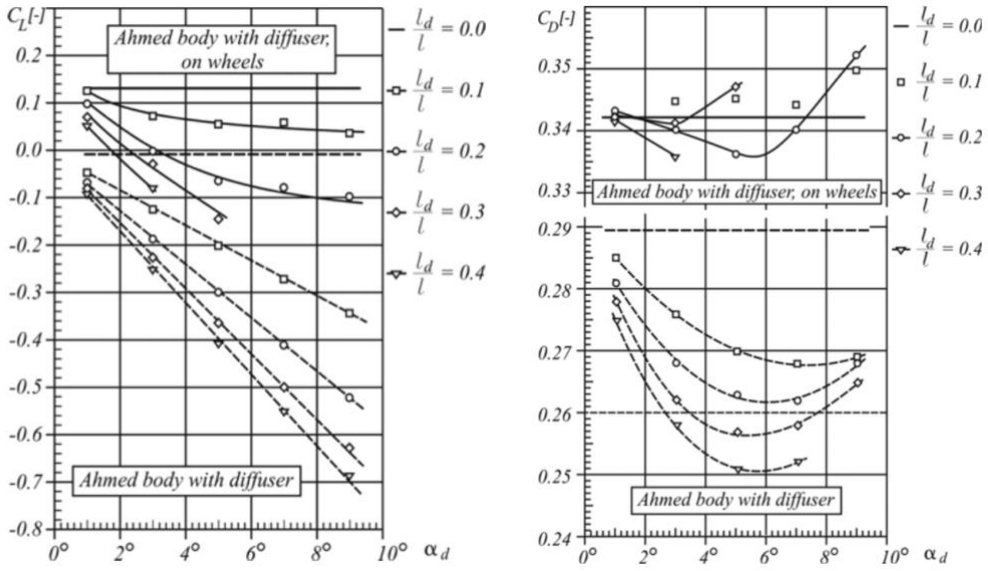


Source: (Huminic, 2015)

Figure 2.29 – Streamlines at the backend of the body

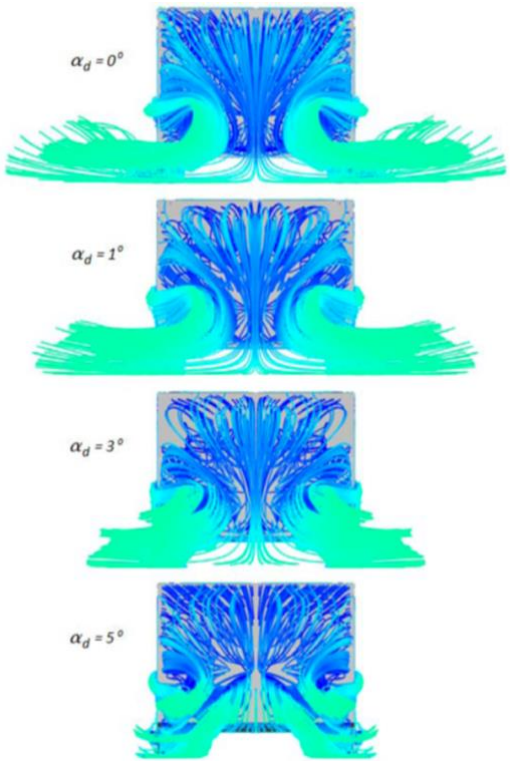


Source: (Huminic, 2015)

The decrement of lift is accomplished also by a decrement of drag for the bodies with an underbody diffuser, due to the Venturi effect. As the pressure rises along the diffuser length, the vortices that originate from the rear wheelhouse are deflected with less intensity causing the amplitude of these vortices to be smaller as shown in Figure 2.29. For high angle values ($\alpha_d > 5^{\circ}$) the boundary layer detaches, and the vortices generated interact with the vortices from the rear wheelhouse increasing the size of the vortices at the base of the diffuser. Separations of airstream occur on the surface of the diffuser and the drag of body starts to increase.

As indicated by the results on the literature, hatchback vehicles are more inefficient in terms of downforce and drag. This performance can be increased by the use of smooth underbody with rear air diffuser. In this context, this work proposes an analysis of the influence of a diffuser on a hatchback car modified for track day events, contributing on the understanding of the diffuser geometry and aerodynamic forces, using aerodynamic balance measurements and flow visualization.

# CHAPTER III

## Bibliographic review

The study of flat underbody with rear air diffusors has been mostly performed in motorsport context; therefore, there are a small number of open articles on the subject. Even though, a general description can be found and a clear increase of related papers on the last decade is perceived.

An aerodynamic underbody is widely considered to be indispensable to car's aerodynamic performance, largely due to its significant downforce contribution. Knight; Spicak; Kuzenko; Haritos; Ren (2018), performed a complete analysis for an inverted Ahmed body. The paper details a numerical investigation of the effects of ride height and diffuser ramp angle to find an optimum downforce and efficiency for the inverted Ahmed model. A short and long diffuser with ratios of 10% and 35% respectively to that of vehicle length are studied. The short diffuser produced lower maximum downforce and efficiency at a lower ride height and lower angle when compared to the longer diffuser. The long diffuser produced highest downforce and the best efficiency with a ramp angle of 25 degrees at ride height ratio of 3.8% when compared to vehicle length. Different ride heights were found to correspond to different diffuser ramp angles to achieve optimum downforce and efficiencies.

Hassan et al. (2013) used CFD to analyze aerodynamic drag of racing cars and different drag reduction techniques such as rear under body modification and exhaust gas redirection towards the rear separation zones. Through a numerical process (Finite Volume Method) of solving the Favre-averaged Navier-Stokes equations backed by k–epsilon turbulence model, the drag coefficient of the car under analysis is found to be 0.3233 and it is evident that the drag can be reduced up to 22.13% by different rear under-body modifications and up to 9.5% by exhaust gas redirection towards the separated region at the rear of the car. It is also evident that if somehow the negative pressure area and its intensity at the rear of the car can be minimized, the separation pressure drag is subsequently reduced.

Another CFD analyze was proposed by Barbut (2011) consist in a study on the influence of the lower part of road vehicles on the global drag characteristics. Reducing overall drag by

redesigning the lower rear part of the vehicle has a potential of 12.7% in the overall drag breakdown, mainly due to the viscous effects and the fluidic interaction of the flow under the car with the typical bluff body flow pattern behind the vehicle.

Marklund et al. (2013) focuses on the aerodynamics of the rear-end and under-body of bluff bodies in general, but also applied to passenger cars, comparing a sedan and state wagon vehicles. The findings were then tested and applied to full–size vehicles, with the focus on under-body flows and the effect of under-body diffusers. Both experimental and numerical tools were used, and scale model as well as full-size test bodies have been investigated. It was observed that the power required to drive the sedan vehicle was reduced 9.5 % by the under-body panels, at 120 km/h; at 80 km/h it was a near 7% power reduction. The added panels to the wagon resulted in reduced power consumption by 2.5% at 120 km/h and 1.8% at 80 km/h. The diffuser generates an upsweep and makes the wake more symmetrical on side view, for the sedan. For the wagon the wake is already symmetrical, and the diffuser can even generate an asymmetric wake.

In 2016, Aulakh analyzed the effect of underbody diffuser on coefficient of drag (Cd) of convoy of two reference car bodies (Ahmed body). CFD analysis of convoy was done using Shear-Stress-Transport model under moving ground conditions. The length of lead body's diffuser was 0.222 m with diffuser angle (degrees) of 0° (no diffuser), 3°, 5°, 7°, 9°, 15°, 20°, 25° and 30° each at intervehicular spacing of 0.25 and 0.75 Ahmed body length. Each configuration thus resulting was analyzed with lead body backlite angle of 25° (pre-critical) and 35° (post-critical) with follow body's backlite angle remaining 25°. CFD analysis were conducted after performing two validation analyses from previous studies. After analysis of convoy, drag on lead and follow vehicles was found to be also dependent on the axial vortices formed due to diffuser in addition to those from backlite surface of lead body. Average drag on cases with diffuser was found to be lesser than the no diffuser cases up to a certain diffuser angle. Thus, applying diffuser had a potential for reducing the overall drag on convoy.

Taiming; Xiaodong; Zhongmin; Zhengqi (2020) propose a drag reduction mechanism of single-channel rear diffuser. The influence of the single-channel rear diffuser on the aerodynamic drag is studied using the Reynolds-averaged method with the 25° slant Ahmed model. The accuracy of the numerical method is validated by means of a wind tunnel test. The aerodynamic performance of the Ahmed model with different vertical diffuser angles, lateral diffuser angles, and channel widths is discussed. The results demonstrate that the vortex location will be influenced by the vertical diffuser angle, and with the vortex core approaching to the model, the aerodynamic

drag will increase. The aerodynamic drag reaches the minimum value with a vertical diffuser angle of 10.46°. Moreover, the aerodynamic drag decreases with increasing channel width. Finally, the aerodynamic drag can be reduced by 5.3%, when the vertical diffuser angle, lateral diffuser angle, and channel width are 10.46°, 0°, and 351 mm, respectively.

In a more recent work, Çalışkan (2022) investigated the effects of varying the diffuser angles on vehicle's performance. The dimensions of the underbody diffuser of a vehicle designed as a 3D model were kept constant and the effects on the lift and drag force at a constant speed of 60 km/h were investigated by positioning the diffuser at 0°, 5°, 10°, 15°, 20°, 25°, and 30° angles. Analyzes were carried out separately for each diffuser position with CFD analysis in Simcenter Star CMM+ program and the results were examined comparatively according to the flat ground geometry. As a result of the study, the peak value of the lift force in the negative direction was calculated as 26.9812 N at a diffuser angle of 20°, where the highest downforce is obtained, a decrease of 200.93% in the lifting force was obtained compared to the 0° position. In case of $C_d$ the use of rear diffuser provided a 14.73% decrease compared to the straight diffuser, considering the diffuser angle of 15°, where the lowest drag force value is obtained.

In a different approach, Guerrero (2022) investigated some different diffuser configurations. A baseline flat-underfloor design, a 7◦ venturi diffuser-equipped setup, a venturi diffuser with diagonal skirts, and the same venturi diffuser with frontal slot-diffusers. The numerical predictions evaluated using RANS computational fluid dynamics (CFD) simulations deal with the aerodynamic coefficients. The configuration that produced the highest downforce coefficient was the one composed of the 7◦ venturi diffuser equipped with diagonal sealing skirts, achieving a $C_l = -0.887$, which represents an increase of around 1780% regarding the baseline model.

Haris (2020) analyzed the drag-reduction effect of a rear air diffuser on a sedan car with computational fluid dynamics (CFD) simulations. A more realistic 3D model was prepared and diffusers with different angles were tested (0°, 3°, 7°, 9°, 12° and 15°). The minimum value of drag coefficient was 0.7487, achieved at a diffuser angle of 7°, what means a reduction of 4.51% when compared to the 0° position.

Pocar; Toet and Gamez-Montero (2022) studied the effect in performance of vertical airfoil endplates on diffusers in vehicle aerodynamics in a simplified geometry. The model was an inversed Ahmed body. Three different diffuser configurations were performed, 0° diffuser and 25° diffuser. A third case was the vertically installed rear vertical airfoil endplates to the 25° diffuser Ahmed body to change the flow field. An inlet velocity of 20 m/s was considered, as this is a typical

velocity when cornering in motorsport. It was concluded that the 25° diffuser configuration generated more downforce than the 0° diffuser, which makes sense as the aim of adding a diffuser is to increase the amount of downforce produced. In addition, and because of the newly proposed configuration, the 25° diffuser Ahmed body with the vertical airfoil endplates emerges in a substantial increase of downforce thanks to the low-pressure zone generated at the back of the body.

For the present work, the study is based in a simplified 1997 Honda Civic VTi model, with some realistic details as wheels, side mirrors and rear wing. A general flow description is presented numerically and experimentally and a study of the influence of the mesh prismatic layer, model geometry, flow velocity and experiment scale are presented.

# CHAPTER IV

## Methodology

This chapter is designated for the presentation and definition of the proposed car model, and the numerical and experimental setups used on this study.

## 4.1. Model geometry

To ensure the similarity of the three-dimensional model, used in the experimental wind tunnel tests, with the real geometry of the car, the blueprint (Figure 4.1) was used as a basis, to ensure the dimensions and shape of the original vehicle. Simplifications were proposed in the details to optimize the development of this work keeping the curves and main characteristics of the car's baseline.

Figure 4.1 – 1997 Honda Civic VTi Type-R blueprint

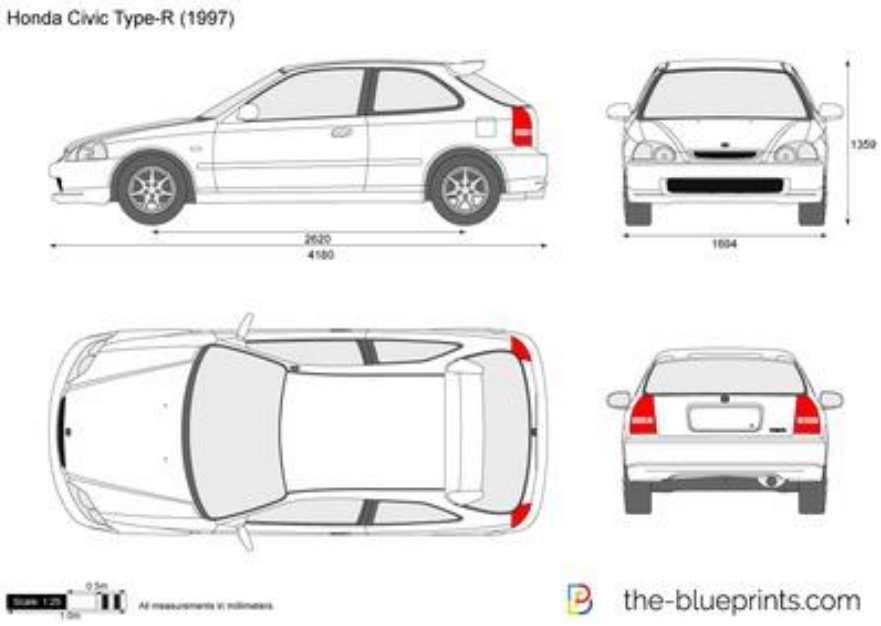


Source: https://www.the-blueprints.com/vectordrawings/show/14005/honda_civic_type-r_ek/

The model was designed in the software CATIA V5R21 using the dimensions as indicated in Figure 4.1. The figure above was cropped so that each face was positioned in the xz, yz and xy planes as shown in Figure 4.2. The Imagine & Shape feature was used to prepare the model surface (Figure 4.3).

Figure 4.2 – Reference images setup

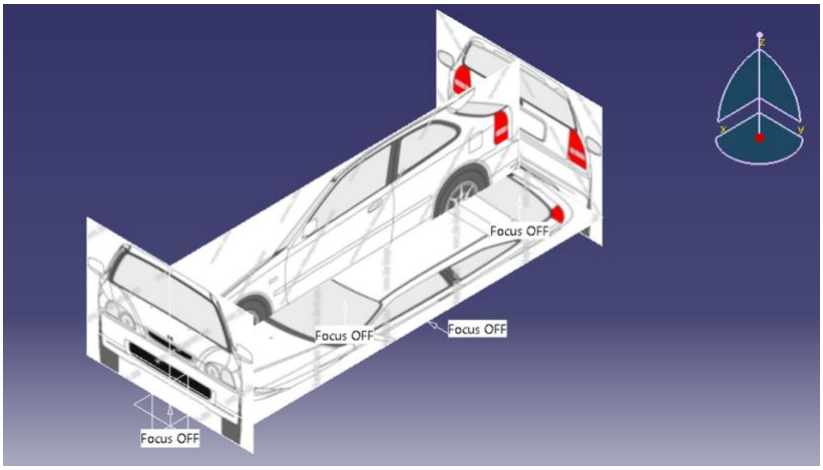


Source: (Own Autor)

Figure 4.3 – Model surface design

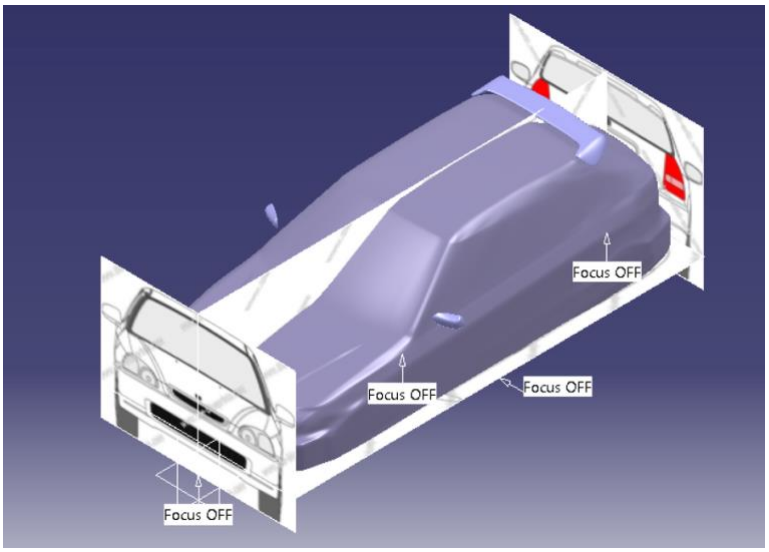


Source: (Own Autor)

In order to achieve a convenient blockage factor on experimental testing, 5% according to Hucho (1987), 1/10 scale is adopted, thus the Length (L) is 418.0 mm, the Height (H) is 135.9 mm, and the Width (W) is 169.4 mm. The 1997 Honda Civic has a frontal area of $1.98\ m^2$, and the designed model has $0.0191\ m^2$. That equals a blockage ratio of 5.30 % on wind tunnel. There were no corrections made on the results presented in Chapter 5 for this blockage ratio.

Figure 4.4 – Model left side view

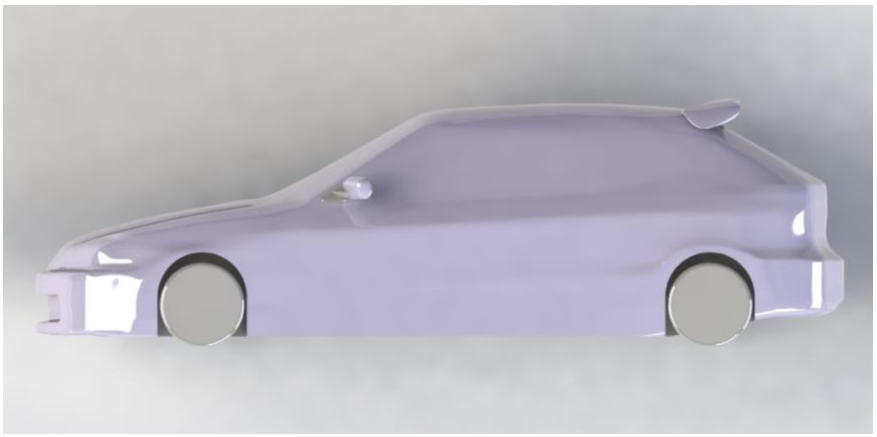

Source: (Own Autor)

Figure 4.5 – Model front view

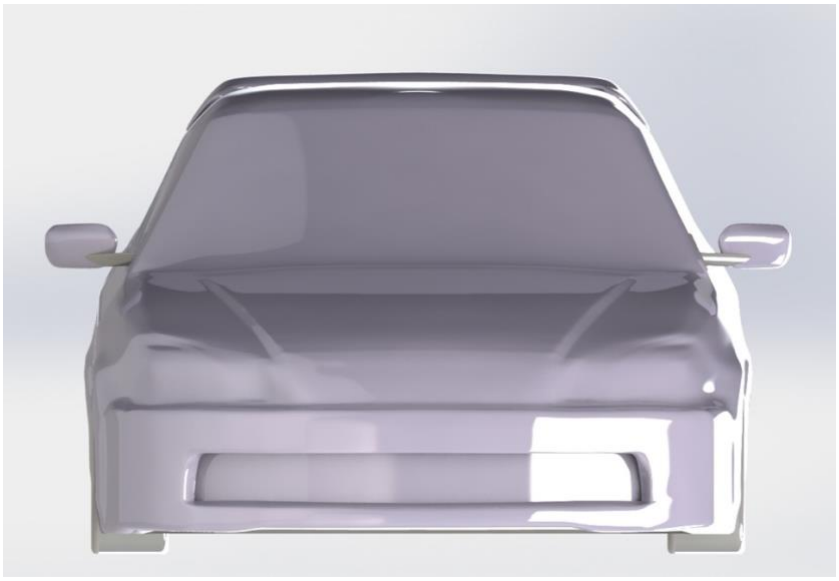

Source: (Own Autor)

Figure 4.6 – Model rear view

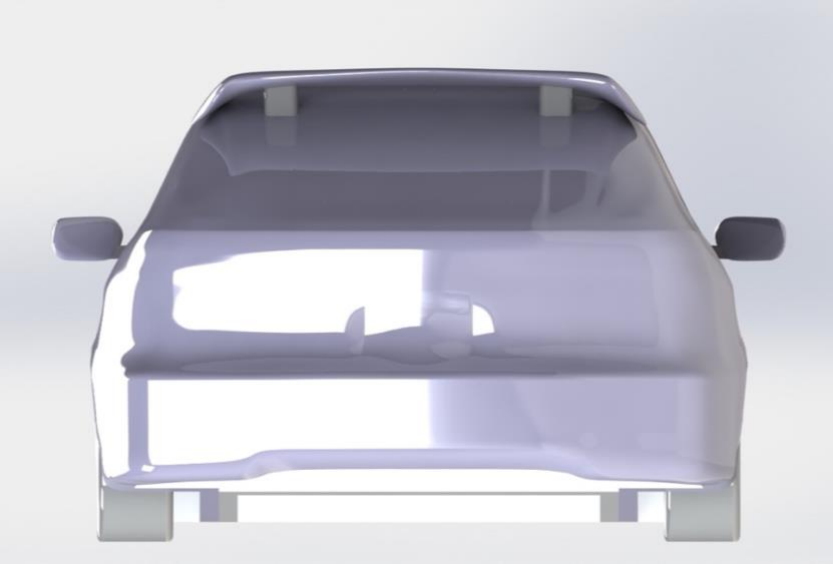

Source: (Own Autor)

Figure 4.7 – Model top view

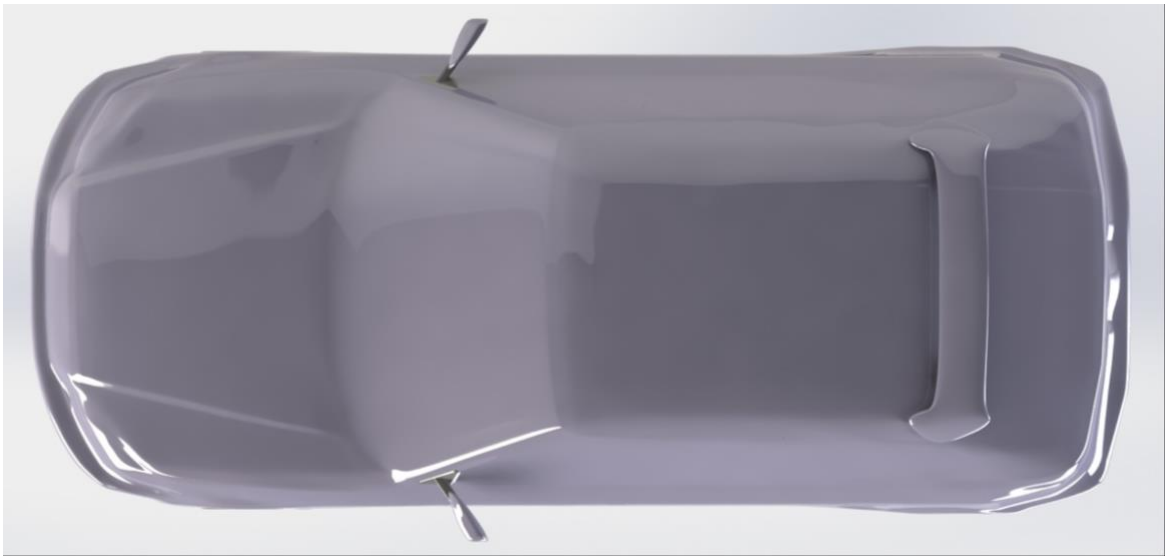

Source: (Own Autor)

Figure 4.8 – Model front isometric view

Source: (Own Autor)

Figure 4.9 – Model rear isometric view

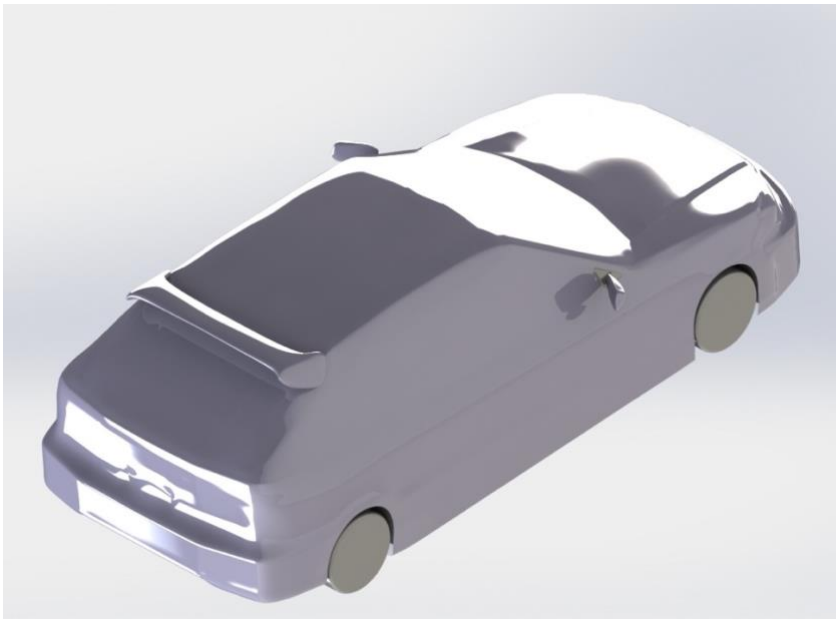

Source: (Own Autor)

The contact of the wheel with the ground is modeled by a chamfer that removed 1% of the diameter parallel to the ground. This modification is closer to reality than the line contact present

if the wheels were completely round. At the center of gravity was positioned a guide for wind tunnel support and balance, in order to measure drag force. First, it was proposed to simulate the model with a flat underbody and without a diffuser.

The rear bumper of the 1997 Honda Civic VTi is naturally upper than the side skirts, this creates an upward angle equals to 10.51°. Due to this geometric limitation, the maximum diffuser angle possible is the existent underbody angle, so it was proposed a set of diffuser angles between 0° and 10.51°, with steps of 2 degrees. The length of the diffusers was a function of the ascent ramp angle, that is, the change in length was performed by changing the angle of the diffuser, not being an object of analysis in this work.

Figure 4.10 – Inclination angle of 1997 Honda Civic underbody

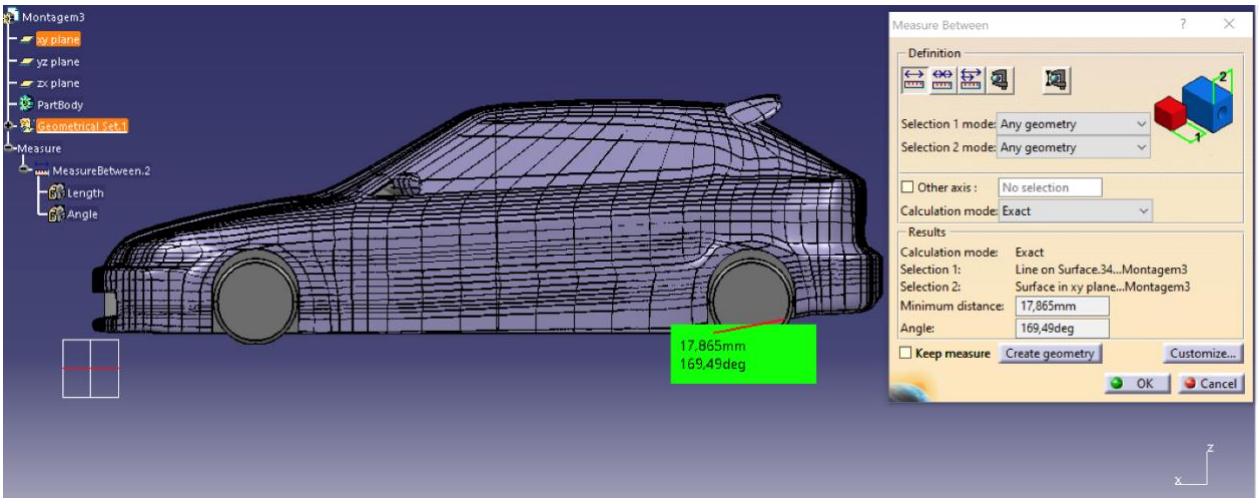


Source: (Own Autor)

## 4.2. Materials and Equipment's

The equipment's that are described in this section belongs to CPAERO - External Aerodynamics Research Center. The main equipment used was a wind tunnel that was responsible to generate a steady and continuous airflow through the test section. For quantitative approaches equipment's like aerodynamics balance and pressure transducer system were used. For qualitative approaches smoke machine, tuffs, and path line (orange wool) were chosen. Other

features like a green table, a green board, and a HD photographic camera. Next follows a more thorough description of these equipment's.

### *4.2.1. Wind tunnel Facility and Model*

The TV-60-Zephyr is a blown-down open section low-speed wind tunnel specially designed for External Aerodynamics Research Center (CPAERO) in Federal University of Uberlândia, Brazil. The wind tunnel contains a four wire-mesh screens and guide vanes after the fan to straight the flow inside the channel to help decrease the turbulence intensity for levels around 0.5 – 0.8% inside the test section (0.6 m x 0.6 m x 1.0 m), providing a good flow quality with minimum distortion provided by the fan blades. Flow momentum is created by a rotor of 12 blades driven by a 25 Hp electrical engine, what provides a maximum air speed of 30 m/s in the teste section with minimal blockage. Air velocity is driven by an electrical inverter (output from 0 to 60 Hz). It is instrumented with pressure taps, Pitot tube and a digital manometer for calibration. The ground of test section is stationary.

Figure 4.11 – CPAERO Wind Tunnel facility


Source: (Own Autor)

The model was printed using a MakerBot 3D printer, model Replicator 2x, with an PLA filament of 1.75 mm diameter. To achieve better contrast on the qualitative flow visualization tests, the black color filament was chosen. The geometry is the same prepared in CATIA for CFD analysis, and the chamfer in wheels is also present. The generation of STL files (for the printer) follows the standard exportation parameters and the tessellation is prepared on printer manufacturer's software (MakerBot Desktop). Due to limitations regarding the printer size, the model was printed in several parts, as presented in Figure 4.12. Printer resolution is 0.5 mm, and the level of infill density is 10%.

Figure 4.12 – Honda Civic model parts

Source: (Own Autor)

Superficial texture and distortions observed on the largest pieces required later preparation for assembling the parts and smoothing the external surfaces and the contacts. The finalized model is presented on Figure 4.14.

Figure 4.13 – Finalized car model without spoiler and side mirrors

Source: (Own Autor)

Figure 4.14 – Finalized car model with spoiler and side mirrors

Source: (Own Autor)

### *4.2.2. Splitter Plate*

When the air flows through test section of the wind tunnel, the boundary layer on the tunnel surface is formed with 4 to 6 mm thick approximately. Due to the proximity of the model to the wind tunnel ground, the model would be influenced by this boundary layer, impairing the measurements and the results. In order to minimize the influences of the existing boundary layer a splitter plate was placed between the tunnel wall and the model. The plate is made of MDF with 10mm thickness. By adding the plate, a new boundary layer starts at the leading edge, and due to the small length of the plate, the boundary layer remains thinner along the length of the car. The leading edge is sharpened to create a smooth start of the boundary layer.

Figure 4.15 – Splitter Plate fixed on wind tunnel test section

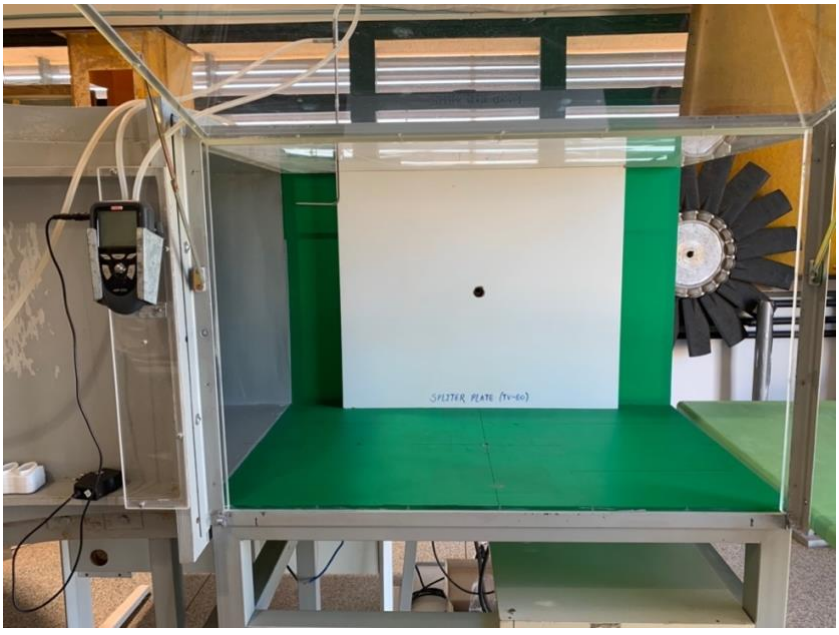

Source: (Own Autor)

Figure 4.16 – Splitter Plate

Source: (Own Autor)

### *4.2.3. Aerodynamic Balance*

The aerodynamic balance is used to measure aerodynamic loads like lift, drag and pitch momentum. It is place external to the test section of the wind tunnel, and once the flow is at a stationary state, the loads are measured in real time by the software of data acquisition AA-DAS at the balance modulus. The modulus itself has two displays, one exhibits the loads, and the other exhibits the angle that the model was positioned.

Figure 4.17 – Aerodynamic Balance


Source: http://aeroalcool.com.br/index.php/acessorios/32-gallery/acessorios/85-ab1-balanca-externa-de-tres-componentes

Fixation of the model is through a cylinder bar that is attached to the balance. When the flow interacts with the model, and depending on the intensity of the interaction, the set may slide from up-down or left-right, which causes an electrical signal captured by three cargo cells. The balance module translates it in a mass measurement in a gram-force scale. The first load cell (load cell 1) measures the effort at the vertical direction, at the downstream. The second (load cell 2), also measures the effort at the vertical direction, but at the upstream, and they are spaced from 77.25 mm form the center of the fixation bar. The third (load cell 3) measures the effort at the horizontal direction. The basic loads in gram force are calculated by the load cells signals as follows:

$$Li\,ft = Cel\,l1 + Cel\,l2$$

$$Drag = Cel\,l3$$

$$Pi\,tch = 77.25(Cel\,l1 - Cel\,l2)$$

The aerodynamics balance used during the tests was designed by the Brazilian manufacture AeroAlcool. The data acquisition system is connected to a computer via USB, where the AeroAlcool software may display the data acquired and translate the gramma-force effort in

Newtons and to calculate the non-dimensional coefficients of drag and lift. This functionality, though, was not available.

### *4.2.4. Pressure Transducer*

The pressure transducer is also designed by AeroAlcool and is a pressure digital unit that allows to capture the pressure measurement through 64 channels. The acquired data is transferred by a module connected on the equipment to a computer to be stored. A time slice must be set up so that a total number of measures per time is capture as wanted for data acquisition. The model AA-TVCFR2 use the same software for analyses the data of the aerodynamics balance.

Figure 4.18 – Pressure Transducer


Source: http://aeroalcool.com.br/index.php/acessorios/32-gallery/acessorios/128-aa-tvcr2

## 4.3. Quantitative Approach

To quantitatively characterize the airflow around the model, two experiments were proposed. The first one was the drag coefficient determination by the aerodynamics balance, followed by the pressure field determination using the pressure transducer equipment.

### *4.3.1. Drag Coefficient Determination*

The determination of the drag coefficient, the aerodynamics balance was used. The experimental process consists in fixing the car by the gravity center to the balance's cylindrical bar, in this way, moments effects around the three axes (coordinate system) could be neglect. Then, the airflow speed must be set. After the flow has achieved equilibrium, three drag forces measures in gram-force are captured and their mean value is calculated. So, appropriating from aerodynamics concepts, the drag coefficient is calculated.

To obtain the evolution of the drag coefficient in function of the speed and in function of the Reynolds number, the velocity range set started on 10 m/s to 22 m/s, with steps of 2 m/s. A total of 50 measures were made for each velocity. For this measurement the model was equipped with a flat underbody without side mirrors and rear spoiler. The following images represent the experimental arrangement.

Figure 4.19 – Drag coefficient determination for baseline model

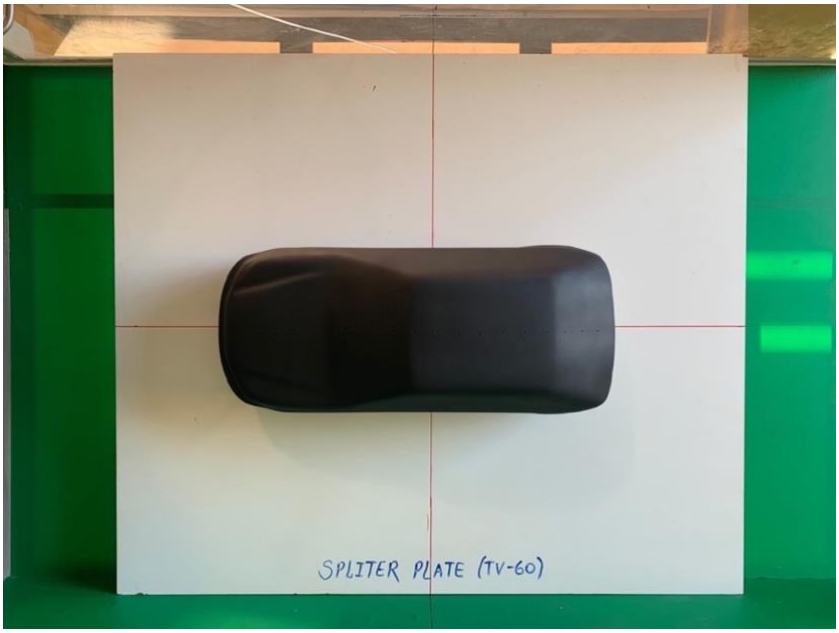


Source: (Own Autor)

Figure 4.20 – Drag coefficient determination for baseline model

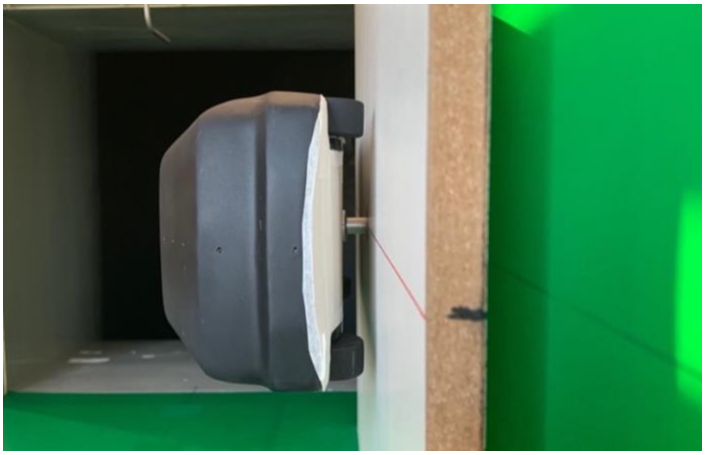

Source: (Own Autor)

Also, to obtain the evolution of the drag coefficient for the complete model, rear spoiler and side mirrors added, keeping the flat underbody, the velocity field stars in 16 m/s to 20 m/s, with steps of 2 m/s. This test was performed to verify the sensitivity of the aerodynamic balance when adding these appendices and to ensure that the delta cd between the two cases is measurable. For this test a total of 30 measures were made for the three velocity values.

Figure 4.21 – Drag coefficient determination for added appendices

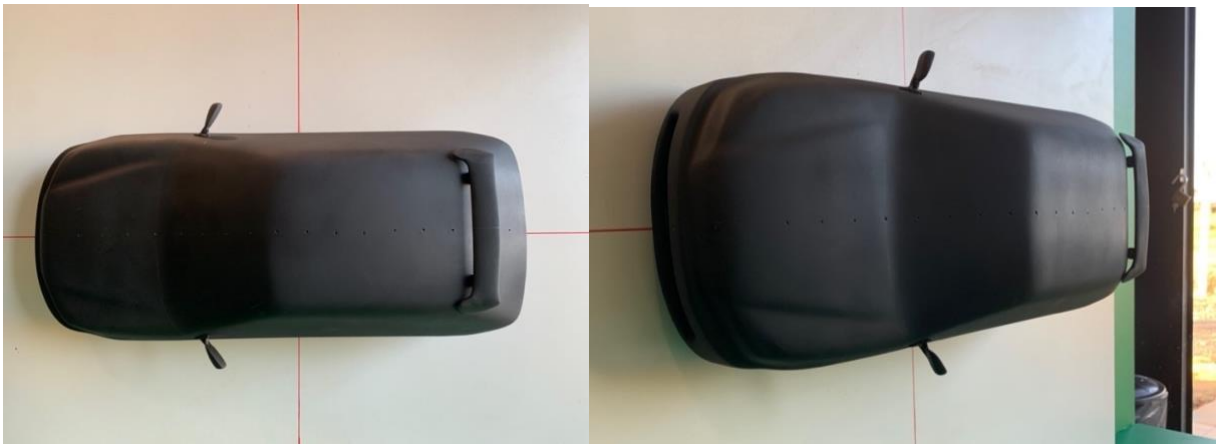

Source: (Own Autor)

After evaluating the influences of side mirrors and rear spoiler, a total of five different diffusers angles were tested. Initially the model was tested with no diffuser, angle of 0°, and then the angle of the ascent ramp was varied up to 10.51° (baseline model), with an interval of 2, totaling 6 configurations (0°, 2°, 4°, 6°, 8° and 10.51°). Later, endplates were installed in the diffusers of 2°, 4°, 6° and 8°. A range of 30 measures were made for each angle with and without endplates. To isolate the effect of the support cylinder bar of the aerodynamic balance, a set of 140 measures were realized, 20 for each velocity. It was subtracted the drag force created by the cylindric bar from the drag force generated by the car, to disregard any external effect.

Figure 4.22 – 0-degree diffuser configuration

Source: (Own Autor)

Figure 4.23 – 2-degree diffuser configuration


Source: (Own Autor)

Figure 4.24 – 4-degree diffuser configuration


Source: (Own Autor)

Figure 4.25 – 6-degree diffuser configuration

Source: (Own Autor)

Figure 4.26 – 8-degree diffuser configuration

Source: (Own Autor)

### *4.3.2. Pressure Field Determination*

In order to determinate the pressure field around the car, 22 points equally spaced were marked to the pressure acquirement and placed at the car longitudinal symmetrical plan. The points were spaced with 20 mm from each other. Then, the model was bored creating 22 through holes, so that the tubes could be attached to it and to transfer the total pressure to the transducer. The model was placed inside the wind tunnel test section and the velocity of 20 m/s was selected. To perform the experiment, it had to be assured that no leak existed.

The experiment was realized for the diffuser angles of 2°, 6° and 10.51°. For the three diffuser angles, three measurements were performed, in which 600 points were obtained in 60 seconds for each measurement. The experimental setup is shown in the Figure 4.27.

Figure 4.27 – Baseline model pressure field determination

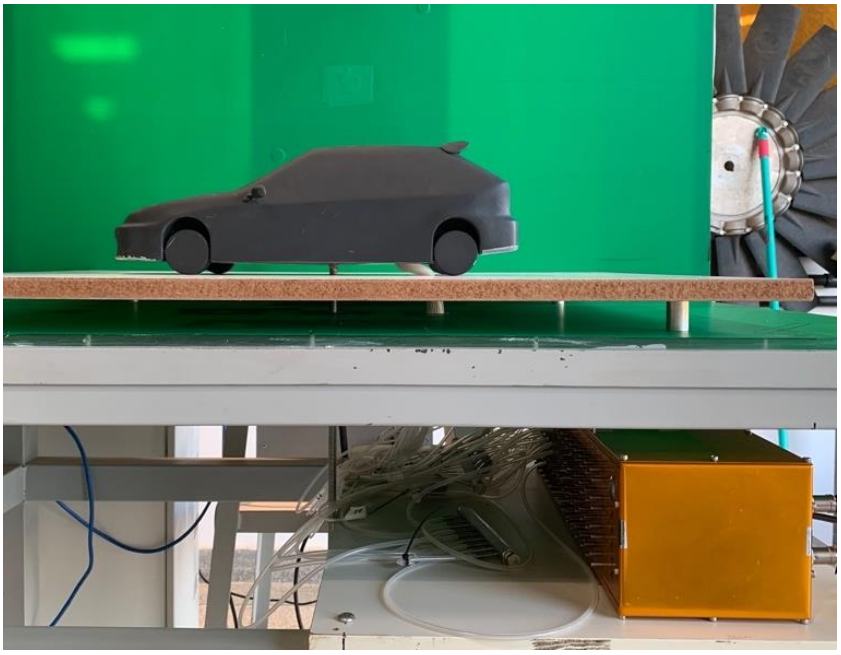

Source: (Own Autor)

### *4.3.3. Pressure Profile Determination*

In order to determinate the pressure behind the model, 13 pressure taps were fixed vertically on a support, equally spaced 10mm apart, with the first pressure tap being 8 mm from the ground. The pressure profile was determined for three different positions relative to the model, so that it was possible to evaluate the influence of the diffusers on the wake. The measurements were performed at 50 mm, 100 mm, and 150 mm from the model. The support containing the pressure inlets was positioned longitudinally, in the direction of flow, on the centerline of the model as shown in Figure 4.28. The model was placed inside the wind tunnel test section and the velocity of 20 m/s was selected.

The experiment was realized for the diffuser angles of 2°, 6° and 10.51°. For the three diffuser angles, three measurements were performed, in which 600 points were obtained in 60 seconds for each measurement. The experimental setup is shown in the Figure 4.28.

Figure 4.28 – Pressure profile determination. Left: 50 mm; Middle: 100 mm; Right: 150 mm.

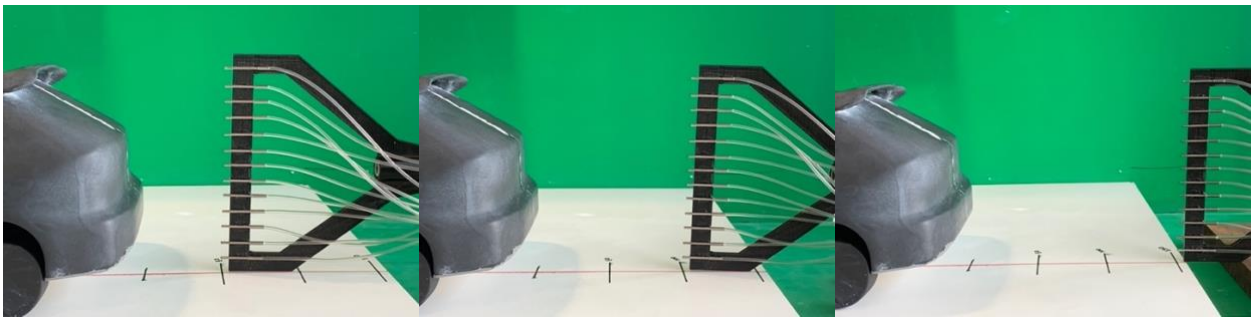

Source: (Own Autor)

## 4.4. Qualitative Approach

The objective of a qualitative method in aerodynamics is to characterize the airflow around a body by visualization methods. This approach helps to shows the coherence or not between the results from the quantitative methods, as they represent the same phenomenon, only the analyses approach is different. Therefore, two visualization tests were proposed: the first, may demonstrate the behavior of the air flow at the rear end of the car, followed by the flow visualization paint

method, which aims to highlight the flow structures. Next, each methodology and experimental set-up is detailed.

### *4.4.1. Wall Tufts*

This is the simplest and most frequently method for surface flow visualization, attach tufts on the surface of interest (Barlow, 1999). It helps to describe flow direction and shows where the flow is steady or unsteady. For the laminar condition, tufts may be aligning with flow direction and describe a relatively steady dynamics; on turbulent and unsteady regions, the movement of tufts is highly oscillating. A tendency to lift from the surface may indicate separated/adverse flow condition (MERZKIRCH, 1987). The possibility of significant influence of the tufts themselves on the flow is very high and must always be kept in mind (BARLOW, 1999).

Figure 4.29 – Wall tufts for surface flow visualization

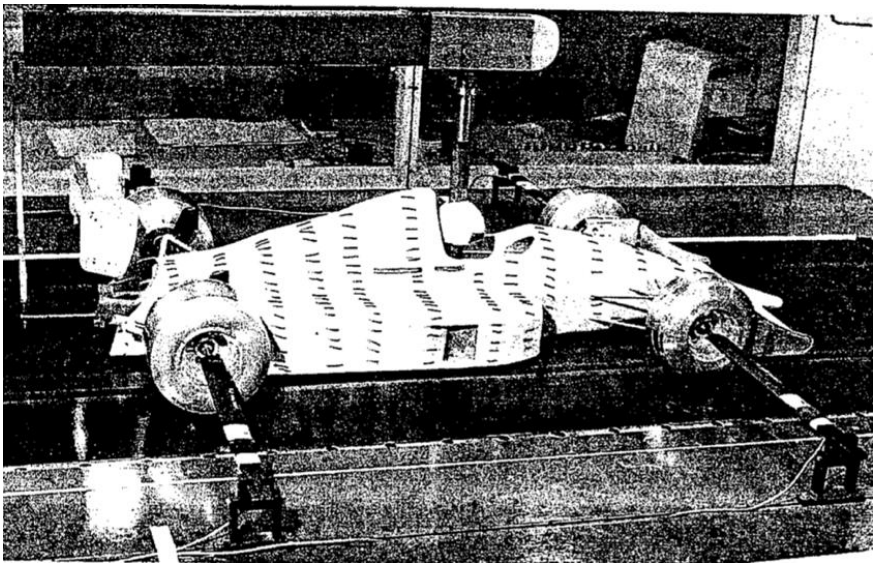

Source: (Katz, 1995)

For this study, 15 mm long wool tufts are attached on the ground of wind tunnel test section, at the roof of the car near the rear spoiler and at the underfloor near the diffuser aera. Tufts are

not placed on the front end. An average distance of 5 mm is considered between the lines of tufts. Figure 4.31 presents the model with the tufts.

Figure 4.30 – Wall tufts at the ground of wind tunnel test section

Source: (Own Autor)

Figure 4.31 – Wall tufts at the rear end of the model

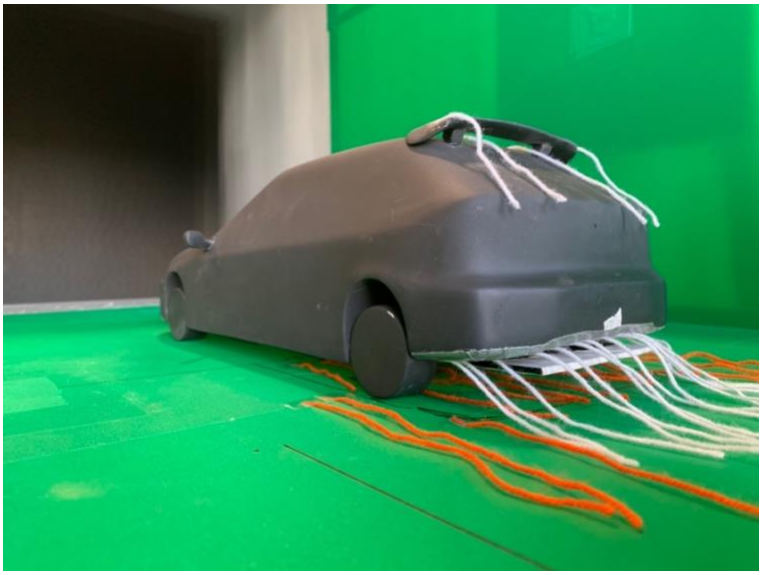

Source: (Own Autor)

The tests are recorded with a cellphone camera posed on the test section windshield. The effects on the rear end were captured for furthermore investigation, and the frames of the recording will be presented in the next chapter. Recording is made on to the velocity of 20 m/s.

### *4.4.2. Flow Visualization Paint*

The viscous fluids are used to show the surface flow. The selected material is usually spread on the areas of interest with a paint brush. It will then flow under the influence of shear stress from the air stream and gravity (Barlow, 1999). This solution is made light enough for it to flow over the car. It also needs to dry quickly so that the airflow over the bodywork can be studied as the car is tested in the wind tunnel. In this work, the solution was made from a mixture of titanium dioxide, kerosene, and oleic acid, and applied on the model with a paint brush.

Figure 4.32 – Painted model for flow visualization

Source: (Own Autor)

# CHAPTER V

## Results and Discussions

This section is dedicated to the presentation and discussion of experimental results.

### 5.1. Drag Coefficient Results

Following the experimental procedure described in Chapter 4, it was possible to obtain the curves presented next. Figure 5.1 show the effect of the cylinder bar on drag force.

Figure 5.1 – The effect of the cylindrical bar on drag force

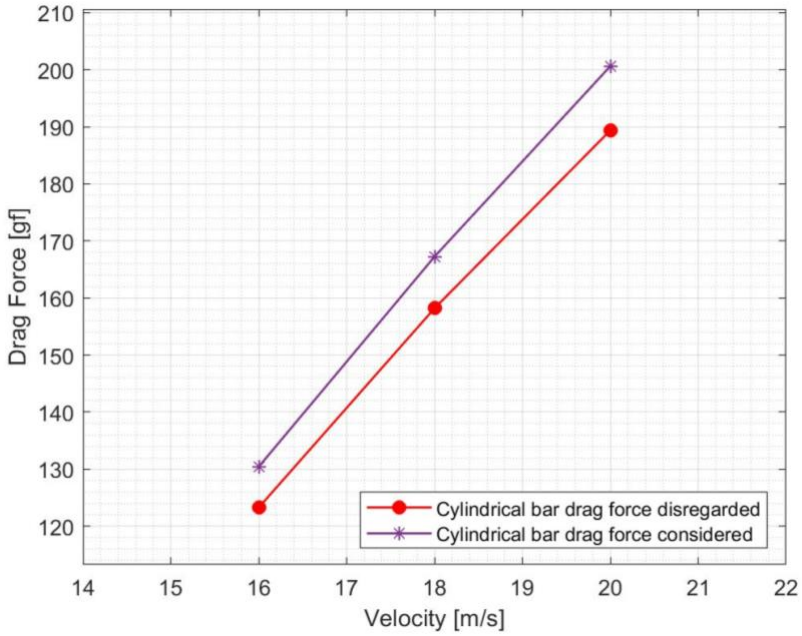


Source: (Own Autor)

Primarily, it was necessary to disregard the drag force generated by the cylindrical bar, from the total drag force calculated by the aerodynamic balance, to eliminate any external effects that may influence the results obtained for the model. It is perceptible that the presence of the cylindrical bar generates a considerable influence on the total drag force, what results in a 6% increase in the drag force at the velocity of 20.0 m/s. The next step was to calculate the drag coefficients of the model. Figure 5.2 and 5.3 shows the results for drag force and coefficient respectively.

Table 1 – Results for baseline model without side mirrors and rear spoiler

| Velocity | Drag Force $(D)$ | Drag Coefficient $(C_d)$ | Reynolds Number $(Re)$ |
|---|---|---|---|
| $10\ m/s$ | $41.94\ gf$ | 0.408 | $2.40\ x\ 10^6$ |
| $12\ m/s$ | $62.90\ gf$ | 0.425 | $2.87\ x\ 10^6$ |
| $14\ m/s$ | $80.37\ gf$ | 0.399 | $3.35\ x\ 10^6$ |
| $16\ m/s$ | $103.75\ gf$ | 0.395 | $3.83\ x\ 10^6$ |
| $18\ m/s$ | $128.93gf$ | 0.387 | $4{,}31\ x\ 10^6$ |
| $20\ m/s$ | $164.61\ gf$ | 0.401 | $4.79\ x\ 10^6$ |
| $22\ m/s$ | $187.79\ gf$ | 0.378 | $5.27\ x\ 10^6$ |

Figure 5.2 – Baseline model, without side mirrors and rear spoiler, drag force

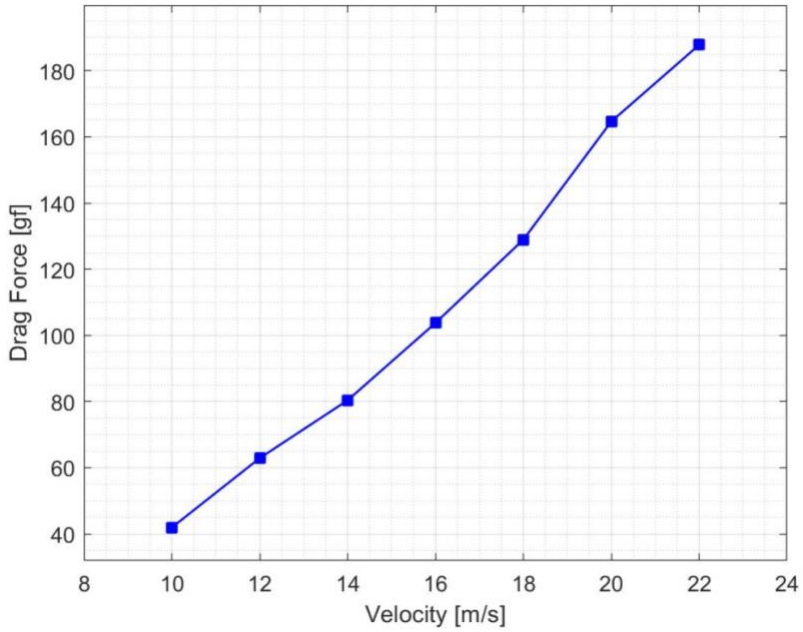


Source: (Own Autor)

Figure 5.3 – Baseline model, without side mirrors and rear spoiler, drag coefficient.

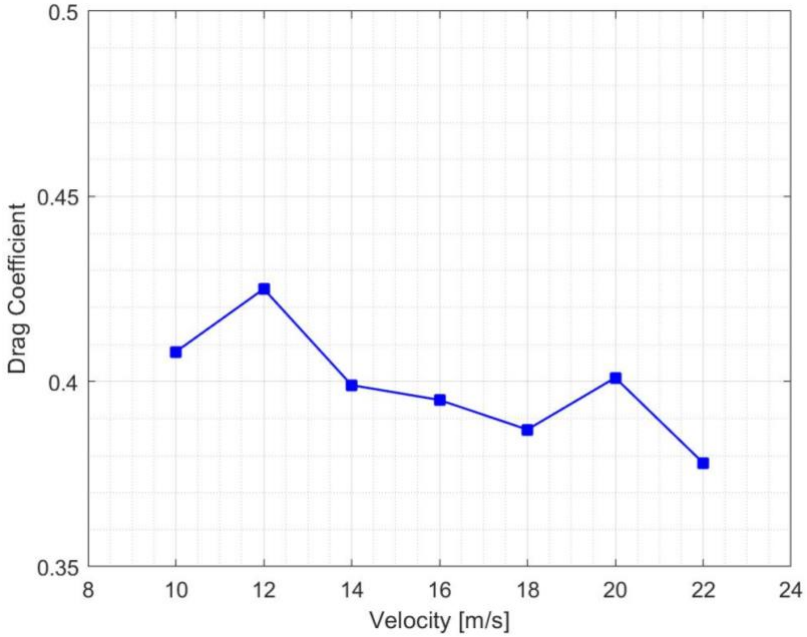


Source: (Own Autor)

Figure 5.4 – Drag force comparison between the models.

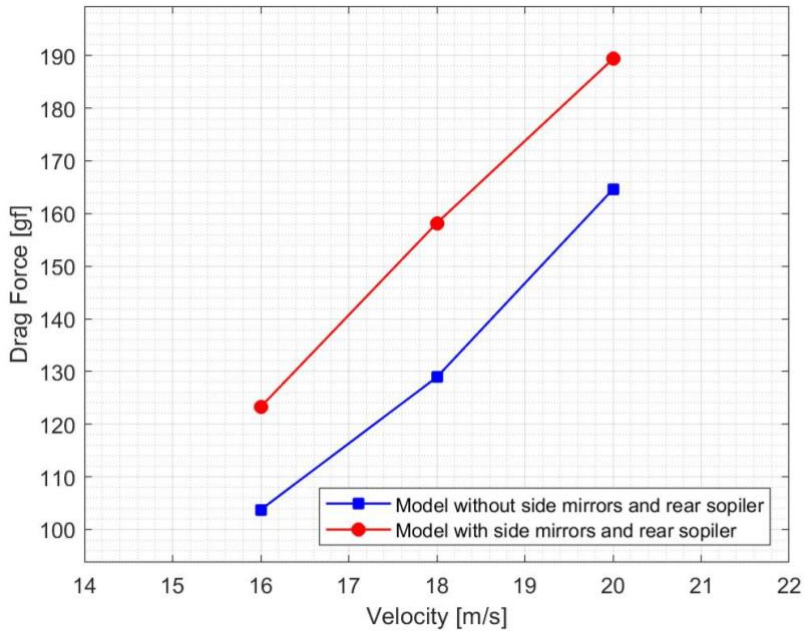


Source: (Own Autor)

Figure 5.5 – Drag coefficient comparison between the models

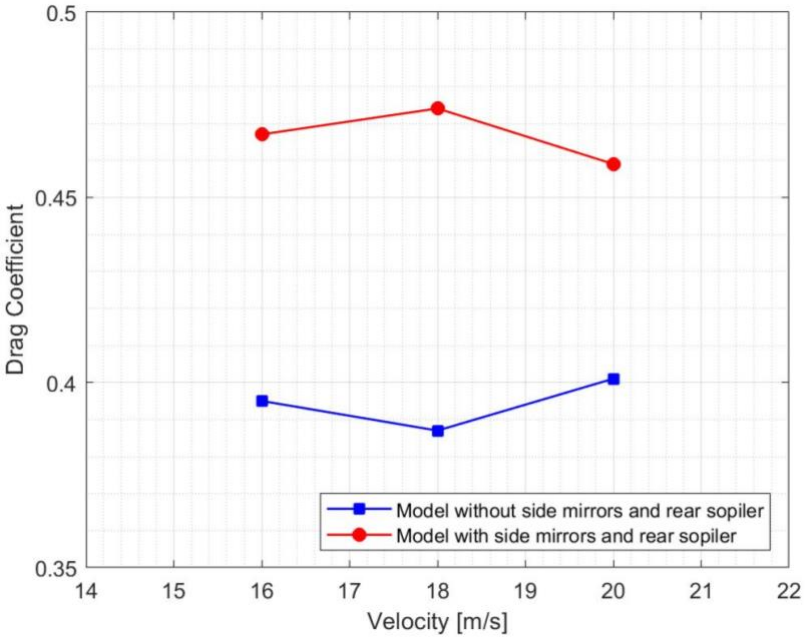


Source: (Own Autor)

From Figures 5.4 and 5.5, it is noticeable the effect that the side mirrors and the rear spoiler causes on the drag force and drag coefficient. For the drag force, at the freestream velocity of 20.0 m/s, the difference between the two cases is about 25 gf, what means an increase of 15.2% when the side mirrors and rear spoiler are installed. For the drag coefficient, at the same velocity, the difference is $\Delta C_D = 0.06$, what means that $C_D$, when the model is equipped with side mirrors and rear spoiler, is increased by 15%. This is explained by the increase in the model frontal area and the generation of vortices, caused by the addition of these devices.

The model with mirrors, rear spoiler and with a smooth floor that has a 10.51° ascent ramp was taken as a reference. The drag coefficient at a velocity of 20.0 m/s was approximately $C_D = 0.463$. To analyze the effects on the model's drag coefficient, tests were carried out with diffusers in which the angle of the ascent ramp was varied from 0° to 8°. The results are presented on Figures 5.6 and 5.7.

Figure 5.6 – Effect of underbody diffuser geometry on drag.

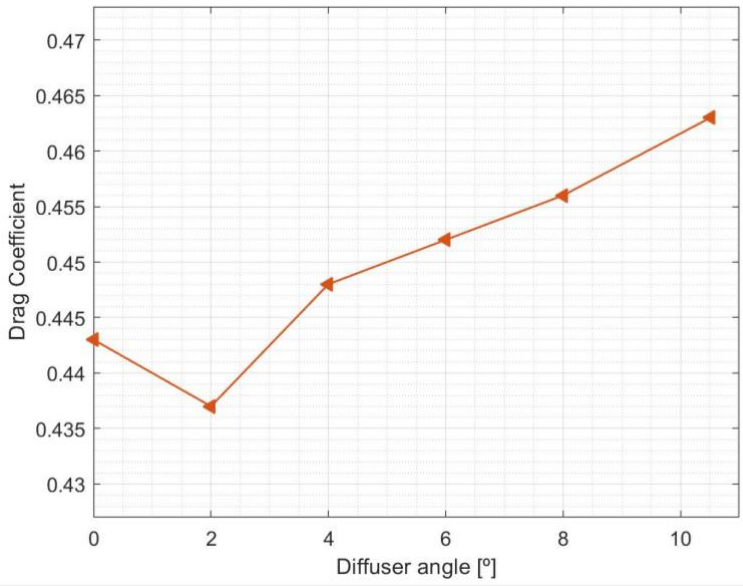


Source: (Own Autor).

Figure 5.7 – Delta $C_D$ by Diffuser angle relating to baseline model

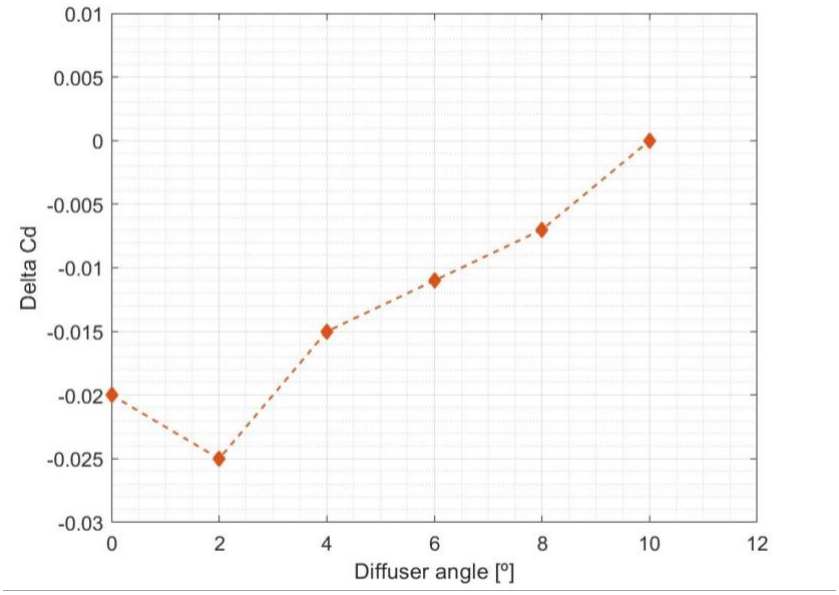


Source: (Own Autor)

For very high angles, three-dimensional separation effects (pairs of vortices formed in the underbody rear end) are expected, which could be the reason for the increase in $C_D$ for angles above 4°, and as the diffuser ramp angle increase, the size and strength of theses vortex pair also increase. Another possible explanation for this increase, would be the detachment of the flow due to slope of the diffuser's rise ramp, which generates turbulence at the diffuser's trailing edge. The improvement for the angle of 2° in relation to the others, can be explained by the non-occurrence of these effects, which indicates that the air flow remained attached to the diffuser. The lowest drag coefficient value found was $C_D = 0.437$, which means a $\Delta C_D = 0.025$ in relation to the reference model, that is, a reduction of 6%, for the diffuser with angle of 2°. For 0-degree, there is no effect of the lateral vortices, since there is no slope, so the increase in the value of $C_D$, in relation to the 2°-angle diffuser, is due to worse pressure recovery at the back of the model.

Endplates were installed in the diffusers of 2°, 4°, 6° and 8°, where the objective was to analyze if the side vortex effects would be neutralized or decreased. The result of the drag coefficient for this case is show in Figure 5.8.

Table 2 – Drag coefficient results at 20 m/s varying diffuser angle with and without endplates

| | Drag Coefficient $(C_d)$ | |
|---|---|---|
| Diffuser Angle | Without Endplates | With Endplates |
| $2^\circ$ | 0.437 | 0.440 |
| $4^\circ$ | 0.448 | 0.453 |
| $6^\circ$ | 0.452 | 0.444 |
| $8^\circ$ | 0.456 | 0.450 |

Figure 5.8 – Effect of underbody diffuser with endplates geometry on drag

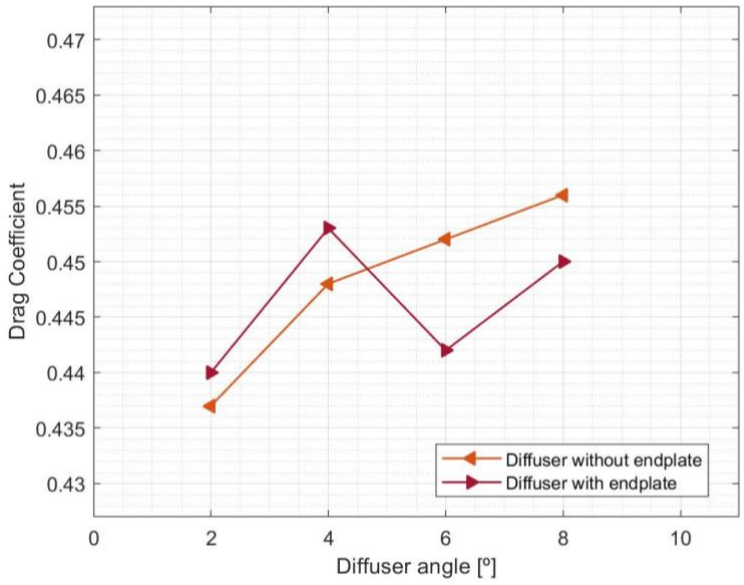


Source: (Own Autor)

By adding endplates on both sides of each diffuser, the results appear not to have a significantly change, unless for the 6-degree diffuser angle, that showed a slight improvement of 2% when compared to the same angle without endplates. The drag coefficient value for this case was $C_D = 0.452$, and when adding the appendices, a reduction of $\Delta C_D = 0.008$ was achieve, totalizing a $C_D = 0.444$. When translate to gramma-force, a 5 gf was obtained. The little gain on 6-degree configuration, may be due to the decrease of the side vortex pair strength. Also, when

compared with the baseline configuration, the 6-degree setup with endplates could reduce drag coefficient in approximately in 5%.

For the 2-degree setting, as there is possibly no effect of the three-dimensional vortices nor the detachment due to tilt, the endplates were irrelevant since they would act to seal the diffuser. In the case of 4-degree diffuser, there is not enough angle to induce the formation of three-dimensional vortices effect, and as the slope is not very high, a small detachment may have occurred at the trailing edge of the diffuser. As for the 8-degree configuration, the size of the three-dimensional vortex pair was enough to keep the value of the drag coefficient practically unchanged, what indicates that the induced drag, generated by these side vortices, is the main responsible.

## 5.2. Pressure Coefficient Results

This section is dedicated to present the data of pressure coefficients determination by following the procedure described in Chapter 4. The results are presented on Figures 5.9 and Figure 5.10.

Figure 5.9 – Upper pressure coefficient for baseline model

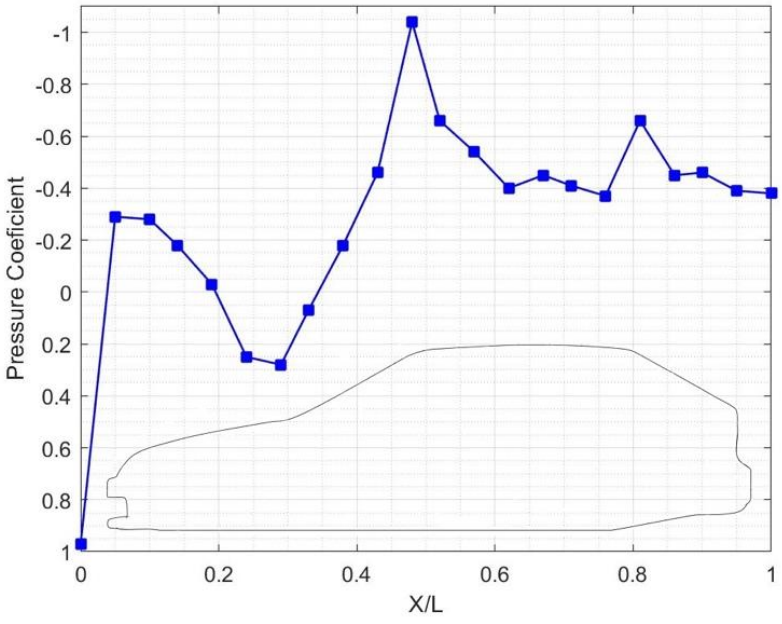


Source: (Own Autor)

Primally, the pressure coefficient curve for the base model was obtained. The upper pressure coefficient of the model follows the expected curve shape for this type of vehicle. As it was shown in the Chapter 2, the stagnation point ($C_p = 1.0$) is also localized at the front of the model, where the highest pressure is found. The first point of low pressure is due to flow acceleration over the hood and $C_P$ becomes negative. As air flow reaches the windshield, it slows down and increases the pressure to a positive value. Air flow began to reaccelerate and reaches the minimum pressure value, for this case $C_p = -1.04$ at the start of the roof. Across the back side of the vehicle the whole sequence is reversed, and the pressure returns to increase. At near $^{X}/_{L} = 0.8$ the second lower pressure peak is due to the presence of rear spoiler, which generates a low-pressure zone by flow detachment. At the back, pressure coefficient does not return to $C_p = 1.0$, due to a large zone of wake that is characterized by low pressure region.

Afterwards, the diffusers that presented the best results for the drag coefficient were installed in the model, being the 2 and 6-degrees diffusers, so that the pressure coefficient curves were obtained and compared with the baseline model, as shown in the Figure 5.10.

Figure 5.10 – Pressure coefficients comparison between the models.

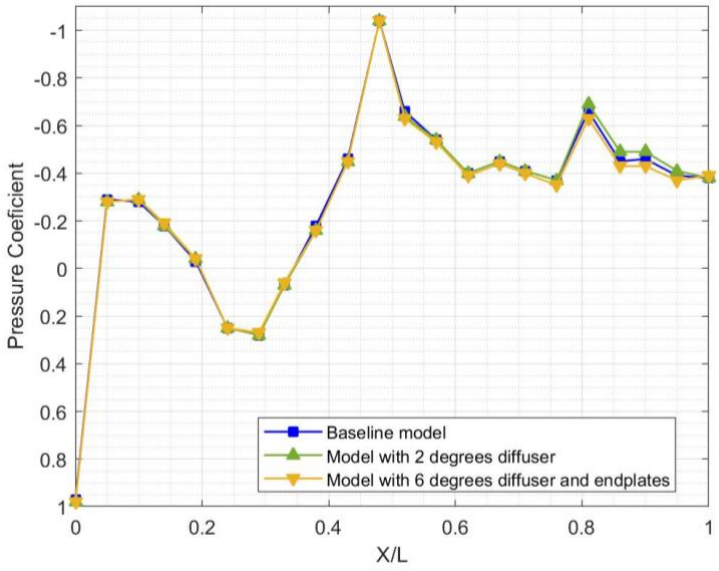


Source: (Own Autor)

The presence of diffusers did not prove to be efficient in terms of pressure recovery at the rear end of the model. This fact can be explained by the reason that for angles of 6° and 10.51°, the flow possibly detaches what keeps the pressure low in the back of the car. The 2-degree diffuser does not have enough inclination to guarantee pressure recovery. The curves remained practically identical, with small variations due to measurement errors.

Figure 5.11 – Pressure hoses arrangement detail.


Source: (Own Autor).

Due to the positioning of the pressure transducer and the configuration of the holes in the test section of the wind tunnel, for the passage of pressure hoses, the way found for the exit of the hoses of the model was through the floor, in the central line. As 22 pressure taps were used, the set of hoses blocked part of the diffuser, and may have caused the flow to detach from the underfloor, which could be an explanation for the non-variation of the pressure coefficient in the rear region just above the diffuser. Also, the diffuser directs the air with high energy into the wake further downstream from the car. As the pressure points are fixed on the model surface, they are not able to measure the pressure difference caused by the diffuser on the flow.

## 5.3. Pressure Profile Results

The pressure profile behind the model was determined by following the procedure described in Chapter 4. The results are presented on Figure 5.12 to Figure 5.14.

Figure 5.12 – Pressure profile comparison for 50 mm from the model

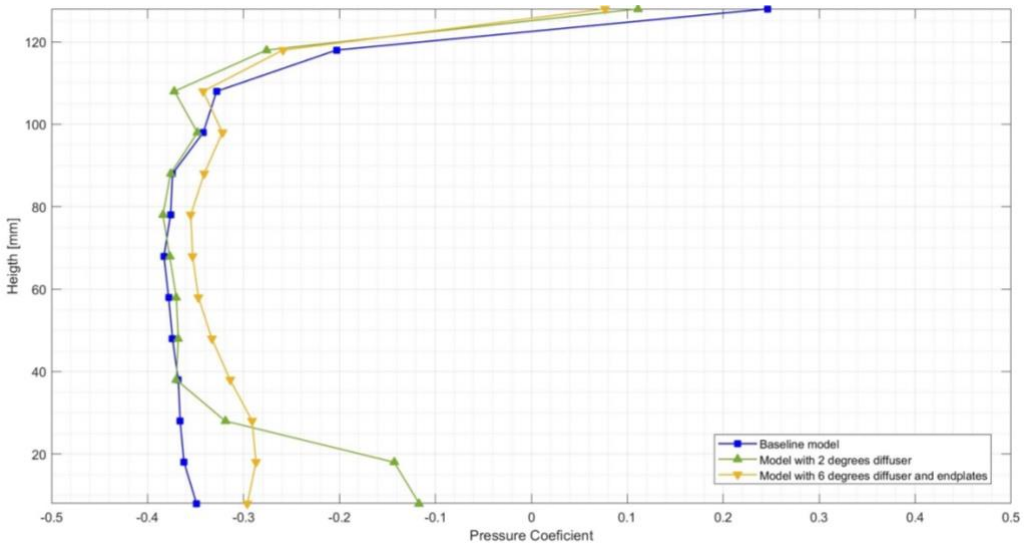


Source: (Own Autor)

Figure 5.13 – Pressure profile comparison for 100 mm from the model

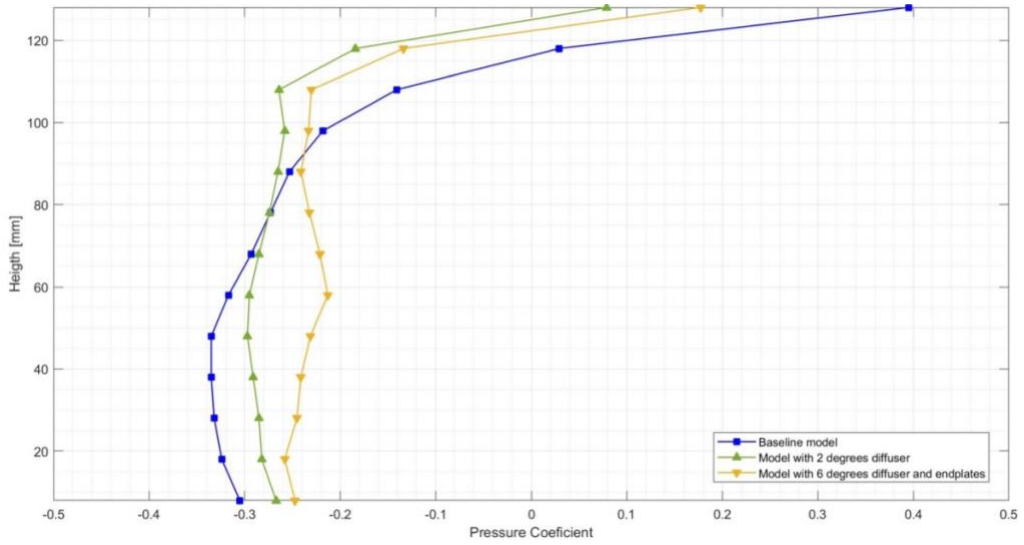


Source: (Own Autor)

Figure 5.14 – Pressure profile comparison for 150 mm from the model

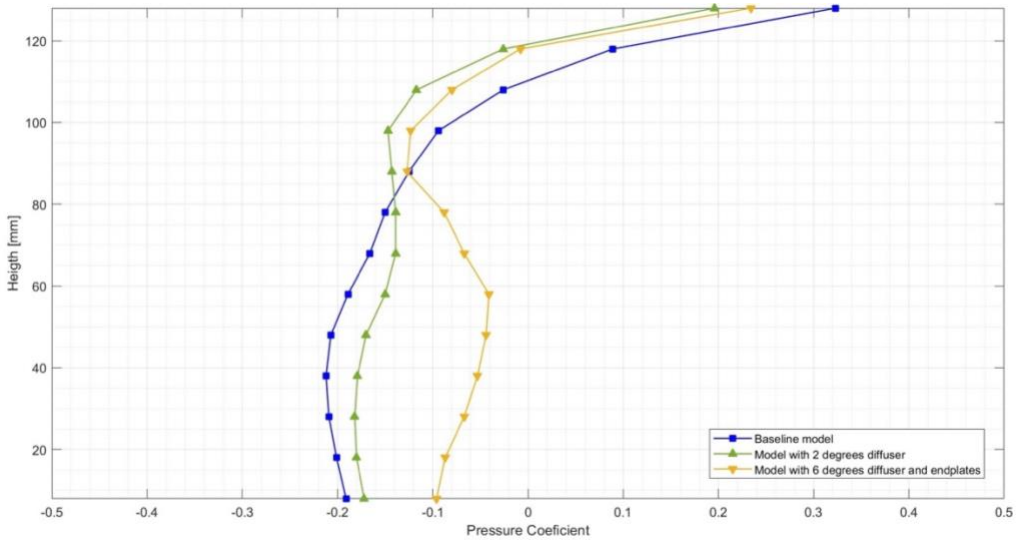


Source: (Own Autor)

For 50 mm position, the pressure profile for the three configurations is quite similar, with some differences that will be pointed next. The baseline shows a low-pressure zone behind the model for almost all pressure taps and the positive values are for those next to the freestream. This zone is characterized by the wake cause by detachment at both top and bottom of the car. The 2-degree diffuser show an increase in pressure on the point closer to the ground, due to the high energy flow directed by the diffuser. As there is a smooth ramp, a small portion of upwash is created, but it isn't enough to direct high energy on the wake for the points above 40 mm, so the pressure profile above the first point is lower similar to the baseline model, which indicates the presence of the wake. The 6-degree diffuser induce a high energy flow on the wake due to the presence of the three-dimensional vortex pair, which slight increase the pressure at 50 mm of the model.

Figure 5.13 indicates an increase on pressure coefficients for all points of the three curves, due to the reduction of the wake. Figure 5.14 show that high energy air directed by 6-degree diffuser has effect on the wake for a lager distance. The other two configuration present a similar pressure behavior and the increase in wake pressure is due to the reorganization of the flow behind the model.

## 5.4. Wall-Tufts Visualization Results

For flow tendency visualization, wool tufts are placed on model wall. Wind tunnel testing was performed at the velocity of 20.0 m/s. Videos were recorded from lateral and from rear of the model. The Figures 5.15 to Figure 5.20 illustrates images registered for each diffuser.

Figure 5.15 – Tufts visualization for 0-degree setup.

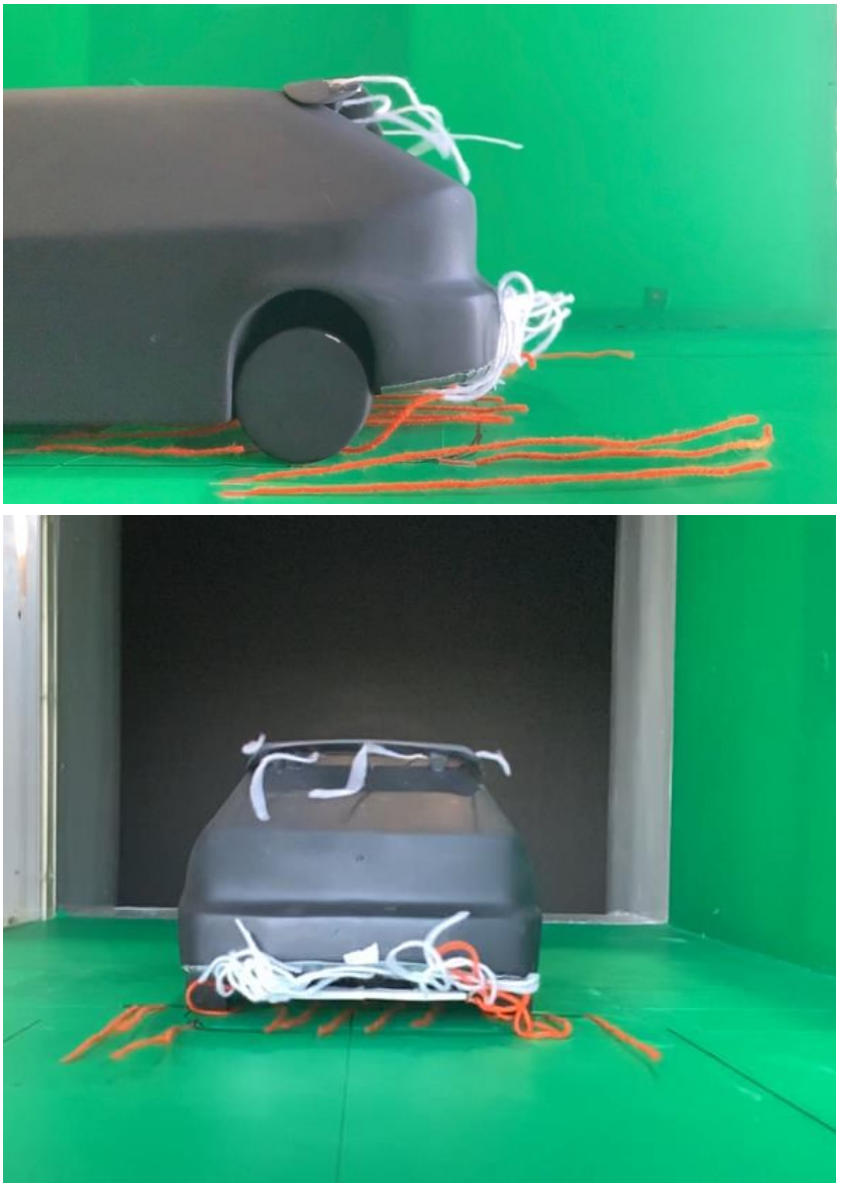

Source: (Own Autor)

Figure 5.16 – Tufts visualization for 2-degree setup

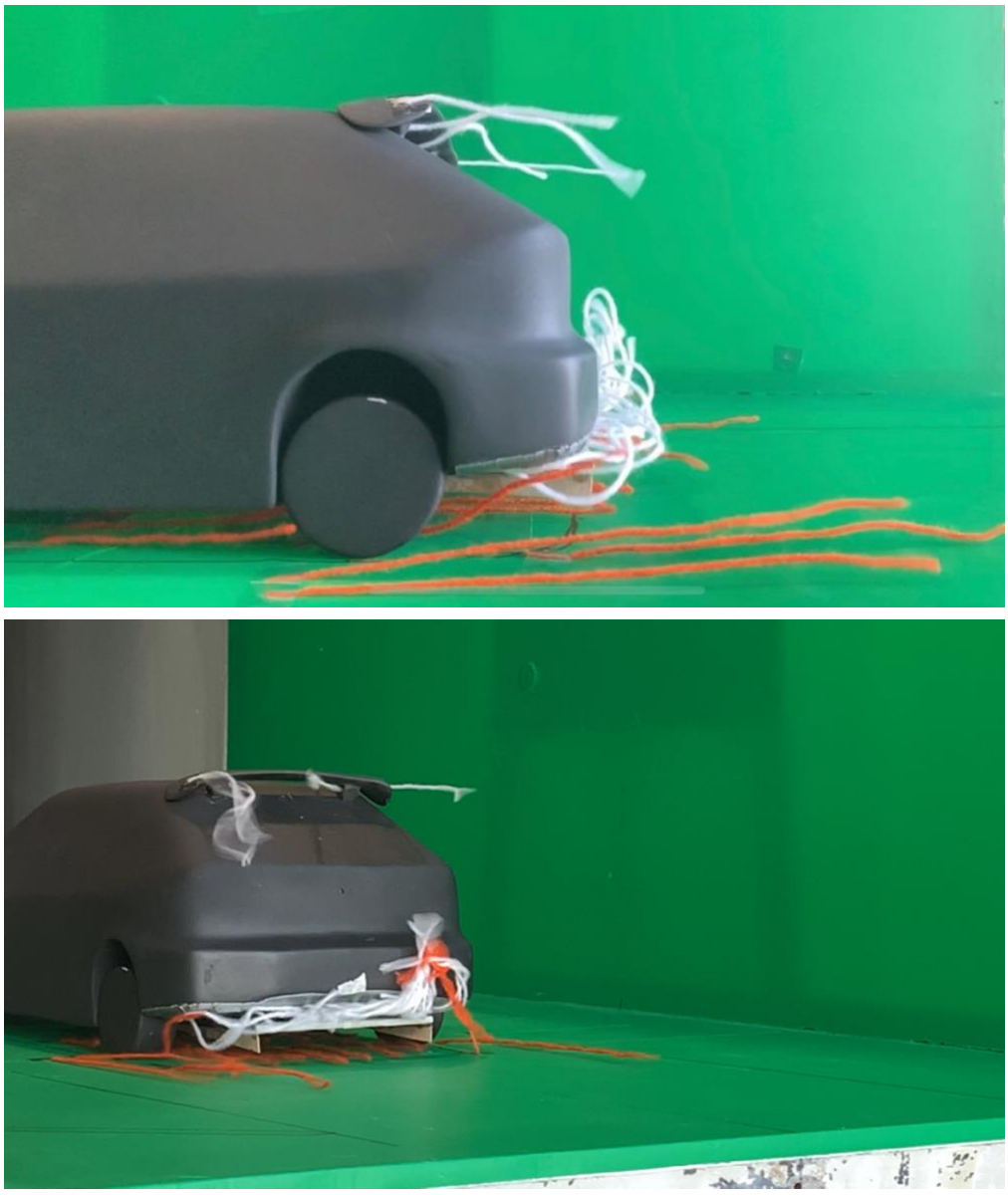

Source: (Own Autor)

Figure 5.17 – Tufts visualization for 4-degree setup

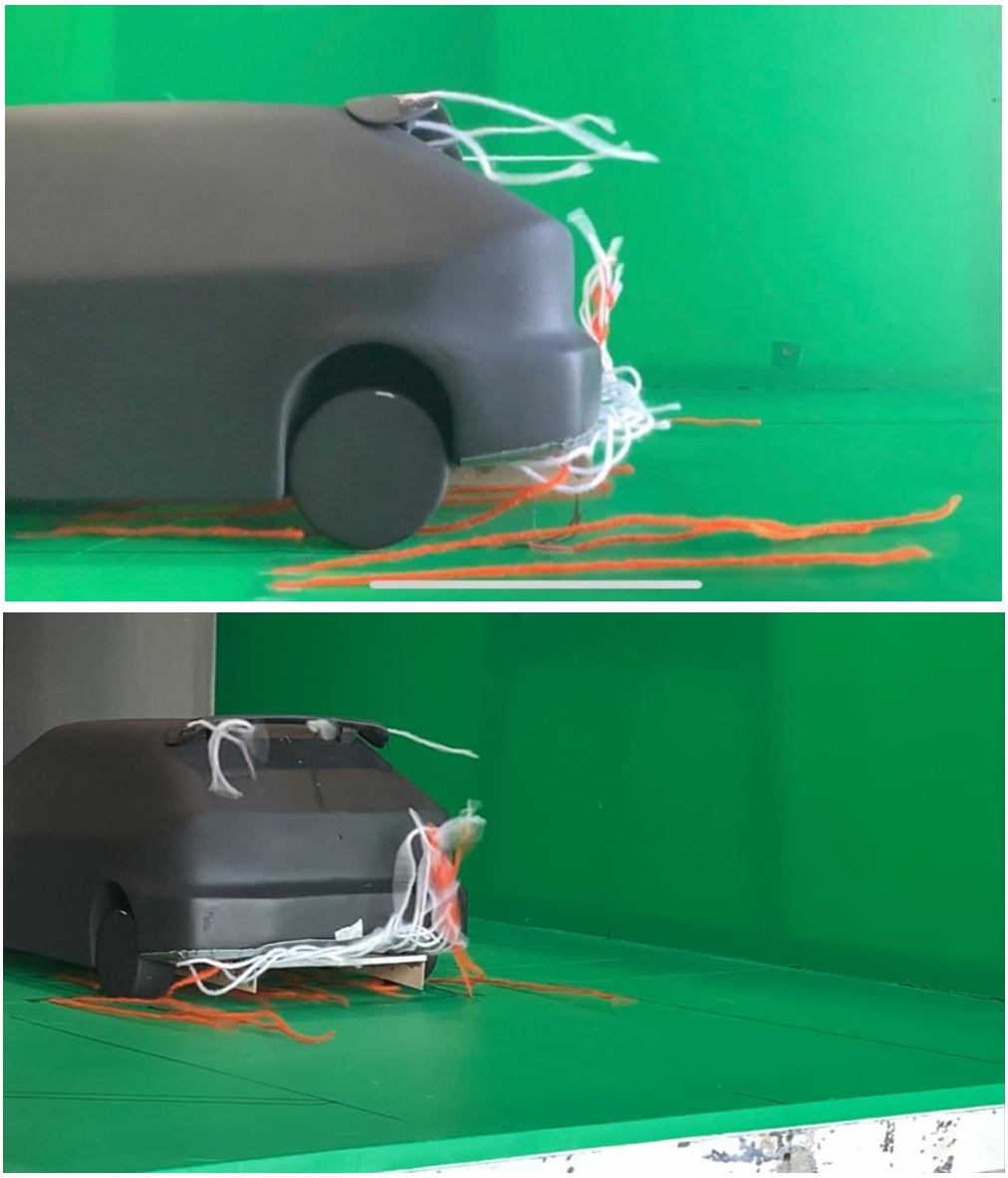

Source: (Own Autor)

Figure 5.18 – Tufts visualization for 6-degree setup

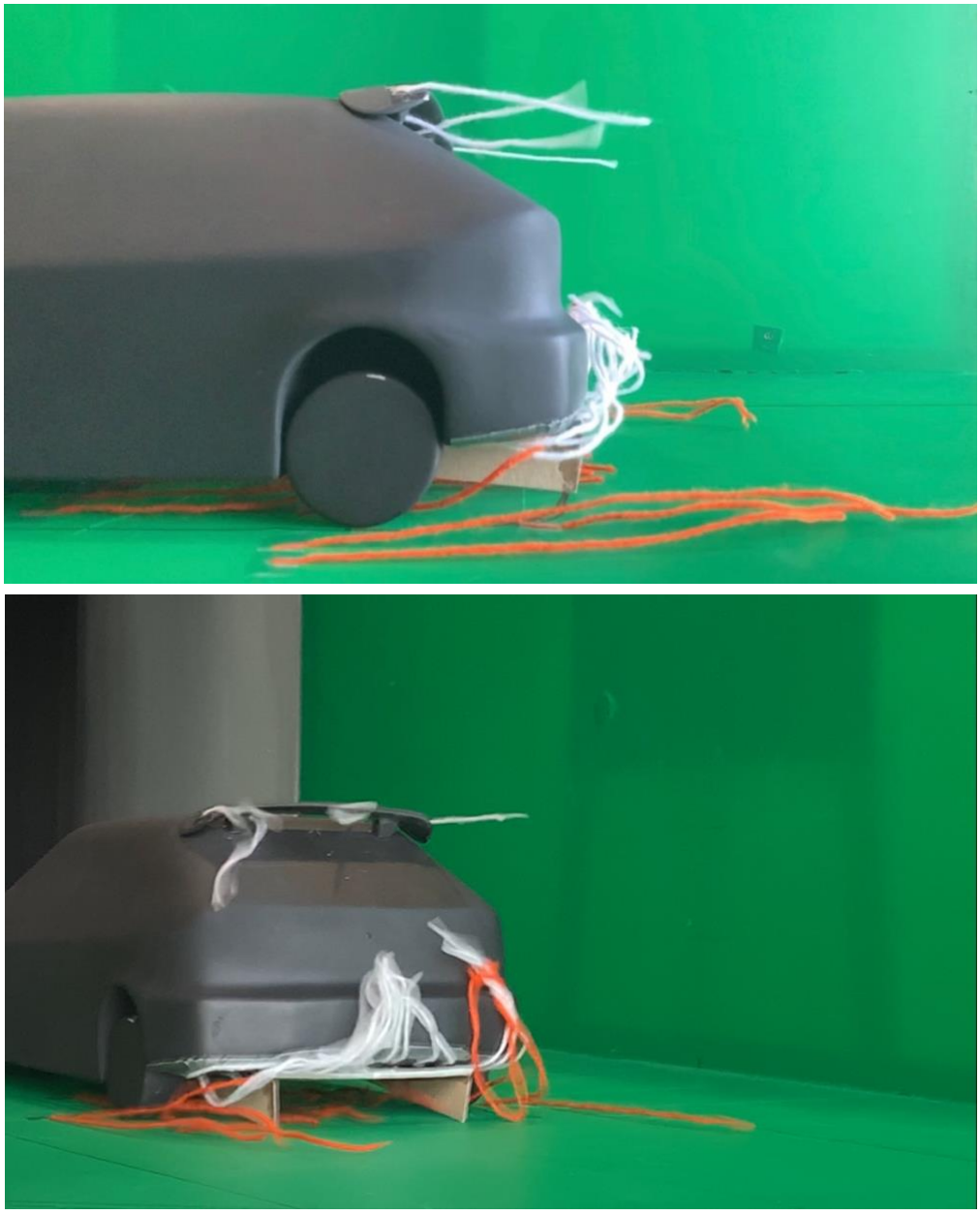

Source: (Own Autor)

Figure 5.19 – Tufts visualization for 8-degree setup

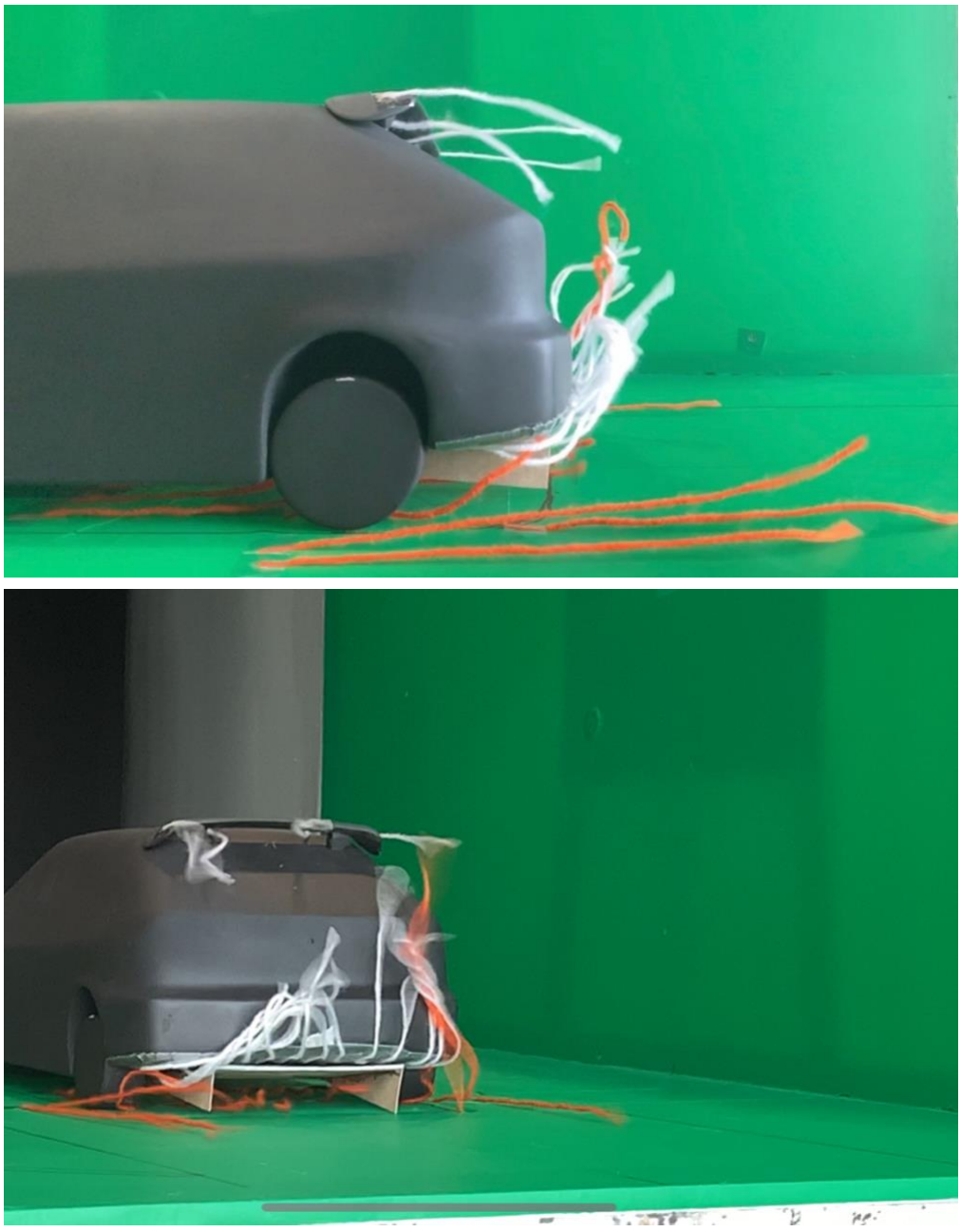

Source: (Own Autor)

Figure 5.20 – Tufts visualization 10.51-degree setup

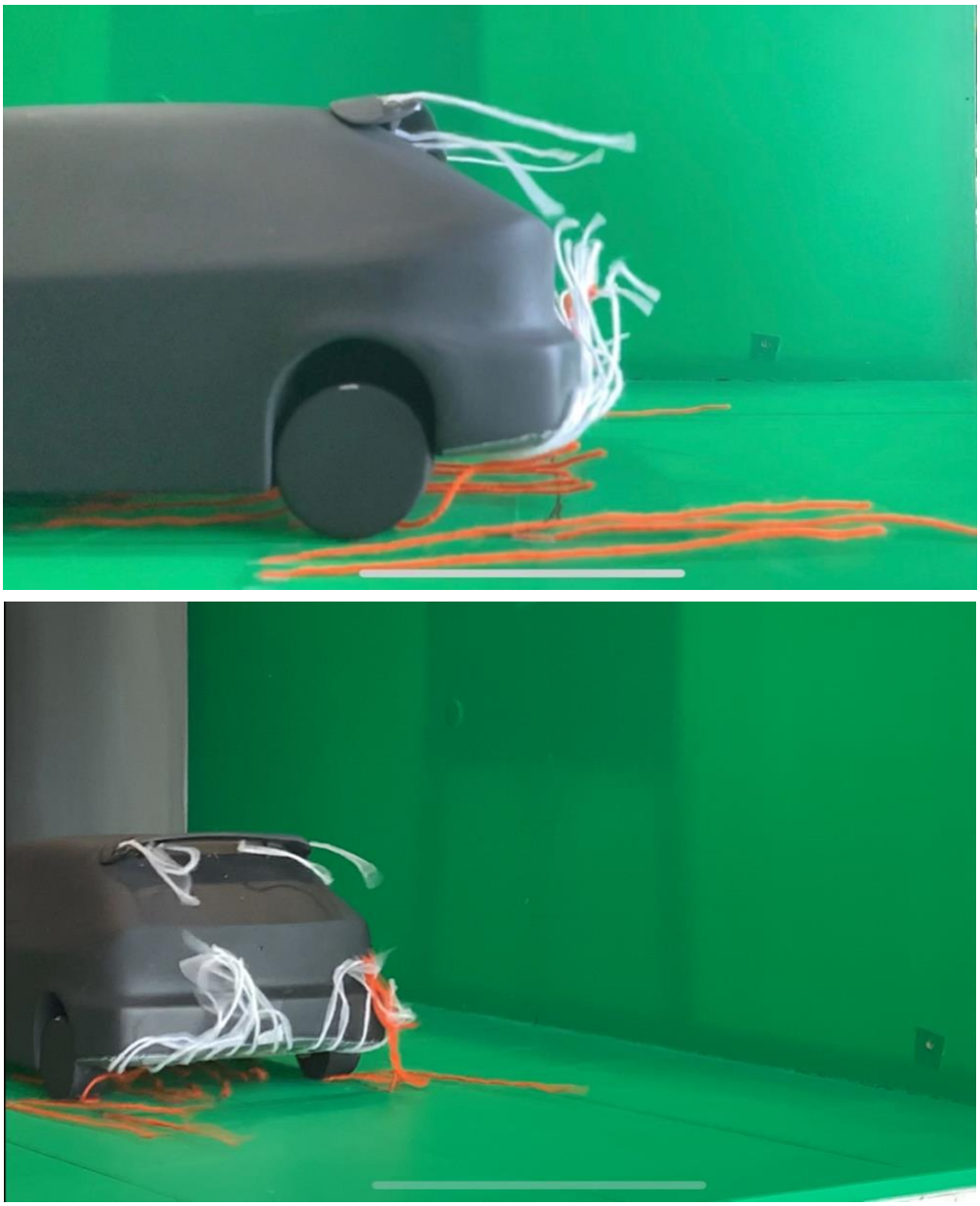

Source: (Own Autor)

The first visualization method shows some interesting phenomenon about the air flow over and under the model. For the two first configurations it's clear that the tufts fixed to the wind tunnel ground remain attached, showing that the air flow is steady along the length of the diffuser. The white tufts seem to have a similar behavior, showing that could be a resembling pressure distribution. At 4-degree angle, the ground tufts start to become unsteady, may be due to the flow

detachment at the end of the diffuser. For the three remain diffuser angles, this turbulence increases as the angle increase. Figure 5.18-b and Figure 5.19-b indicates a rotating orange tuft near the right endplate, which means the formation of three-dimensional side vortex due to the diffuser ramp which induce lateral inflow. The white tufts attached to the car were high lifted at the back, maybe due to the bigger vortex structure. But some cases (6-degree and 8-degree diffuser angle) were possible to see the orange tufts, under the car, lifting from the ground, so downforce could be expected for this high angle's diffusers. The 10.51° setup didn't lift the tufts as expected, what could be explained by the diffuser height from the wind tunnel ground and the flow detachment from the body.

Figure 5.21 – Ground tufts lifted for 6-degree diffuser

Source: (Own Autor)

Figure 5.22 – Ground tufts lifted for 8-degree diffuser

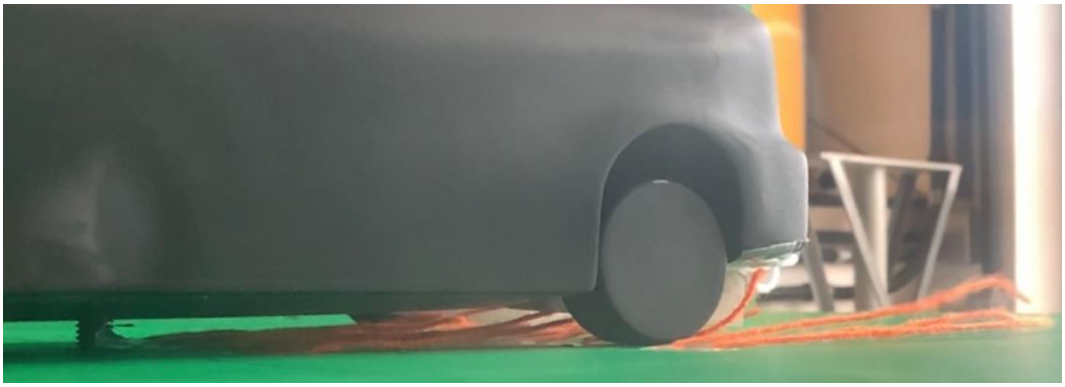

Source: (Own Autor)

The use of wall tufts permitted the clarification of flow behavior close to the model, especially for zones under adverse pressure or flow recirculation.

## 5.5. Flow Visualization Paint Results

For the next flow visualization method, a solution was prepared according to the Chapter 4. Wind tunnel testing was performed at the velocity of 20.0 m/s. Videos were recorded from lateral and from top view of the model. The Figures 5.23 and 5.24 illustrates images registered for each diffuser.

Figure 5.23 – Painted model side view

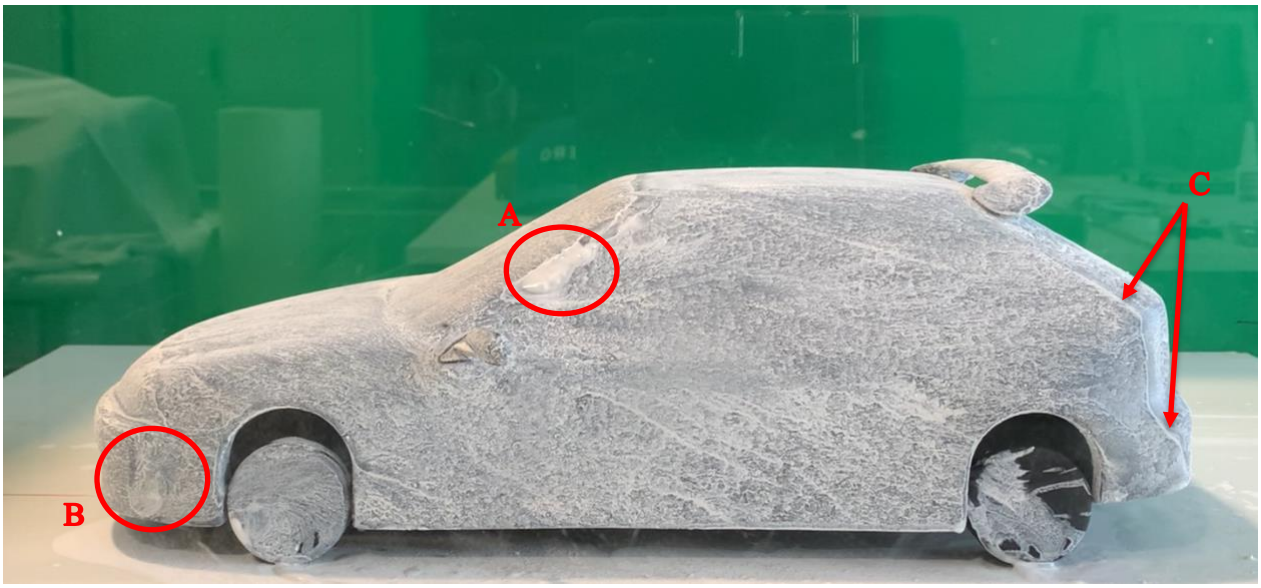


Source: (Own Autor)

This type of flow visualization enables to understand the air flow streamlines passing over the model and where detachment occurs. At the point A, as indicated in the Figure 5.19, it's possible to see the detachment of the flow in the A-pillar. The accumulation of paint shows a low-pressure zone and the presence of vortices in this region. The point B shows another accumulation region, evidencing a detachment region on the front bumper. C indicates where the air flow separates from the model, and where the wake zone begins.

Figure 5.24 – Painted model top view

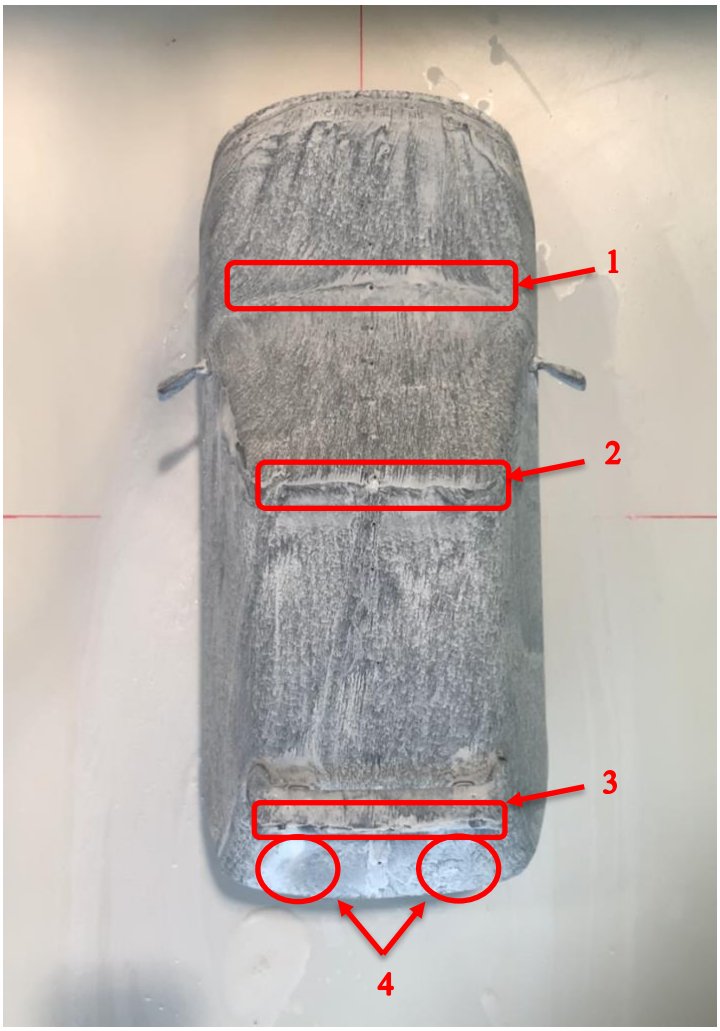


Source: (Own Autor)

From the top view some interesting phenomenon can be observed. First, at the start of windshield a high-pressure zone is identified by paint accumulation, as expected according to the pressure field results. At the point 2, a bubble recirculation appears at the end of windshield, because this region is a transition mechanism present in low Reynolds flows and reattached right after at the roof. It is also possible to observe the air flow detachment occurring in rear spoiler trialing edge. Maybe due to the spoiler upper surface. The last one, is a pair of vortices cause by rear spoiler fixation support.

The use of oil painting is a complement for visualize flow behavior over the model, especially for zones under adverse pressure or flow recirculation.

# CHAPTER VI

## Conclusion

An experimental study of the aerodynamics of diffuser's angles were performed. The model was prepared to be faithful to the real vehicle shape. Baseline model is composed by the main vehicle characteristic, including side mirrors and rear spoiler; and the existent rear diffuser of 10.51° with a flat underbody. A set of five different diffuser angles (0°, 2°, 4°, 6° and 8°) were prepared, and endplates were placed in each diffuser configuration. The model was printed 1:10 scale for wind tunnel testing. On experimental procedures, qualitative (wall tufts visualization) and quantitative (drag coefficient determination and pressure field determination) tests revealed main structures on wake and on the close wall.

The balance was able to measure the effects made by each diffuser on drag coefficient. The small angles seem to be the best choice for drag reduction, being that the 2-degree diffuser was capable to reduce drag force by 6%. Adding endplates show to be inefficient for this study, unless for the 6-degree setup, in which reduce in 5% when compared with baseline configuration. Lift forces was unable to analyze due to way of the aerodynamic balance was already assemble in wind tunnel test section. The upper pressure field of the car presented the expected result for a hatchback car model, but when compared different diffuser angles, there was no significant changes observed. The pressure profile shows that 6-degree diffuser induced high energy flow on the wake, which could recover the pressure behind the model.

The visualization method revealed that, the presence of diffuser and its angle variation, are capable to change the flow behavior behind the model. For lower angles, air flow under the car did not suffer variation, remaining in steady condition, while for high angles, turbulence was observed, indicating detachment of the flow by separation and vortex generation. Oil painting visualization helps to understand how the air flows over the model and to determine the detachment points.

The study of the airflow passing by a diffuser it's not a simple task. The reduced scale of the model hinders the analyses of different configurations and geometries, since the diffuser is a small appendicle on the car. Experimental tests must be combined with numerical studies, to

ensure a better analysis of how the airflow interacts with the proposed geometry, so that one approach can complement the other.

Therefore, trying to analyze this interaction with complex models closer to a hatchback car for the first time, may lead to false, incomplete, or irresolute conclusions. Most articles found used more simplified models, that made it possible to studied higher diffuser angles. Yet, the study from automobiles manufactures and racing teams are already in the stage of proposing geometries to deliver the best lift-drag ratio, once they have large investment, so that they can test in full scale.

The next step of the project is to do CFD analysis to predict the flow behavior under the model and compare it with the results of the wind tunnel tests. With computer simulations, lift can be evaluated and thus how much downforce can be generated with each diffuser. For better wind tunnel test results are recommended to fix the car by upper surface to minimize the external effects on the underbody. Design separated rear ends with diffuser attached may be a better approach to avoid imperfections in the assembly of each diffuser. Another change in the model would be to decrease its height in relation to the ground since the literature and other works point to this as a way to improve the efficiency of the diffuser. For pressure field quantification, a hole at upper surface of the model to pass hoses, might be the best way to avoid external effects. And to quantify the underbody pressure coefficient, pressure taps on flat underfloor is recommended to analyze the influence of different diffuser angles on air flow.

# ▪ REFERENCES


KATZ, J.; Race Car Aerodynamics: Design for Speed. 2nd ed. Cambridge: Bentley Publishers, Inc., 1995.

HUCHO, W.-H.; Aerodynamics of Road Vehicles: From Fluid Mechanics to Vehicle Engineering. 1st ed. London: Butterworth-Heinemann, 1987.

ANDERSON, J. D.; Fundamentals of Aerodynamics. 5th ed. New York: The McGraw-Hill Companies, 2011.

SMITH, C.; Tune to Win: The Art and Science of Race Car Development and Tunning. California: Aero Publishers, Inc., 1978.

KATZ, J.; Race Car Aerodynamics. Annual Reviews, 2006.

HOERNER, S. F.; Fluid-Dynamic Drag: Theoretical, Experimental and Statistical Information. 1965.

TOET, W.; Aerodynamics and Aerodynamic Research in Formula 1. **Aeronautical Journal**, Vol. 117, No. 1187, 2013.

COOPER, K. R.; BERTENYI, T.; DUTIL, G.; SYMS, J.; SOVRAN, G.; The Aerodynamic Performance of Automotive Underbody Diffuser. **Society of Automotive Engineers**, 1998.

COOPER, K. R.; SYMS, J.; SOVRAN, G.; Selecting Automotive Diffusers to Maximize Underbody Downforce. **SAE Paper 2000-01-0354**, 2000.

HUMINIC, A.; HUMINIC, G.; Aerodynamic Study of a Generic Car Model with Wheels and Underbody Diffuser. **International Journal of Automotive Technology**, Vol. 18, No. 3, pp. 397−404, 2017.

BARLOW, J. B.; REA, W. H.; POPE, A.; Low-Speed Wind Tunnel Testing. 3rd ed. New York: John Wiley & Sons, Inc., 1999.

MERZKIRCH, W.; Flow Visualization. 2nd ed. Florida: Academic Press, 1987.

YAKKUNDI, V.; MANTHA, S.; SUNNAPWAR, V.; Hatchback Versus Sedan – A Review of Drag Issues. **SSRG International Journal of Mechanical Engineering**, Vol. 4, 2017.

BHAGIRATHSINH; RATHOD, P. P.; ARVIND, S.; I JOSHI, H.; Comparative Assessment of Drag Force of Hatchback and Sedan Car Model by Experimental Method. **International Journal of Advanced Engineering Research and Studies**, Vol. 1, 2012.

EHIRIM, O. H.; Downforce–enhancement of Automobile-type Diffuser Using Two Devices. Patent No.: US9,957 B1, 2018.

KNOWLES, K.; SADDINGTON, A. J.; A Review of Ground-Effect Diffuser Aerodynamics. **Journal of Fluids Engineering**, 2018.

KNIGHT, J.; SPICAK, N.; KUZENKO, A.; HARITOS, G.; REN, G.; Investigation of Vehicle Ride Height and Diffuser Ramp Angle on Downforce and Efficiency. **Proceedings of the Institution of Mechanical Engineers Part D Journal of Automobile Engineering**, 2018.

HASSAN, S. N. R.; ISLAM, T.; ALI, M.; ISLAM, MD. Q.; Numerical Study on Aerodynamic Drag Reduction of Racing Cars. Elsevier Ltd, 2013.

BARBUT, D.; NEGRUS, E. M.; CFD Analysis for Road Vehicles - Case Study. **Incas Bulletin**, Vol. 3, 2011.

MARKLUND, J.; Under-body and Diffuser Flows of Passenger Vehicles. Sweden, 2013.

Effect of underbody diffuser on the aerodynamic drag of vehicles in convoy, Deepinder Jot Singh Aulakh, Cogent Engineering (2016), 3: 1230310.

TAIMING, H.; XIAODONG, Z.; ZHONGMIN, W.; ZHENGQI, G.; Experimental and numerical investigations of the vehicle aerodynamic drag with single-channel rear diffuser. **SAGE Journals**, Vol. 234, pp. 2216-2227, 2020.

ÇALIŞKAN, M.; BAKIRCI, A.; An Investigation of the Different Diffuser Positions Effect on Vehicle Aerodynamic Performance. **International Journal of Automotive Science and Technology**, Vol. 6, No.1, pp. 75-82, 2022.

Guerrero, A.; Castilla, R.; Eid, G. A Numerical Aerodynamic Analysis on the Effect of Rear Underbody Diffusers on Road Cars. Appl. Sci. 2022, 12, 3763. https:// doi.org/10.3390/app12083763.

HARIS, M. N.; SAPIT, A.; MOHAMED, N. H. N.; Study of Airflow Due to Rear Diffuser of Supercar. **Journal of Complex Flow**, Vol. 2, No. 2, pp. 32-36, 2020.

Porcar, L.; Toet, W.; Gamez-Montero, P.J.; Study of the Effect of Vertical Airfoil Endplates on Diffusers in Vehicle Aerodynamics. Designs2021,5,45. https://doi.org/10.3390/designs5030045.

DUXBURY, A.; HOLDING, J.; How fast is an F1 car? Top speeds of F1, IndyCar, MotoGP and more. Autosport.com, 2022. Available in: <https://www.autosport.com/f1/news/how-fast-is-an-f1-car-top-speeds-of-f1-indycar-motogp-and-more-4980734/4980734/>.

- **APPENDIX I**


31
VTEC


60
HONDA
CVY·7788
VTi
YTEC
YO!
CARS


31
NELSON PACHECO.COM


16 16
31

*“In Memory of Nelson Batista Neto”*

*1998 – 2022*